TRACKING ERROR BASED SLIDING MODE CONTROLLER DESIGN WITH APPLICATION TO FLIGHT CONTROL

by

GIRESH KUMAR SINGH

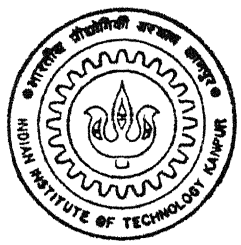

DEPARTMENT OF ELECTRICAL ENGINEERING

Indian Institute of Technology Kanpur

FEBRUARY, 1998

TRACKING ERROR BASED SLIDING MODE CONTROLLER DESIGN WITH APPLICATION TO FLIGHT CONTROL

A Thesis Submitted

in Partial Fulfillment of the Requirements

for the Degree of

Doctor of Philosophy

by

GIRESH KUMAR SINGH

to the

DEPARTMENT OF ELECTRICAL ENGINEERING

INDIAN INSTITUTE OF TECHNOLOGY, KANPUR

February, 1998

To
Mini, Baby, Papa,
&
Sweet Memories of Mummy

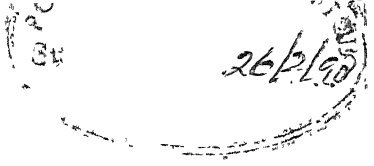

CERTIFICATE

It is certified that the work contained in this thesis entitled *Tracking Error Based Sliding Mode Controller Design with Application to Flight Control* by *Giresh Kumar Singh* has been carried out under my supervision and that this work has not been submitted elsewhere for a degree.

Professor K. E. Holé
Department of Electrical Engineering
Indian Institute of Technology
Kanpur

February, 1998

Acknowledgments

I would like to take this opportunity to firstly thank all those who have taught me and from whom I have learnt. It is mainly because of the efforts of so many *gurus* that I have reached this stage. It is a great pleasure for me to express my deep sense of gratitude to Prof. K.E. Holé for his sincere and constant guidance throughout the present work. I have always found him very approachable, communicative, patient, and always willing to help in all aspects of life. His gentle proddings have been greatly responsible for bringing the present work to a logical conclusion.

I am thankful to Profs. S.C.Raisinghani and C.V.R. Murthy for having introduced the fascinating area of aircraft dynamics and control and Dr. R.K. Bera for inspiring me to work on it. I am indebted to Profs. A.K. Raina, V.R. Sule, P.K.Kalra, and my guide for guiding me through the maze of control theory and for the valuable suggestions and advice they gave me from time to time.

The time spent in the *Control System Laboratory* has been a very memorable one. It is only during my involvement in the setting up of laboratory experiments along with Dr. A.K. Raina, Shri Gurucharan Singh and Shri Uday Majumdar that I realized the difficulties in instrumentation and implementation of control systems. The company of Uday, Qadeer, Sashmita and Ramnath in the laboratory was always refreshing and encouraging.

I would like to thank IIT Kanpur for the various facilities including the scholarship, the computer centre and the central library.

I would like to thank my seniors Drs. I.N. Kar, Deepak Murthy, and Shiv Narayan, and friends Ryali Venkat, Vydyanathan, Rajiv Kumar, Ashish Balaya and many others, who were always ready for a discussion or an argument on various technical aspects of

the work. These long talks have helped me in developing a better appreciation of the area. They have always been a source of inspiration.

All work and no play! It is difficult to think of life without friends. During my stay in IIT Kanpur, I was fortunate enough to have many close friends, whose company will be remembered forever. The pleasure of being in the company of Swapan, Alok, Sujoy Fatta, Dipak, Raghu, Rahul, Abır, Him, Shivgovind, Khanna, Ajju, Bpandey, Kak, Kaki, Jauhari, Anjani, Shankha, Pankha, Medh, Sharma, Suman, Kishore, Mama, PK Dada, Bogada, Jawed, Immi, Kashi, Ksri, Palani, Govind, Mogambo, Tapo, Shanti, Mangsuli, Joydeep. Rogers, and others, can hardly be described in words – it is best experienced. I have always found them by my side when need be. The canteens of the various halls have been quite instrumental in nurturing our friendships, and their role is gratefully acknowledged.

I can hardly ever forget the staff, hall4 and the faculty cricket teams and the matches between the three, and the discussions following them. These have gone a long way in making my stay here pleasant and memorable. I would like to thank the members of the family of Shri Uday Majumdar for extending warm hospitality during my stay in the campus.

Closure: Last, but not the least, it is impossible for me to express in words my deep feelings towards my family. Looking back, I find myself lacking in the roles of a son as well as a brother. It is my parents' and sisters' whole-hearted love, support, and encouragement which has kept me going. Also the affection and support extended by friends and relatives back home during some of the turbulent periods of life has been very helpful. It saddens me to think of how my mother would have reacted on the completion of this thesis. To her, papa and my sisters, I dedicate this work.

G.K. Singh

Synopsis

The Flight Control System (FCS) design for modern fighter aircrafts is one of the major problems encountered in its development phase. This design problem has assumed more importance with unstable airframes, ever expanding flight envelopes and involved technological developments. These developments are directed to enhance the combat agility and survivability. In fact, the development of new tactical maneuvers and strategies now hinges on the capability of the FCS. Conventionally, gain-scheduling has been the most widely used method to design the FCS. However, the method is rather ad hoc in nature and requires extensive simulation before it can be applied in flight. Recent developments in nonlinear control theory, namely the feedback linearization or the dynamic inversion, have also been applied to FCS design. However, guaranteeing stability and performance robustness in the presence of uncertainty and disturbances is not very straightforward and has been tackled using the approaches developed in the linear control theory.

The present work is a study of the feasibility and applicability of the Sliding Mode Control (SMC) method for the FCS design. The SMC method uses a nonlinear discontinuous control law and offers attractive robustness properties. The method originated in the Soviet literature. The method involves a) the selection of a sliding surface (SS), and b) the choice of a control law to make the SS attractive. The evolution of trajectories may be considered in two distinct phases, a reaching phase, in which a trajectory reaches the SS, and a sliding phase where it will evolve according to the dynamics specified by the selected SS. Invariance to unknown but bounded matched uncertainties and disturbances in the sliding phase has been established. This is made possible by using a high gain or switching type of control law. However, practical applications

of the method are limited by the facts that

1. It is directly applicable to input affine systems only.

2. Robustness in the presence of unmatched uncertainties is not guaranteed.

3 The inputs to any practical system are the outputs of a dynamic actuation system with a finite bandwidth, and thus instantaneous changes in the input cannot be achieved ruling out the use of a discontinuous term as in the conventional SMC method.

These issues are addressed in this work for the aircraft longitudinal FCS design problem.

The Chapter 2 considers the design of a constant plus proportional rate reaching law SMC for second order nonlinear systems. Conventionally, the controller parameters are selected so as to minimize the reaching time, i.e the time taken to arrive at the SS, and use the guaranteed invariance property offered by the SMC. However, a quick tracking performance in terms of the time taken to reach a small output tracking error (OTE) is of primary interest and should govern the parameter selection. For this, firstly it is established that this composite rate reaching law has a robust performance even before the onset of sliding. A new method of selection of the controller parameters based on the criterion of minimizing the time to reach a pre-specified OTE is proposed. It is established that controllers designed using the criterion of the time to OTE, while using similar peak levels of control effort, are expected to take substantially shorter times to the OTE as compared to designs based on the reaching time criterion. The method is applied to two second order mechanical systems, and the simulation results show that control laws designed based on the new criterion result in appreciably faster output tracking, verifying the parameter selection approach.

Although the SMC method has excellent robustness properties, its applications to the FCS design problem have been few. The forces and moments generated are known to be complicated nonlinear functions of the aerodynamics and control surface deflections. Most of the published works use linearized approximations of the nonlinear aerodynamics to develop input-affine models for the aircraft dynamics, as the SMC is

directly applicable to this class of systems. In this work, the forces and moments are directly treated as inputs to the aircraft instead of the conventional control surface deflections, with the assumption that appropriate methods of generation of the desired forces and moments exist. A bounded multiplicative uncertainty is assumed between the command force vector and the actually realized force vector to account for any errors that might be involved in generating the desired force-moment vector. An explicit model following (MF) structure is used to design a SMC (MF-SMC) based full-envelope control law, using full state feedback, for the nonlinear longitudinal dynamics of an aircraft for the case of matched uncertainties and disturbances in Chapter 3. Analytical control laws for two operational modes of the aircraft, namely i) the velocity tracking mode, and ii) the trimming mode are derived. Results of the numerical simulation using parameters of the F-16 aircraft confirm the robustness of the control law and establish the applicability of the design method.

The SMC method is next extended to include the presence of unmatched uncertainties and disturbances as it would be present in most practical systems. The SMC design for this case is developed based on a multi-loop (ML) strategy. With the velocities as primary outputs of the aircraft system, the uncertainties/disturbances present in the dynamics of the position state variables would be unmatched. It is assumed that model responses for the velocity and position state variables are available. The outer loop control law is designed so as to track the position state variables by treating the command signals for the velocity variables as the input. The ML strategy passes on the effect of the unmatched disturbances in the outer loop to the inner loop. A SMC based inner loop control law is then designed to track the command velocity variables. The difference between the model and the command velocity variables has been derived and is shown to depend on the magnitude of the unmatched uncertainties. The ultimate boundedness of the position and velocity errors is established and their time domain bounds are obtained as functions of the controller parameters. These bounds can thus serve as a guideline for their selection. The method is applied to the design of the velocity tracking mode controller for the aircraft longitudinal dynamics. Numeri-

cal results for various choices of the controller parameters are presented in Chapter 4. The ML approach is then applied to single input (SI) higher order nonlinear systems with unmatched uncertainties. Analysis for a third order system shows that, with the proposed method of selection of the switching term gain, the conventional SMC design can be applied to tackle unmatched uncertainty. The errors in the various loops are shown to be ultimately bounded. Numerical simulation on a nonlinear system confirms the developed bounds and verify the applicability of the ML strategy.

The chattering phenomenon, due to the use of a discontinuous control law, is one of the most serious limitations of the SMC approach which restricts its application to practical problems. Moreover, the control inputs to any system are generally applied through an actuation system with a finite bandwidth, ruling out the possibility of instantaneous switching capability. In this work, the input is considered to be the output of a specified first order system with disturbances and uncertainties. Available studies use higher order sliding modes and a differential algebraic approach to address this problem. However, both of these methods involve higher order derivatives of the states and thus the propagation of disturbances and uncertainties becomes complicated making robustness analysis very difficult. The ML strategy, developed in Chapter 4, is extended to the SMC design for such systems in Chapter 5. The propagation of disturbances in the ML strategy is better handled and obviates the need of derivatives of the uncertainties/disturbances leading to a simpler robustness analysis. The state and input errors are shown to be ultimately bounded. The method is first developed for a SI nonlinear system and applied to the nonlinear spring mass problem. Simulation results verify the approach. The method is then applied to the MI aircraft velocity tracking problem, considered earlier, with specified first order input dynamics, and the ultimate boundedness of the the velocity, position, and input errors is established. A parametric study of the choice of controller parameters is done. Results of the numerical simulation in the velocity tracking mode establish the applicability of the ML approach to this problem.

Contents

List of Tables

List of Figures

Chapter 1

Introduction

1.1 The Aircraft Flight Control Problem

The aircraft flight control system (FCS) design is amongst the most critical problems faced in an aircraft development project. This design problem has become more critical with unstable nominal aircraft designs, ever expanding flight envelopes, and ongoing technological developments. McRuer and Graham [1] chart out the historical developments in the controller design since the first flight in 1901 by the Wright Brothers. The onset of high speed digital computers revolutionized the conventional control schemes resulting in the fly-by-wire and the active control technology [2, 3]. Novel concepts such as the Control Configured Vehicles (CCVs) [2, 4, 5] have been tried out on many operational aircrafts with associated benefits. Another such emerging technology area is the thrust vectoring (TV) which will be equipping almost all the future generation fighter aircrafts [6–9]. This makes use of the fact that the engine thrust remains almost constant as compared to the flow dependent conventional flight control (CFC) surfaces, namely the elevator, aileron and the rudder, and hence can be used even after the CFC surfaces are ineffective. To increase combat effectiveness and survivability, fighters are being pushed not only to the limits of the conventional flight envelopes but also beyond to acquire a tactical edge over the contemporary fighters. So much so that the development of new combat tactics and strategies is now governed by the capability of the FCS. The 'Pougachev's Cobra maneuver' routinely displayed by the

Sukhoi fighters [9] is one of the so called super-maneuvers. Other examples include the 'Herbst Maneuver' in which the aircraft rotates its velocity vector through 180^0 in a minimum possible time. The governing theme guiding these developments is that maneuverability of manned flight should be bounded by the limitations of the human pilot and not the airframe.

The aircraft is conventionally modelled as a 6 degree of freedom (dof) rigid body [10] (3 for the translational and 3 for rotational). This results in a highly coupled and nonlinear set of dynamic equations. The dynamic modes of the aircraft may be broadly classified into two categories, i) Rotational modes, and ii) Flight path modes. The responsiveness of an aircraft to maneuvering commands, i.e its agility, is determined by the speed of the rotational modes. The natural frequencies of these modes are sufficiently high so as to make it impossible for the pilot to control the aircraft if these are lightly damped or unstable. Control systems are needed to augment the natural modes to have a suitable damping and frequency characteristics. These are popularly called the Stability Augmentation Systems. In addition to these, there are the Control Augmentation Systems, which help in achieving a desired response to the the pilot control inputs as in tracking etc. Autopilots are also used to perform pilot relief functions such as attitude hold or for navigational purposes. These control systems are intended to perform the functions designated to them over the entire flight envelope. The uncertainties and disturbances are an unavoidable feature of any practical dynamic system. These arise either because of the inexact knowledge of the parameters in the system (structured uncertainty) or because of unmodeled dynamics (unstructured uncertainty). A practical control system design besides performing stabilization should also provide

- robustness to uncertainty and disturbances, and
- some desired response characteristics- popularly known as Flying /Handling qualities (HQ).

This necessitates the design and use of a flight control system (FCS) to meet stability and performance specifications over an entire flight envelope.

Linearized aircraft dynamics has been conventionally used to design linear control laws [10]. One approach was to design a single linear controller for the entire flight envelope. Hence the variation in aircraft dynamics at different flight conditions was modeled as a nominal plant with an additional uncertainty term. Yedavalli [11] considers robust linear controller design under structured uncertainties. Houpis et.al. [12] using quantitative feedback techniques design a robust control law for the F-16 aircraft accounting for four different flight conditions and six failure modes, i.e. a total of 24 possible flight configurations. However, any scheme using a single linear control law for the entire flight envelope would achieve stability robustness only at the cost of sacrifice in performance. Moreover, the nature of changes involved in the aircraft dynamics with varying flight conditions is not completely unknown and may be incorporated in the design procedure.

Thus, a better control strategy was the gain-scheduled (GS) approach. In this method, linearized models of the aircraft, which would approximate the actual dynamics better in some local neighbourhood, at the specified operating points are obtained. Separate linear controllers, with desired stability and performance robustness in a local sense, are then designed for each linear model obtained earlier. These point designs are then 'stitched together' using a gain schedule to obtain the overall control law. Scheduling is heuristically done on parameters which i) vary slowly so that the actual plant may be considered quasi-steady, and ii) which capture the plant nonlinearities. Gangsaas et.al. [13] report practical applications of the LQG based gain-scheduled control law design. Adams et.al. [14] developed a a full envelope nonlinear control law for the longitudinal and lateral modes. Blight et.al. [15] design GS control law using LQG and structured singular value techniques to design for robust point designs. Shue et.al. [16] use a mixed H_2/H_∞ method for the point controller designs and schedule the controllers over the mach numbers. The main advantage of GS is that the wealth of linear control methods, performance measures, design intuition and computational tools may be used on the multi-variable nonlinear systems. However, the choice of the number of operating points and the point itself is not very well laid out, and therefore

the GS law has to be verified by extensive nonlinear simulation before it can be actually applied to an aircraft. Traditionally, this approach has been the most popular and widely used control law with both analog and digital versions of the method being used in various fighter aircrafts such as the Mirage 2000, and the F-16 among others. However, there have been notable failures also, for e.g. the JAS-39 and the YF-22 crashes [17, 18]. Shamma and Athans [19] discuss the application of this approach to non-linear plants. Shamma and Athans [20] point out some pitfalls of the method.

With the recent developments using differential geometric concepts in nonlinear control theory [21, 22], nonlinear inverse dynamics or feedback linearization based flight control design has been investigated by many researchers. The main advantage of the method was that it directly results in a global/ full-envelope control law. It also offers generality of application to different aircraft types. Smith and Meyer [23] used model inversion techniques to the aircraft control design problem treating the accelerations as pseudo-inputs. Lane and Stengel [24] used the method to decouple specific state variables that are of some particular interest to the pilots and used it to enhance stall prevention capabilities. They observed that 'Flight control systems based upon nonlinear inverse dynamics offer the potential of providing improved levels of safety and performance over conventional designs developed using linearizing assumptions'. Vukobratović and Stojić [25] discuss the centralized and decentralized control schemes using the inverse aircraft model. Singh [26] and Romano and Singh [27] design controllers for large nonlinear maneuvers of the aircraft. Durham et.al. [28] use a nonlinear model following approach to airplane control. Sun and Clarke [29] study auxiliary control devices, namely the flaps and spoilers for direct force control, for active control of the aircraft. Enns et.al. [17] apply the method to the F-18 HARV executing a Herbst maneuver.

However, this approach does not lead to an easy robustness analysis. This issue was addressed by using a multi-loop strategy with the inner loop performing the linearization of the unperturbed plant, and an outer loop was designed to take care of any uncertainties in the actual system. Adams and Banda [30] following the method

developed in [31] applied the structured singular value analysis to incorporate robustness in this approach. In another related work Sparks et.al. [32] use a gain-scheduled inner loop to obtain dynamic inversion. Enns et.al. [17] use loop shaping techniques to obtain robustness properties. An alternative method which uses a nonlinear discontinuous control law and offers attractive robustness properties, namely the sliding model control method, is next considered for this control design problem.

1.2 The Sliding Mode Control Method

The Sliding Mode Control (SMC) originated in the Soviet literature [33]. Some of the recent survey /review papers on this topic are Utkin [34], DeCarlo et.al. [35], and Hung et.al. [36]. They reflect the increasing interest of the control community in the method and report the developments and applications of the SMC to a myriad of control problems. The SMC design method involves two steps, i) the selection of a stable hyperplane in the state/error space on which motion should be restricted, called the sliding surface (SS), and ii) the synthesis of a control law which makes the selected surface attractive. In this method a trajectory, starting from a non-zero initial condition, evolves in two phases :

- A Reaching phase, in which it reaches the SS, and
- A Sliding phase, in which the trajectory on reaching the SS, remains there for all further times and thus evolves according to the dynamics specified by the SS.

The sliding surface specifies the dynamics in the second phase. Trajectories from any starting point can be shown to arrive at the SS in a finite time [37]. It has been shown that the trajectories on the SS exhibit invariance to unknown but bounded matched uncertainties and disturbances [21, 38]. This is achieved by using a switching/relay type of control law. However, the sliding motion commences only after the trajectory reaches the SS. Thus, to reap the benefits of the invariant response on the SS, it has been considered imperative to reduce the reaching time, i.e. the time spent in the first phase, and this has been traditionally used to select the controller parameters.

However, for a tracking task the quickness of response in terms of the time required to reach a small output tracking error (OTE) is of paramount interest and should be considered for the parameter selection. For the class of second order nonlinear systems, it is shown that a constant plus proportional rate reaching law as proposed in [37] offers a robust performance in the reaching phase also. Using this result, a new method of selection of controller parameters based on the time to OTE as the criterion is proposed. Simulations on two second-order mechanical systems show that the proposed parameter selection method takes substantially lower times to reach the OTE, while using similar levels of control effort, as compared with the selection method based on the traditional criterion of the reaching time.

The SMC method has been used to design controllers for various practical applications [36] including the aircraft FCS design. However, the method primarily applies to input affine systems, i.e. systems linear in the input, and has been applied to such systems. The SMC needs to be extended to tackle the presence of unmatched uncertainties and disturbances. Moreover, inputs to any practical system are generally generated by a dynamic actuation system and hence a discontinuous control law is not readily implementable. These issues need to be properly addressed for the method to gain more acceptance among the practising engineers and find more practical applications. The present work attempts to study these factors as related to an aircraft FCS design problem.

1.3 Application of SMC to Flight Control Design

The SMC, with its robustness properties, is an attractive alternate method for the aircraft flight control design problem. However, its application to the FCS design has been rather slow to pick up as is indicated by the method finding no application in the special issue of the *International Journal of Control* on aircraft flight control design [17, 39]. Calise and Kramer [40] were among the pioneers to adopt the SMC method for designing the FCS. They considered the linearized dynamics of the AV-8A Harrier in a hover mode under matched uncertainties. Singh [41] designed control laws for

large simultaneous longitudinal and lateral maneuvers of aircraft with linearized aerodynamics and matched uncertainty. Hedrick and Gopalswamy [42] reported the pitch axis control system design with nonlinear dynamics and linearized aerodynamics under matched uncertainty. They also considered various response criteria as developed by HQ engineers. Thukral and Innocenti [43] consider a linear model for the longitudinal problem. They consider the stabilization and tracking problems. Fossard [44] coupled the SMC with model following for the helicopter problem.

The above cited works model the nonlinear aircraft at best as an input affine system as the SMC technique is easily applied to such systems. However, the aircraft system of equations is known to be nonlinear in the states as well as the inputs [10]. Also, the number of independent inputs limit the number of outputs that may be exactly tracked. Thus the use of CFC surfaces, which is basically intended to control the three moments, imposes a fundamental limit on the number of tracked outputs. If, however, independent control of all the accelerations or equivalently the complete force-moment vector is possible, then these may be treated as pseudo-inputs, and the assumption of input affineness remains valid. It also increases the number of trackable outputs. Smith and Meyer [23] considered the accelerations as pseudo-inputs to the aircraft system. However, their design did not include robustness properties. Franklin [39] uses the forces as input for the low speed longitudinal landing control problem. Since, the generated forces depend on the bounded (with estimate of the bounds known) but uncertain time-varying inertia properties, the forces and moments have been treated as inputs to the aircraft system in this work, and is thus called the force control approach (FCA). To realize the forces as desired by the controller, appropriate control effectors are assumed to be present. With TV-FCS gaining popularity [6, 9, 45] independent control of the forces and moments affecting the motion is a feasible assumption. In fact flight tests on unmanned scaled fighter models have shown the practicality of a pure TV-FCS [46]. It is however observed that a proper mix of the CFC surfaces and TV leads to maximized safety agility and controllability levels. Presence of more alternatives, via the CFC surfaces, may be used to advantage by choosing control surface deflections that also

perform the CCV functions such as maneuver load control [2, 4]. This inverse problem of control allocation is being actively pursued in various development projects [7]. The constrained control allocation problem has been considered by Durham [47, 48]. The control surface deflections thus selected, on application to the airframe, are expected to generate the desired forces and moments. However, in practice the actually generated force vector would be different from its desired values, because of various reasons including the unsteady uncertain aerodynamics and the generally neglected aeroelastic effects. This discrepancy between the desired and the actually generated force vector has been modeled as a bounded multiplicative uncertainty in this study.

The explicit model following (MF) approach has been used to design the FCS. It offers many advantages. Firstly it facilitates the incorporation of various flight modes for different operational requirements. The HQs of an aircraft may be easily optimized by varying the models in-flight. One of its biggest advantages is that simulators can be widely used to train pilots with obvious advantages. In this work, a MF-SMC based full-envelope controller design for the nonlinear longitudinal dynamics of an aircraft has been done under matched uncertainties as is considered in almost all of the above cited works. A practical system however would not readily satisfy this assumption, and this is considered next.

1.3.1 The Unmatched Uncertainty Case

As seen earlier, there is a limit on the number of outputs that can be exactly tracked. The control of the remaining states is however still desirable. This was attempted by making use of the fact that there is a significant difference in time scales between the fast and slow states of an aircraft [49, 50]. In this multi-loop (ML) approach, a dynamic inversion based control law was synthesized for the slow states treating the fast states as the the input for the outer loop. Then an inner loop control law is designed so that the fast states actually track the command signals generated in the outer loop. Snell et.al. [49] report that better responses are obtained with this ML strategy as compared to the conventional gain-scheduled control law. The robustness of the control law was

however not dealt with. An integral error feedback in the outer loop was introduced by Azam and Singh [50] to obtain robustness while using a similar control structure.

As seen earlier, the SMC law guarantees invariance against the matched uncertainties and disturbances only, however, the presence of unmatched disturbances and uncertainties is not uncommon in practical systems. This would adversely affect the intended system performance. Design of control laws for the unmatched uncertainty case has been considered by many researchers [51–53] under various assumptions on the types of mismatch. In this work, the ML strategy is extended to include the effects of unknown but bounded unmatched uncertainties. The propagation of disturbances and uncertainties, from the outer to the inner loops, in this approach is worked out. Using the ML approach, a SMC law is developed for a general multi-input (MI) mechanical system under unmatched uncertainty and applied to the nonlinear longitudinal aircraft dynamics. The ultimate boundedness of the position and velocity tracking errors is established and the associated bounds are calculated as functions of the selected controller parameters. This can thus serve as a guideline for their selection. Application of the ML analysis, to a third order nonlinear system with unmatched uncertainties and disturbances, shows that conventional SMC design procedure, with a new method of selection of the gain of the switching term, may still be applied to tackle unmatched uncertainty. The ultimate boundedness of the errors in the various loops is established.

1.3.2 SMC with Input Dynamics

The switching control law as used by SMC is not practically feasible as it would require an infinite switching frequency to achieve the 'ideal' sliding. However, in practice any actuation system will have a finite bandwidth and delays resulting in 'real' sliding [54, 55]. Thus the invariance property is in effect lost and motion within some boundary of the SS can be guaranteed. This leads to the high frequency chattering effects which may excite the high frequency unmodeled dynamics in the system. To circumvent this difficulty, researchers have used two approaches i) use of continuous approximations of the discontinuous control law [21, 56], and ii) application of higher

order sliding methods [54, 55]. The control law then results in a continuous control law with discontinuities in the input rates. Ramirez and coworkers [57–59] using a differential algebraic approach construct input dependent sliding surfaces, and obtain similar results. The higher order sliding methods require higher order derivatives of the states and thus of the disturbances and uncertainties. This complicates the analysis of robustness properties, as the propagation of disturbances and uncertainties through the time derivatives is not very straight forward [60].

In this work, the input is considered to be the output of a first order actuator system. The ML strategy as discussed earlier is extended to address this problem. The propagation of disturbances and thus the robustness issues are more simply dealt with in the developed procedure. The method is first developed for a single input (SI) nonlinear system and ultimate boundedness of the state and the input errors are established. It is then applied to the MI aircraft velocity tracking problem with unmatched uncertainties. The position, velocity and input errors in the various loops are shown to be ultimately bounded. A parametric study of the involved feedback gains is required for their proper selection.

1.4 Organization of the Thesis

In this thesis, the aircraft control design problem using the SMC approach has been considered. Chapter 2 considers the design of a constant plus proportional rate reaching law based SMC design for second order mechanical systems. A method of selection of parameters for the SMC which results in lower times to an acceptable level of OTE is proposed. Simulation results obtained for a single input (SI) nonlinear spring-mass-damper and a two input two-link robot problems verify the method. Chapter 3 introduces the aircraft longitudinal dynamics and the force control approach. A MF-SMC based full-envelope controller design for the nonlinear longitudinal dynamics of a fighter aircraft has been done under the assumption of matched uncertainty. The desired model responses are obtained from a linear aircraft model given in Appendix D. The aircraft parameters, the assumed disturbances and uncertainties used in the

simulation are also given there. Analytical control laws for two operational modes, namely i) the Velocity Tracking Mode, and ii) the Trimming Mode, are derived for the case of matched uncertainty. A ML strategy is used to develop a SMC design procedure in the case of unmatched uncertainty in Chapter 4. Results of numerical simulation for the aircraft in the velocity tracking mode ascertain the robustness properties. This approach is then applied to SI higher order systems. Synthesis of a SMC law with first order input dynamics is discussed in Chapter 5. The method is first developed for the SI nonlinear spring-mass problem. Simulation results are presented to verify the feasibility of the approach. The design procedure is then applied to the MI aircraft problem. Simulation results for the velocity tracking mode with unmatched uncertainties are presented. Conclusions and scope of further research form Chapter 6.

Chapter 2

Design of Proportional plus Constant Rate Reaching Law SMC for Second-order Systems

2.1 Introduction

Many mechanical systems are modeled as second order systems e.g. as in the trajectory following robots, or the angular position control in aircrafts as nose pointing or pitch hold autopilots. Other examples include the classical inverted pendulum, or the antenna pointing of satellites among others. The SMC method has been used for many such applications as is evident from [36, 37]. Thus it is of particular interest to study the effect of the SMC parameters for this class of systems. As discussed earlier the sliding motion, and thus the invariant performance, occurs only after the trajectory reaches the SS, while the tracking behaviour in the reaching phase depends on the uncertainties. Thus, a smaller reaching time would imply that sliding begins earlier and this has been conventionally used to select the SMC parameters.

Gao and Hung [37] proposed a reaching law method which specifies the error dynamics in the reaching phase. They suggested three structures- the constant rate reaching, constant plus proportional rate, and the power rate reaching. The time taken to reach the SS is also evaluated. By appropriately selecting parameters the dynamic quality of the SMC system can be controlled. Choi et al. [61] suggest the use of a stepwise

time-varying SS, in which the SS is shifted and/or rotated as a function of time. They applied this method to a non-linear spring mass damper system and reported a handsome decrease in time to achieve zero tracking error. However, the resulting controller is cumbersome to implement because the parameters of the SS need to be calculated at different time instants. Bartoszewicz [62] proposed a continuously time-varying SS that gives still faster tracking. The choice of the time varying SS is extended in [63] so as to minimize the integral of the absolute error. However, the parameter selection is dependent on the initial error conditions.

In this chapter a study on the design of constant plus proportional rate reaching law for second order systems is done. Using Lyapunov theory, it is shown that the constant plus proportional rate reaching law imposes a second-order dynamics on the error variables, and thus guarantees a robust performance in the reaching phase also. The selection of controller parameters based on minimizing the reaching time is shown to be inadequate with regard to the time to reach a small output tracking error (OTE). A new method of the selection of the control law parameters based on the criterion of time to a specified OTE is proposed. To illustrate the method, it is applied to a nonlinear spring mass problem taken from Choi et al. [61] and a two-input two link robotic arm trajectory following problem [37]. Simulation results show that, for similar peak levels of control effort, considerably faster tracking performances are obtained for control laws designed using the proposed method.

2.2 The Reaching Law based SMC Design Method

Consider a single input, second order input-affine non-linear system of the form

$$\ddot{x} = f(x, \dot{x}) + g(x, \dot{x})u + d_f \tag{2.1}$$

where u is the control input, and d_f represents the bounded uncertainties and external disturbances, with $|d_f| < D$. Since the uncertainties and/or disturbances which are in the range space of the input are called matched, it is obvious that any uncertainty entering in the scalar system as given above is matched. The arguments of f and g are

dropped from now on for brevity. The uncertainty in the input distribution function g is expressed as $g = \hat{g}(1 + \tilde{g})$, where $\hat{g}$ represents its nominal value, and $\tilde{g}$ is bounded, i.e., $|\tilde{g}| < G < 1.0$.

Defining the state variables as $x_1 = x$ and $x_2 = \dot{x}$, (2.1) can be written in the state space form as

$$\begin{pmatrix} \dot{x}_1 \\ \dot{x}_2 \end{pmatrix} = \begin{pmatrix} x_2 \\ f + gu + d_f \end{pmatrix}. \tag{2.2}$$

Let the trajectory to be followed (desired trajectory) be given as x_{1d} and $x_{2d} = \dot{x}_{1d}$. Then the error between the actual and the desired trajectories can be expressed as $e = x_1 - x_{1d}$ and $\dot{e} = x_2 - x_{2d}$. In vector form,

$$\begin{pmatrix} e \\ \dot{e} \end{pmatrix} = \begin{pmatrix} x_1 - x_{1d} \\ x_2 - x_{2d} \end{pmatrix}. \tag{2.3}$$

Let $y = (e, \dot{e})^{\mathrm{T}}$, where the superscript T denotes the transpose. Taking the time derivative of the above equation and using (2.2) results in the dynamics

$$\dot{y} = \begin{pmatrix} \dot{e} \\ f + gu + d_f - \ddot{x}_{1d} \end{pmatrix}. \tag{2.4}$$

The switching function s for second order systems is conventionally defined as a combination of the errors in (2.3) [21, 37] as

$$s = \dot{e} + \alpha e, \tag{2.5}$$

where, $\alpha > 0$ sets the dynamics in the sliding mode. The SS selected above should be made attractive so that trajectories starting from a non-zero value of s approach the SS, and then stay on $s = 0$ for all future time instants. For this, using $\ddot{e}$ from (2.4), the time derivative $\dot{s}$ is obtained from (2.5) as

$$\begin{aligned} \dot{s} &= \ddot{e} + \alpha\dot{e}, \text{ or} \\ &= f + gu + d_f - \ddot{x}_{1d} + \alpha\dot{e}, \\ &= f + \hat{g}(1 + \tilde{g})u + d_f - \ddot{x}_{1d} + \alpha\dot{e}. \end{aligned} \tag{2.6}$$

The input u remains to be chosen so as to make s go to zero for sliding. The normal procedure for its selection [21] is to express the input u as a sum of two terms. The first term is chosen, using the nominal plant parameters, so as to make $\dot{s} = 0$, when $s = 0$, and is called the equivalent control. The second term is then chosen to tackle the uncertainties in the system. Note that in (2.6) $\hat{g}$ is the nominal g. Thus, the first term of u is chosen to cancel out the known terms in the right hand side of (2.6) and is seen to be $\hat{g}^{-1}(\ddot{x}_{1d} - f - \alpha\dot{e})$. The second term is selected as $\hat{g}^{-1}(-\epsilon s - K\text{sgn}[s])$ to introduce stabilizing terms in the s dynamics (2.6). The complete u thus becomes

$$u = \hat{g}^{-1}(\ddot{x}_{1d} - f - \alpha\dot{e} - \epsilon s - K\text{sgn}[s]), \tag{2.7}$$

where, $\epsilon, K > 0$ are positive real numbers to be selected, and sgn[$\cdot$] is the *signum* function. It is established later on in this section that the above control law actually imposes a constant plus proportional rate reaching law [37]. Note that the u in the above equation may be simplified by using the definition of s in (2.5) and defining a and b as

$$\begin{aligned} a &= \alpha\epsilon, \text{ and} \\ b &= \alpha + \epsilon, \end{aligned} \tag{2.8}$$

both of which are obviously positive real numbers. Thus u becomes

$$u = \hat{g}^{-1}(\ddot{x}_{1d} - f - ae - b\dot{e} - K\ \text{sgn}[s]). \tag{2.9}$$

Using this u in (2.6) and substituting $g = \hat{g}(1 + \tilde{g})$ gives

$$\begin{aligned} \dot{s} &= f + g\hat{g}^{-1}(\ddot{x}_{1d} - f - ae - b\dot{e} - \epsilon s - K\ \text{sgn}[s]) + d_f - \ddot{x}_{1d} + \alpha\dot{e} \\ &= \tilde{g}(\ddot{x}_{1d} - f - ae - b\dot{e}) - (ae + b\dot{e}) - (1 + \tilde{g})K\text{sgn}[s] + d_f + \alpha\dot{e} \\ &= -ae - (b - \alpha)\dot{e} + \tilde{g}(\ddot{x}_{1d} - f - ae - b\dot{e}) - (1 + \tilde{g})K\text{sgn}[s] + d_f. \end{aligned} \tag{2.10}$$

Let

$$R = \ddot{x}_{1d} - f - ae - b\dot{e}. \tag{2.11}$$

Using R as above, a and b as defined in (2.8), and s from (2.5), $\dot{s}$ in (2.6) may be simplified to get

$$\dot{s} = -\epsilon s + \tilde{g}R - (1+\tilde{g})K \text{ sgn}[s] + d_f, \text{ or} \tag{2.12}$$

$$s\dot{s} = -\epsilon s^2 + s(\tilde{g}R + d_f) - (1+\tilde{g})K|s|. \tag{2.13}$$

The scalar K should be chosen so that $\dot{s}$ above satisfies a constant plus proportional rate reaching law [37] as

$$\dot{s} = -\epsilon s - \eta \text{ sgn}[s], \text{ or} \tag{2.14}$$

$$s\dot{s} = -\epsilon s^2 - \eta|s|, \tag{2.15}$$

where, η is a positive real number to be selected later. For $s\dot{s}$ in (2.13) to satisfy the above equation, K should be chosen large enough so that $-(1+\tilde{g})K|s|$ in (2.13) always dominates the $s(\tilde{g}R + d_f)$ and in the worst case, $-(1+\tilde{g})K|s| + s(\tilde{g}R + d_f)$ is at least $-\eta|s|$. Thus K may be selected [21] as

$$K = \frac{G|R| + D + \eta}{1 - G}. \tag{2.16}$$

For this choice of K, it may be easily seen that the $-(1+\tilde{g})K|s| + s(\tilde{g}R + d_f)$ term in (2.13) is always $\leq -\eta|s|$. The term may thus be equivalently written as $-\eta'|s|$ where $\eta' \geq \eta$. The $s\dot{s}$ in (2.13) thus becomes

$$s\dot{s} = -\epsilon s^2 - \eta'|s|, \text{ or} \tag{2.17}$$

$$\dot{s} = -\epsilon s - \eta' \text{sgn}[s]. \tag{2.18}$$

It may be easily established for the s dynamics above that $s = 0$ is the only stable equilibrium point. The control law (2.9) is thus seen to satisfy the above reaching condition, i.e. it makes the $s = 0$ plane an attractive surface. It can be easily shown that the s dynamics as above will have better decay characteristics (See Appendix A) than the reaching law specified in (2.14). Furthermore, estimates of the reaching time i.e. the time to reach the SS ($s = 0$) may be evaluated using (A.7). Note that η' as defined above can be shown to be bounded with a maximum possible value of $\eta_M = \eta + 2K$. The effect of the controller parameters, namely the positive scalars α, ϵ and η are next studied.

2.3 Selection of SMC Parameters

In this section a method of selection of the parameters in u (2.9) is proposed. Using s from (2.5), and $\dot{s} = \ddot{e} + \alpha\dot{e}$ from (2.6), (2.18) may be rewritten as

$$\ddot{e} = -\alpha\epsilon e - (\alpha + \epsilon)\dot{e} - \eta' \text{sgn}[s], \text{ or} \tag{2.19}$$

$$\ddot{e} = -ae - b\dot{e} - \eta' \text{sgn}[\dot{e} + \alpha e], \tag{2.20}$$

with a and b as defined in (2.8).

With this, the y dynamics in (2.4) may be rewritten as

$$\dot{y} = Ay + \bar{q} \tag{2.21}$$

where,

$$A = \begin{bmatrix} 0 & 1 \\ -a & -b \end{bmatrix}, \tag{2.22}$$

and,

$$\bar{q} = \begin{pmatrix} 0 \\ -\eta' \text{sgn}[s] \end{pmatrix}. \tag{2.23}$$

With a and b defined as in (2.8), the A matrix above is seen to have its poles at $-\alpha$ and $-\epsilon$. These poles govern the response of the linear homogeneous part (i.e. the A-dynamics). Conventionally, these are selected to achieve a desired error response and lower reaching times. Also, the choice of α in (2.5) gives the rate of error decay in the SS. Note that K specifies the magnitude of the discontinuity in the control law in (2.9). The value of K in (2.16) is seen to increase with an increase in η. A higher value of η leads to smaller reaching times as discussed in Appendix A and has been shown to give rise to more chattering [37].

Next the effect of the α and ϵ parameters on the tracking performance is studied. This is done using the Lyapunov approach. A candidate Lyapunov function V for the y dynamics as specified in (2.21) is selected as

$$V(y) = y^{\mathrm{T}} P y \tag{2.24}$$

where, P is a positive definite symmetric matrix and is taken as

$$P = \begin{bmatrix} \alpha^2 + \beta & \alpha \\ \alpha & 1 \end{bmatrix}, \tag{2.25}$$

and, $\beta > 0$ guarantees the positive definiteness of the P matrix. The time derivative of $V(y)$ may be obtained as

$$\dot{V} = \dot{y}^{\mathrm{T}} P y + y^{\mathrm{T}} P \dot{y}. \tag{2.26}$$

Using (2.21) in the above equation gives on simplification

$$\dot{V} = y^{\mathrm{T}}[A^{\mathrm{T}} P + P A] y + 2 y^{\mathrm{T}} P \bar{q}. \tag{2.27}$$

Since A in (2.22) is a Hurwitz matrix, it satisfies the Lyapunov equation

$$A^{\mathrm{T}} P + P A = -Q \tag{2.28}$$

where, the Q can be derived from the above equation using A and P as given in (2.22) and (2.25) as

$$Q = \begin{bmatrix} 2\alpha^2\epsilon & 2\alpha\epsilon - \beta \\ 2\alpha\epsilon - \beta & 2\epsilon \end{bmatrix}. \tag{2.29}$$

Note that positive definiteness of Q is guaranteed if

$$\beta < 4\alpha\epsilon. \tag{2.30}$$

From $\bar{q}$ and P as defined in (2.23) and (2.25) respectively, the $y^{\mathrm{T}} P \bar{q}$ is seen to be equal to $-s\eta'\mathrm{sgn}[s]$. Using this and Q as obtained above in (2.29), $\dot{V}$ in (2.27) may be simplified to

$$\begin{aligned} \dot{V} &= -y^{\mathrm{T}} Q y - 2s\eta'\mathrm{sgn}[s], \text{ or} \\ &= -y^{\mathrm{T}} Q y - 2\eta'|s|, \end{aligned} \tag{2.31}$$

which is seen to be always negative definite. Thus, the stability of e dynamics in (2.21) or equivalently in (2.20) is guaranteed. To study the time decay performance of V in the above equation, the following result is required.

Claim 1 *For the second order error dynamics as given in (2.19), a Lyapunov function may be selected as in (2.24). For the Q matrix in (2.29), as obtained from the Lyapunov equation (2.28), there exists a positive real number $\delta > 0$ such that*

$$Q = \delta P + H, \tag{2.32}$$

where H is at least a positive semi-definite matrix.

Proof: It can be easily shown by a constructive proof that for the system under consideration, there is always a range of values that δ can take. The detailed proof is presented in the Appendix B. In particular, it is established that permissible range of values of δ lies in an open set and is given by $\delta \in (0, \min[2\alpha, 2\epsilon])$, where $\min[\cdot, \cdot]$ gives the minimum of its arguments. ■

Using the decomposition of Q as in (2.32), the $\dot{V}$ in (2.31) may be rewritten as

$$\begin{aligned} \dot{V} &= -y^{\mathrm{T}}[\delta P + H]y - 2s\eta' \mathrm{sgn}[s], \text{ or} \\ &= -\delta V - y^{\mathrm{T}} H y - 2\eta' |s|. \end{aligned} \tag{2.33}$$

From the developments in Appendix A, it follows that the V decay response of the above system will be better than the response of the system described by

$$\dot{V} = -\delta V. \tag{2.34}$$

It is interesting to find out the A_b matrix with the dynamics specified as

$$\dot{y} = A_b y, \tag{2.35}$$

that satisfies (2.34). The A_b should thus satisfy the Lyapunov equation (2.28) with the P as selected in (2.25), i.e. $A_b^{\mathrm{T}} P + P A_b = -\delta P$, for some feasible choice of $\delta > 0$ as in (2.34). For this, the general form of the A_b matrix is taken as

$$A_b = \begin{bmatrix} 0 & c' \\ -a' & -b' \end{bmatrix}, \tag{2.36}$$

where, a', b', c' are to be determined. The Lyapunov equation for A_b matrix as given above is solved for these unknowns for a general value of δ. These may be easily obtained by the solution of a set of simultaneous linear equations in a', b', c' as

$$\begin{aligned} a' &= \frac{\delta(\alpha^2+\beta)}{2\alpha} \\ b' &= \delta \\ c' &= \frac{\delta}{2\alpha}. \end{aligned} \tag{2.37}$$

It is known that (see Appendix B) δ can take values as large as 2ϵ or 2α, in the limit as $\beta \to 0$, depending on whichever is smaller. Using (2.37), the A_b matrix for $\delta = 2\alpha$ may be obtained as

$$A_b = \begin{bmatrix} 0 & 1 \\ -(\alpha^2+\beta) & -2\alpha \end{bmatrix}, \tag{2.38}$$

and is seen to have both of its poles at $-\alpha$, for $\beta = 0$. Similarly, for $\delta = 2\epsilon$, the A_b matrix becomes

$$A_b = \begin{bmatrix} 0 & \epsilon/\alpha \\ -(\epsilon\alpha + \epsilon\beta/\alpha) & -2\epsilon \end{bmatrix}, \tag{2.39}$$

and for $\beta = 0$, both the poles of the above A_b matrix are easily seen to lie at $-\epsilon$. It follows from Appendix A that the decay of the Lyapunov function (2.24) as obtained in (2.33), i.e. for the dynamics in (2.21) with the A matrix in (2.22) having its poles as $-\alpha$ and $-\epsilon$, is guaranteed to be better than the decay response in (2.34), which is achievable by a A_b matrix as selected in (2.38) or (2.39) which has both of its poles at $-\min[\alpha, \epsilon]$. This implies that the error dynamics in (2.21) in the reaching phase is bounded by the response of the second order A_b dynamics in (2.35) and a robust performance in the presence of the matched uncertainties and disturbances is achievable even before the onset of sliding. Estimates of the guaranteed times to reach the OTE may be obtained using the A_b dynamics. It is obvious that shorter times to the OTE are expected as both α and ϵ are increased. However, the control law in (2.9) will also require larger control magnitudes as a and b will also increase as can be seen from (2.8). Next the effect of the relative values of these parameters is considered.

2.3.1 The Relative Choice of α and ϵ

Let the poles of the A matrix in (2.22) be selected as $-p$ and $-q$, where p and q are positive real numbers satisfying $p > q$ This could be achieved in the following two ways:

- Case CP: $\alpha = p$ and $\epsilon = q$. This would result in the SS being $\dot{e} + pe$, say S_p.
- Case CQ: $\alpha = q$ and $\epsilon = p$, with which the SS becomes $\dot{e} + qe$, say S_q.

It follows from (2.8) that $a = pq$ and $b = p + q$ remain the same in both the cases resulting in the same A matrix in (2.22). With a and b being the same, R in (2.11) and thus K (2.16) are expected to have comparable magnitudes for both the cases. Thus the peak values of the control effort u in (2.9) should also be nearly equal. The performance obtained in the two cases is compared next. For this, a common Lyapunov function is first constructed as follows.

Claim 2 *Let P and Q be symmetric positive definite matrices as specified in (2.25) and (2.29) respectively, for the Case CP, i.e. $\alpha = p$ and $\epsilon = q$. Then, there exists a sufficiently large positive scalar M such that*

$$V(y) = y^{\mathrm{T}} P y + M|S_p| + M|S_q| \tag{2.40}$$

where, $y = (e, \dot{e})^{\mathrm{T}}$, is a valid common Lyapunov function for Cases CP and CQ.

Proof: For V to be a Lyapunov function, at least negative semi-definiteness (n.s.d.) of its time derivative must be established for the two cases. Detailed derivations are given in the Appendix C. Let $\dot{V}_i$, $i = p, q$ represent the time derivative $\dot{V}$ of the Lyapunov function in (2.40) for the cases denoted by the subscript 'i'. The $\dot{V}_p$ has been derived in (C.6) - (C.9) for the Case CP and $\dot{V}_q$ in (C.12) - (C.17) for the Case CQ respectively. The negative definiteness of the time derivatives in the two cases is shown for a choice of M as in (C.19). ■

The discussion in the Appendix C shows that (C.6) - (C.9) giving $\dot{V}_p$ for the Case CP may be combined to give the time derivative as in (C.10). Similarly (C.20) gives

$\dot{V}_q$ for the Case CQ. Further, for the Case CQ, it is shown in the Appendix C that there exists a $0 < \delta_q < q$ ($< p$ by selection), using which $\dot{V}_q$ in (C.20) may be rewritten as

$$\dot{V}_q \leq -y^{\mathrm{T}}Qy - \delta_q M[|S_q| + |S_p|] - (p - \delta_q)M|S_q|. \tag{2.41}$$

From Claim 1, it is known that the Q matrix may be decomposed as given in (2.32) as $Q = \delta_q P + H_q$, where H_q is a positive definite matrix, since $\delta_q < q < \min[2q, 2p]$. Using this decomposition, the $\dot{V}_q$ above may be expressed as

$$\begin{aligned} \dot{V}_q &\leq -\delta_q y^{\mathrm{T}}Py - y^{\mathrm{T}}H_q y - \delta_q M[|S_q| + |S_p|] - (p - \delta_q)M|S_q|, \text{ or} \\ &\leq -\delta_q V_q - (p - \delta_q)M|S_q|, \end{aligned} \tag{2.42}$$

using the definition of V in (2.40) where the subscript 'q' represents the Case CQ. As $p > q > \delta_q$, the $(p - \delta_q)M|S_q|$ term in the above equation is always non-negative, and thus the results of Appendix A imply that the V_q decay response of this system will be better than the exponential decay response offered by

$$\dot{V}_q = -\delta_q V_q, \text{ where } \delta_q \in (0, q). \tag{2.43}$$

Note that δ_q can assume a maximum value of $\bar{\delta}_q = q$ in the limit.

For the Case CP, the $\dot{V}_p$ is seen from (C.10) to be given as

$$\dot{V}_p \leq -y^T Qy - M[q|S_p| + p|S_q|] - 2\eta'|S_p|. \tag{2.44}$$

The Q matrix in this case is decomposed as $\delta_p P + H_p$, where $0 < \delta_p < 2q = \min[2q, 2p]$ has to be found out. Following the steps as for the Case CQ, the $\dot{V}_p$ above may be rewritten as

$$\begin{aligned} \dot{V}_p &\leq -\delta_p V_p - y^{\mathrm{T}}H_p y - (p - \delta_p)M|S_q| - (q - \delta_p)M|S_p| - 2\eta'|S_p|, \text{ or} \\ &\leq -\delta_p V_p - y^{\mathrm{T}}H_p y - (p - \delta_p)M|S_q| - (q - \delta_p + \frac{2\eta'}{M})M|S_p|. \end{aligned} \tag{2.45}$$

Thus, it is seen that if $\delta_p < \min[p, q + \frac{2\eta'}{M}]$, then the $(p-\delta_p)M|S_q| + (q-\delta_p+\frac{2\eta'}{M})M|S_p|$ term in the above equation is always guaranteed to be non-negative. As discussed in

the Appendix C, the condition on M for V_p to be a Lyapunov function is $M \geq 0$. For $M \to 0$, the $2\eta'/M$ term will increase, However, since the decomposition in (2.32) is possible only for $\delta_p < 2q = \min[2q, 2p]$, the δ_p may be selected to be smaller than $\min[p, 2q]$. It thus follows that the V_p decay response of the above system will be better than the response of the system given by

$$\dot{V}_p = -\delta_p V_p, \text{ where } \delta_p \in (0, \min[p, 2q]). \tag{2.46}$$

Thus the upper limiting value of δ_p is seen to be given by $\bar{\delta}_p = \min[p, 2q]$. Thus it is obvious that $\bar{\delta}_p > \bar{\delta}_q$.

With the guaranteed decay responses of V_q and V_p being given as in (2.43) and (2.46) respectively, it is clear that Case CP guarantees a faster exponential decay of the Lyapunov function (2.40) as compared to the Case CQ. These guaranteed decay performances may be used to develop an estimate of the time to reach a specified level of OTE in terms of the Lyapunov function. Thus, given an initial value $V(0)$ at $t = 0$, the time t_f required for V_i, i $=q, p$ dynamics, in (2.43) and (2.46) respectively, to decay to a final value of V_f may be evaluated as

$$t_f = \frac{1}{\bar{\delta}_i} \ln \left[\frac{V(0)}{V_f} \right], \tag{2.47}$$

where, i $=q, p$, and $\bar{\delta}_i$ are as defined earlier and represent the maximum limiting value of δ_i for the δ_q and δ_p as given in (2.43) and (2.46) respectively. For the same $V(0)/V_f$, it is obvious that t_f in the Case CP will be smaller than in the Case CQ, as the right hand side of the above equation will be smaller because of the fact that $\bar{\delta}_p > \bar{\delta}_q$. The t_f in (2.47) gives conservative estimates for the decay of the Lyapunov function. The actual times t_{OTE} required, for the V decay responses in (2.42) and (2.45) for the Cases CQ and CP respectively, to reach the V_f are expected (see Appendix A) to be smaller than the t_f, i.e. $t_{OTE} \leq t_f$. Thus the α and ϵ parameters should be selected as in the Case CP to have a smaller value of t_f, i.e. for a given choice of the poles of the A matrix in (2.22), ϵ should be selected as the magnitude of the dominant pole, and α as the magnitude of the other, or simply $\alpha > \epsilon$. This is summarized as follows.

Lemma 1 *The choice of α and ϵ parameters, for the constant plus proportional rate reaching SMC law as in (2.9), with a and b selected as in (2.8) and the sliding surface as in (2.5), such that*

$$\alpha > \epsilon. \tag{2.48}$$

guarantees a faster decay of the Lyapunov function (2.40).

Note that the above lemma indicates that the choice of α and ϵ as in (2.48) only ensures that t_f will be smaller. It however does not guarantee that the t_{OTE} for the Case CP will be smaller than the Case CQ, although it is so expected and can actually be seen from the simulation results presented in the next section. There may however be parameter combinations where this would not hold.

A smaller value of V implies a smaller tracking error in the sense of the norm (as defined by the Lyapunov function). Thus, since the Case CP has a faster guaranteed decay performance, it is expected to take lesser times as compared to the Case CQ to reach an acceptably small OTE. As discussed earlier, the control effort is expected to be almost the same for both the CP and CQ cases. Note that, lower reaching times correspond to the case of $\epsilon > \alpha$ (Case CQ) as can be seen from the results in the next section. However, the above theoretical developments show that shorter times to a desired OTE are expected for the cases where $\alpha > \epsilon$ (Case CP). The estimates of the time to the OTE using (2.47) showing the effect of the relative choices of α and ϵ as suggested in Lemma 1 are verified by applying the design method to two mechanical systems. The systems and the obtained simulation results are presented next.

2.4 Simulation Results

For the illustration of the proposed SMC design method, the results presented in the previous section have been used to design controllers for two practical problems. The numerical results of these examples ascertain the validity of Lemma 1.

2.4.1 Nonlinear Spring Mass Damper System

The first example concerns a non-linear mass-spring-damper system from Choi et. al. [61]. The governing differential equation is

$$m\ddot{x} + \nu(\dot{x}, t) + \mu(x, t) = u(t) + d(t), \tag{2.49}$$

where, $x, \dot{x}$ represent the position and the velocity of the mass m, $u(.)$ represents the applied input force, and $d(.)$ the disturbance signal. $\nu(.,.)$ and $\mu(.,.)$ represent the damping and spring force term respectively. The system parameters and functions are given to be $m = 1$, $f = f_1 + f_2 + f_3 + f_4$, which are given as $f_1 = \mu_0 x$, $f_2 = -\mu_1 x^3$, $f_3 = -\nu_0 \dot{x}$, and $f_4 = -\nu_1 \dot{x}|\dot{x}|$ with $\mu_0 = 0.5$, $\mu_1 = 0.5$, $\nu_0 = 0.3$, and $\nu_1 = 0.3$. The system also has uncertainties expressed as $a_1 f_1 + a_2 f_2 + a_3 f_3 + a_4 f_4$ with $a_1 = -.05 + 0.25\sin(5\pi t)$, $a_2 = -.05 + 0.25\sin(5\pi t)$, $a_3 = -.05 + 0.15\sin(7\pi t)$, and $a_4 = -\ 05 + 0.15\sin(7\pi t)$ and disturbance $d = 0.05 + 0.25\cos(3\pi t)$. The signal to be tracked is given by $x_{1d} = -0.5\cos(\pi t/5)$. The above system in (2.49) may be expressed in standard form as in (2.1). The initial conditions are taken as 0.5 and 0 for the two states respectively.

Simulation was done using the fourth order Runge-Kutta method with a time step of 2.5ms. The remaining parameters were selected as $\beta = 1$ and $\eta = 1$. Several combinations of α and ϵ were used.

- **Case 1:** $\alpha = 2$ and $\epsilon = 6$
- **Case 2:** $\alpha = 6$ and $\epsilon = 2$
- **Case 3:** $\alpha = 3$ and $\epsilon = 4$
- **Case 4:** $\alpha = 4$ and $\epsilon = 3$
- **Case 5:** $\alpha = 4$ and $\epsilon = 5$
- **Case 6:** $\alpha = 5$ and $\epsilon = 4$

Table 2.1: Comparison of time for OTE and Reaching: Example 1.

Case no.	α	ϵ	Time to OTE ($< 1 \times 10^{-3}$) in (s)		Reaching time (s) (A.7)	t_f (s) (2.47) for $\frac{V_0}{V_f} = 10^4$
			Bound obtained from A_b dynamics (2.35)	Actual		
1	2	6	4.24	3.30	0.183	4.605
2	6	2	4.24	2.00	1.472	2.302
3	3	4	2.83	2.35	0.426	3.070
4	4	3	2.83	2.00	0.732	2.302
5	4	5	2.13	1.80	0.439	2.302
6	5	4	2.13	1.65	0.650	1.842

The time to OTE (defined as the time after which the error is less than 1.0×10^{-3}) obtained for the bounding A_b dynamics in (2.35), the actual tracking times, the reaching times calculated from (A.7) and the t_f for $V_0/V_f = 1.0 \times 10^4$ as evaluated from (2.47) for all the cases are presented in Table 2.1. It can be seen from the table that the actual time to achieve the OTE is appreciably smaller for Case 2 as compared with Case 1. The Table 2.1 also shows that similar results are obtained for Cases 4 and 6. In all these cases $\alpha > \epsilon$, thus verifying Lemma 1. It is noticed from Table 2.1 that, for all of these cases, the reaching time is greater than the corresponding Cases 1, 3 and 5. Although Cases 1,3 and 5 have smaller reaching times, they require about 65%, 17.5%, and 9.1% more time to the OTE than the time required by the Cases 2,4, and 6 respectively. Thus, from the table it is clearly evident that parameter selections giving lower reaching times actually take longer times to reach the specified OTE. Moreover, the time bounds t_f calculated from (2.47) are seen to be better than those obtained from the A_b dynamics (2.35) in the sense of being able to bring out the effect of the relative values of α and ϵ.

Choi et al. [61] reported a time of 2.58 seconds to achieve a zero tracking error (OTE). It can be observed from Table 2.1 that in almost all the cases under consid-

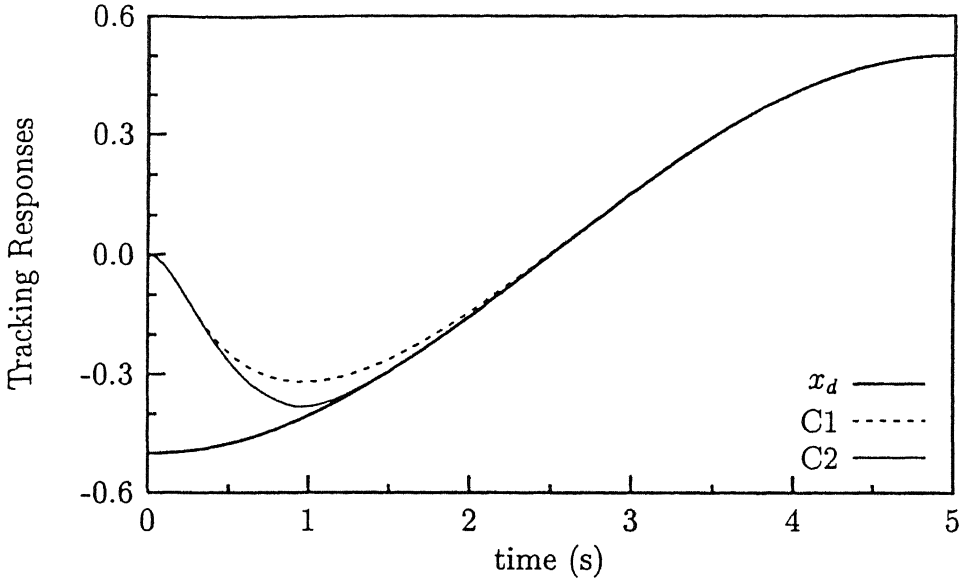

Fig. 2.1: Tracking responses for Case 1 ('C1') and Case 2 ('C2').

eration, a lesser tracking time is achieved by this approach. In fact the best tracking time achieved is 1.65 seconds for Case 6. In all of the cases the actual time to reach OTE is smaller than the bound given by the A_b dynamics and the t_f. As qualitatively similar responses were obtained, the responses obtained for the parameter combination in Cases 1 and 2 are presented in Figs. 2.1, 2.2, and 2.3 respectively. The responses are indexed by the case numbers in these figures. Note that Case 1 corresponds to Case CQ, and Case 2 to Case CP. Fig. 2.1 shows the tracking response obtained in the two cases. It is evident from the figure that the 'C2' (satisfying the Lemma 1) trajectory approaches the OTE in appreciably lower time as compared to the 'C1' trajectory. Fig. 2.2 shows the s response in the two cases. The 'C1' response has a lower reaching time (see also Table 2.1) as compared to 'C2'. Fig. 2.3 shows the error decay with time for both the cases and also for the solution of the A_b dynamics in (2.35), labeled as e_A. Although, only a better decay of the Lyapunov function in (2.24) is guaranteed for the control law in (2.9), the figure shows that the decay of e obtained in the two cases are better than the solution of the A_b dynamics in (2.35).

The required control effort in the two cases are shown in Fig. 2.4. As discussed in

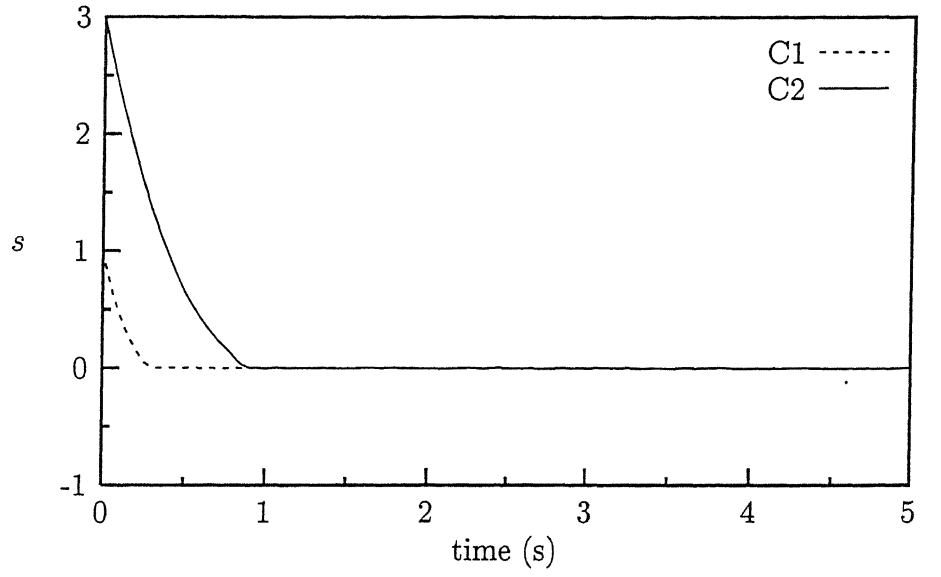

Fig. 2.2: The s responses for Cases 1 and 2.

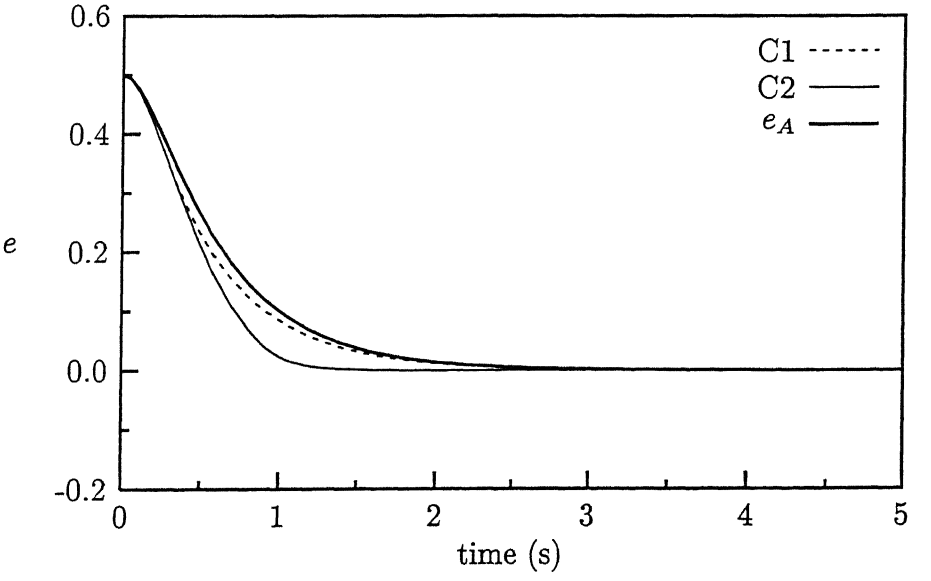

Fig. 2.3: The error dynamics for Cases 1 and 2 and that given by the A-dynamics (e_A).

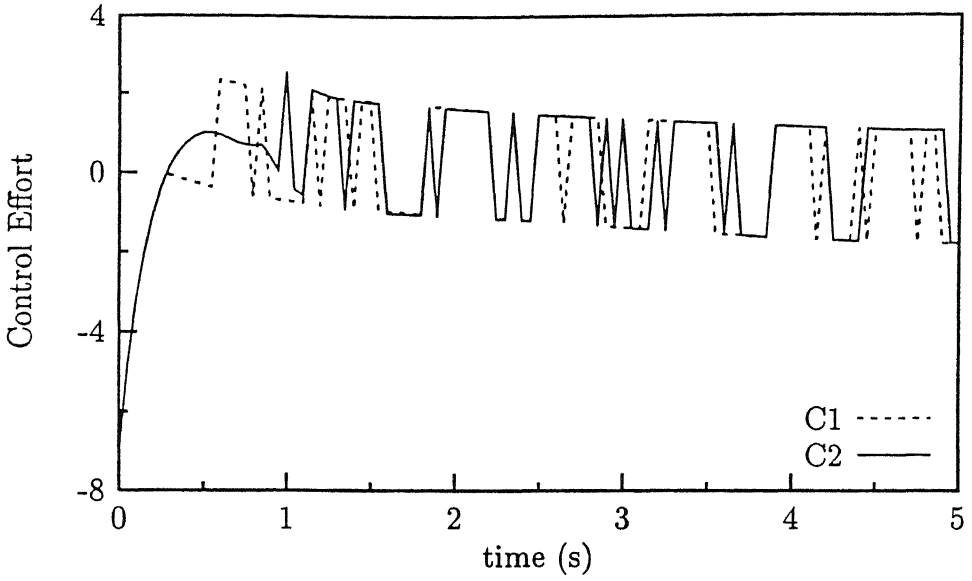

Fig. 2.4: The control effort u required for Cases 1 and 2.

the previous section, since $a = 12$ and $b = 8$ from (2.8) are same for the cases 'C1' and 'C2', thus the control efforts in these cases should be of about the same magnitudes This can indeed be seen from Fig. 2.4, thus it verifies that that the proposed method uses about the same control effort to achieve the same tracking accuracy much faster. However as the reaching time in 'C1' is smaller, the input in Case 'C1' begins chattering earlier as can be seen from the figure. Thus the selection of the parameters can be easily done drawing on the experience of the initial condition responses of linear second order systems. If the α and ϵ are chosen so as to satisfy Lemma 1, better results are expected.

2.4.2 Two-link Robotic Arm

The design method given in Section 2.3 is extended to multi-input case consisting of the two-link robot arm problem [37]. The equations governing the dynamics are given as

$$H(q)\ddot{q} + C(q,\dot{q})\dot{q} = \tau + d \tag{2.50}$$

where, $q = (\theta_1, \theta_2)^{\mathrm{T}}$ gives the angles of the two links in radians. $H(q)$ is the positive definite inertia matrix. The vector $\tau = (\tau_1, \tau_2)^{\mathrm{T}}$ is the control torque vector, and

$d = (d_1, d_2)^{\mathrm{T}}$ represents the disturbance vector with bounds on their magnitude given as $|d_1| < D_1$, and $|d_2| < D_2$. The expressions for all the functions in the above equation are taken from [21]. The above equation can be rewritten as

$$\ddot{q} = H^{-1}(q)[\tau + d - C(q, \dot{q})\dot{q}]. \tag{2.51}$$

The trajectory to be followed is given as $q_d = (\theta_{1d}, \theta_{2d})$, and its time derivatives. The error vector is defined as before.

$$\begin{pmatrix} e_1 \\ \dot{e}_1 \\ e_2 \\ \dot{e}_2 \end{pmatrix} = \begin{pmatrix} \theta_1 - \theta_{1d} \\ \dot{\theta}_1 - \dot{\theta}_{1d} \\ \theta_2 - \theta_{2d} \\ \dot{\theta}_2 - \dot{\theta}_{2d} \end{pmatrix}. \tag{2.52}$$

Following the developments in Section 2.2, the input torques are selected as

$$\begin{pmatrix} \tau_1 \\ \tau_2 \end{pmatrix} = H(q) \begin{pmatrix} \ddot{\theta}_{1d} - a_1 e_1 - b_1 \dot{e}_1 - \bar{D}_1 \mathrm{sgn}[s_1] \\ \ddot{\theta}_{2d} - a_2 e_2 - b_2 \dot{e}_2 - \bar{D}_2 \mathrm{sgn}[s_2] \end{pmatrix} + C(q, \dot{q})\dot{q}. \tag{2.53}$$

where, the quantities $a_1, b_1, a_2, b_2 > 0$ are selected by appropriate choices of α_1, α_2 and ϵ_1, ϵ_2. Also $\bar{D}_1 = D_1 + \eta_1$, and $\bar{D}_2 = D_2 + \eta_2$. Under the application of the control law the system decouples into two single input systems. It is easily seen that the above control law satisfies the following constant plus proportional rate reaching law

$$\begin{aligned} \dot{s}_1 &\leq -\epsilon_1 s_1 - \eta_1 \mathrm{sgn}[s_1], \text{ and} \\ \dot{s}_2 &\leq -\epsilon_2 s_2 - \eta_2 \mathrm{sgn}[s_2]. \end{aligned} \tag{2.54}$$

Then the choice of the parameters can be done based on the discussion in Section 2.3.

Simulation was done as in the previous example, but with a time step of 500μs. The parameters of the robot, the disturbance signals, and the controller parameters are taken from [37] in which the SMC parameters were taken as $\alpha = 1$, and $\epsilon = 15$ (Case *CQ* of Section 2.3). The Lemma 1 indicates that the choice of the two parameters should be the other way round. β and η were selected as in the earlier example. The Table 2.2 presents the various time bounds and the actual tracking times for four parameter combinations.

Table 2.2: Comparison of time for OTE and Reaching: Example 2. (L1) and (L2) denote responses for the Links 1 and 2 respectively.

Case no.	α	ϵ	Time to OTE ($< 1 \times 10^{-3}$) in (s)		Reaching time (s) (A.7)	t_f (s) (2.47) for $\frac{V_0}{V_f} = 10^4$
			Bound obtained from A_b dynamics (2.35)	Actual		
1	2	6	4.24	3.128 (L1) 2.890 (L2)	0.183	4.605
2	6	2	4.24	1.095 (L1) 0.910 (L2)	1.472	2.302
3	1	15	2.83	5.683 (L1) 5.475 (L2)	0.027	9.210
4	15	1	2.83	0.563 (L1) 0.423 (L2)	4.732	4.605

It is seen from the table that the Cases 1 and 3, corresponding to the Case CQ, have very small reaching times as compared to the Cases 2 and 4 which correspond to the Case CP. Although the Case CP exhibits a much larger reaching time, it is expected from Lemma 1 and the results in the previous section that it should exhibit a faster tracking performance as compared to the Case CQ. The times to OTE for the Case CP is indeed seen to be substantially smaller than the corresponding Case CQ.

Since the qualitative nature of the responses in the Cases 2 and 4 are similar, as was also observed for the the other two cases, the error responses obtained only for the Cases 3 (labeled as $C3$) and 4 (labeled $C4$) for the first link is presented in Fig. 2.5, and that for the second link in Fig. 2.6. As is indicated by the very small reaching time for the Case CQ, it was observed from the numerical simulation results that in Case CQ, sliding begins almost instantaneously as compared to the Case CP. However, from the CQ response in the figures, the time to OTE is seen to be about 5.5s as compared to about 0.5s for the Case CP. This again shows that substantially better performances are achievable by satisfying Lemma 1. It also substantiates the view that

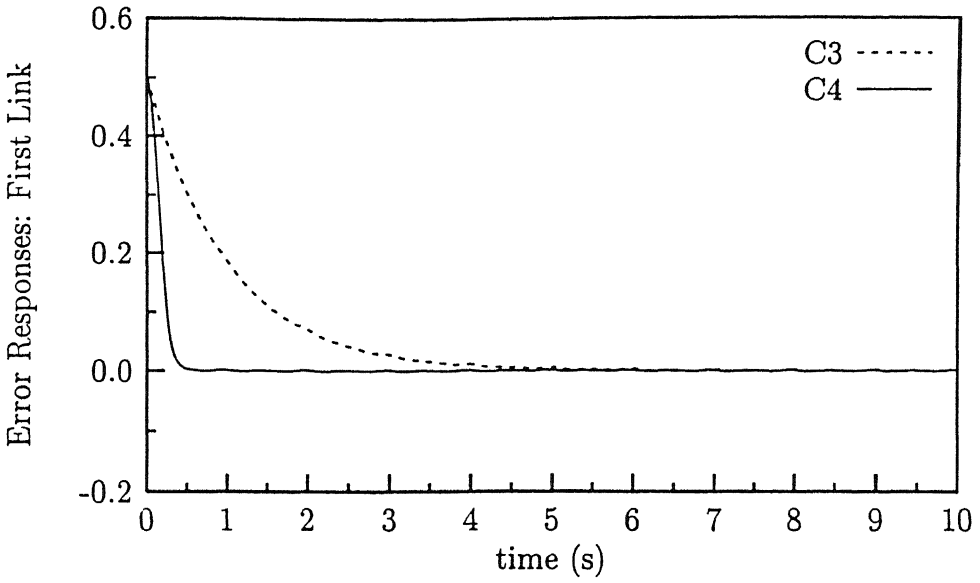

Fig. 2.5: Error responses for the first link for Cases C3 (CQ) and C4 (CP).

a lower reaching time does not imply faster tracking. Thus, it may be concluded that the time to OTE should be used as the criterion to select the controller parameters rather than the reaching time.

The required control efforts τ_1 and τ_2 (2.53) for parameter combinations in Cases 3 and 4 are presented in Figs. 2.7 and 2.8 respectively. It is observed that required torque levels for both cases are similar.

2.5 Conclusions

In this chapter the design of the constant plus proportional rate reaching SMC for second order nonlinear systems has been studied. An investigation of the effect of the choice of the controller parameters has been done. Using a Lyapunov approach it has been shown that the design method imposes a bounding second order dynamics on the error variables, and thus a robust performance in the reaching phase is guaranteed. A new method of selection of the SMC parameters which results in smaller times to reach a given level of OTE, while using almost similar levels of maximum control effort, is proposed. It is seen that for the class of systems under study, a small reaching time does

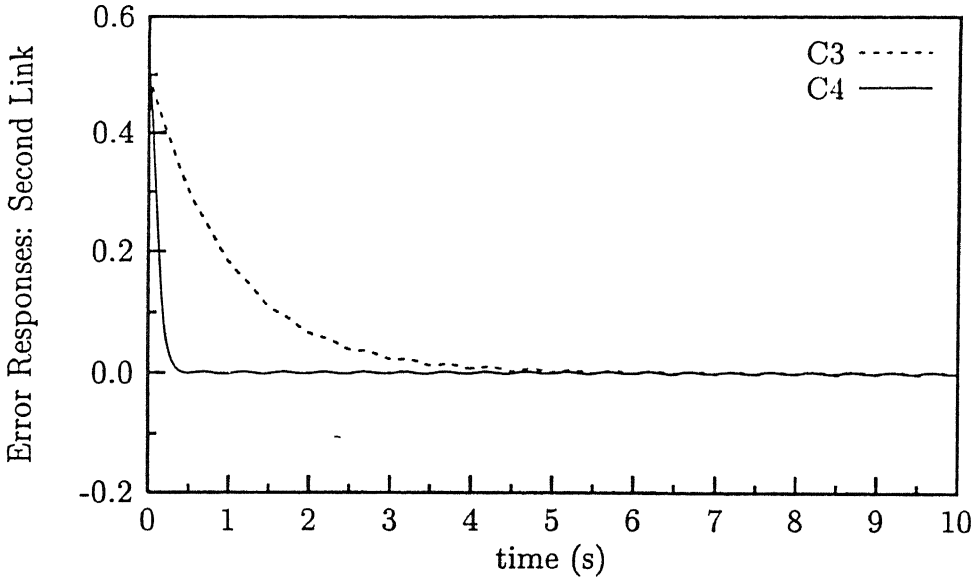

Fig. 2.6: Error responses for the second link for Cases C3 (CQ) and C4 (CP).

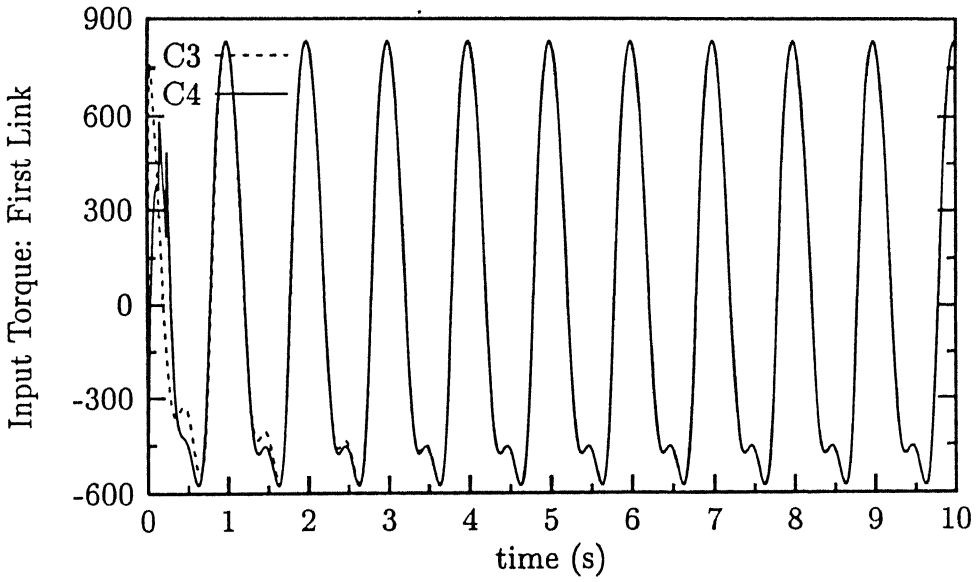

Fig. 2.7: The input torque τ_1.

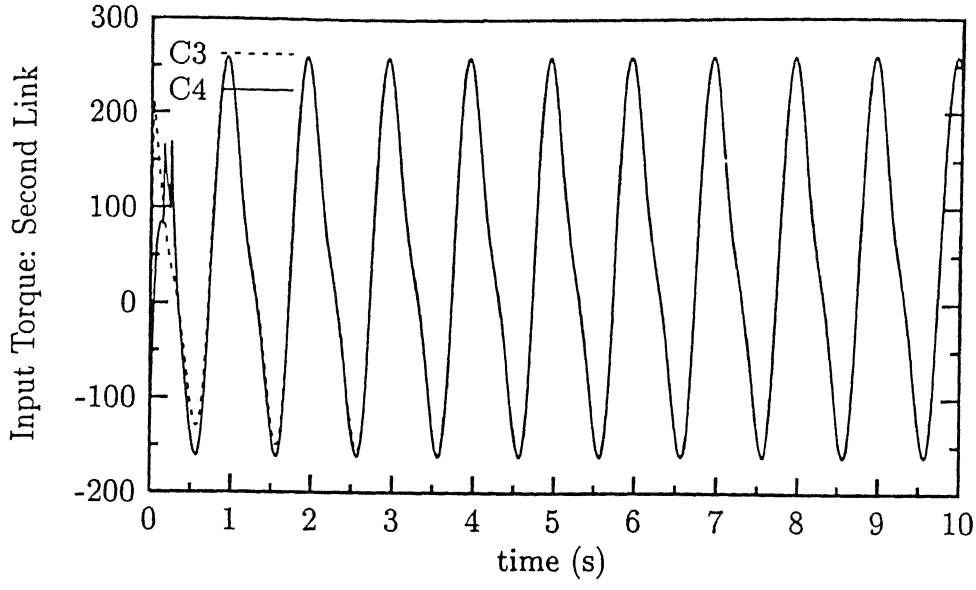

Fig. 2.8: The input torque τ_2.

not guarantee a fast tracking response. The method of parameter selection should thus be based on the time to OTE, rather than on the criterion of the reaching time. The design technique has been applied to a nonlinear spring-mass-damper system under matched uncertainties and exogenous disturbances. From the simulations done it is seen that the control laws based on the lower reaching times require approximately $10 - 60\%$ more time as compared to the proposed control laws to reach the same level of OTE, while using the same levels of control magnitudes. The method developed for a single input system has been extended to a two input two link robotic arm problem. Results of numerical simulation for the parameters used show that significantly faster tracking is obtained with the proposed control law, thus establishing the utility of the method. However, more work is required to develop better estimates of the time to OTE.

Chapter 3

SMC for the Longitudinal Dynamics of a Fighter Aircraft

3.1 Introduction

The aircraft flight control system (FCS) forms the backbone of the current generation fighter aircrafts. This chapter discusses the application of the SMC method for the design of FCS for fighter aircrafts. The aircraft is conventionally modelled as a 6 degree of freedom (dof) rigid body [10]. As discussed in Chapter 1, the nonlinear inverse dynamics based flight control design has been applied in many works [17, 23, 24, 27–29, 39] to various aircrafts for varying purposes. However, the issue of robustness of the feedback linearization techniques to disturbances and uncertainties still needs to be addressed. The SMC, with its robustness properties, offers an alternative method for this problem. However, it has not been readily used for the FCS design problem as is evident from the lack of a single application paper in the the special issue of the *International Journal of Control* (Vol. 59 no.1, 1994) on aircraft flight control design [17, 39].

The SMC method has earlier been used for FCS design problem by some researchers. Calise and Kramer [40] applied the SMC design method to the linearized dynamics of the AV-8A Harrier in a hover mode under matched uncertainties and compared the obtained responses with those obtained using a LQ based design. They observed that the SMC method outperformed the linear controller in the presence of disturbances

and uncertainties. Mudge and Patton [64] designed SMC laws with eigenstructure assignment for a remotely piloted vehicle and provide frameworks for assessment of robustness. Singh [41] defined a switching function which included the integral of the tracking error also and led to improved closed loop performance. Control laws for large rapid rotational maneuvers of aircraft under the perturbational model for aerodynamics and matched uncertainty are developed. Hedrick and Gopalswamy [42] show that the undesirable zero-dynamics could be tackled by output redefinition. They designed control laws for the nonlinear pitch axis system dynamics with linearized aerodynamics under matched uncertainty. The HQ criteria were incorporated into the design procedure. They also developed a method of selection of sliding gains for a MIMO system. Thukral and Innocenti [43] designed SMC laws for a linearized model of the longitudinal dynamics for the stabilization and tracking problems. They also presented a review of related work.

In this chapter, the longitudinal or the pitch axis control problem for the nonlinear aircraft dynamics has been studied. The aircraft longitudinal dynamics and the force control approach (FCA) are explained briefly in the next section. In addition to the uncertainties and disturbances generally considered, an error between the command force vector and the actually obtained force vector is taken into consideration. A model following (MF) structure is next described and is used to design a full envelope SMC law taking these uncertainties into account. Analytic control laws for the tracking and the trimming modes of the aircraft are developed and simulations are done using the inertia parameters of the F-16 aircraft to show the effectiveness of the MF-SMC (model following-SMC) approach.

3.2 Longitudinal Dynamics and Force Control Approach

The aircraft longitudinal dynamics in the body fixed frame is defined by the set of ordinary nonlinear differential equations [10] as given in (3.1).

$$\begin{pmatrix} \dot{U} \\ \dot{W} \\ \dot{Q} \\ \dot{\theta} \\ \dot{p}_x \\ \dot{p}_z \end{pmatrix} = \begin{pmatrix} -QW - g_0 \sin(\theta) \\ QU + g_0 \cos(\theta) \\ 0 \\ Q \\ U\cos(\theta) + W\sin(\theta) \\ U\sin(\theta) - W\cos(\theta) \end{pmatrix} + \begin{pmatrix} R_m F_x \\ R_m F_z \\ c_7 M \\ 0 \\ 0 \\ 0 \end{pmatrix} \tag{3.1}$$

The system states are U, W, the velocities along the body X and Z axes respectively, the pitch rate Q, the pitch angle θ, and p_x, p_z the positions along X and Z axes respectively from an earth frame of reference. F_x, F_z represent the forces along the X and Z directions respectively; and M is the pitching moment. Also g_0 denotes earth's gravity, R_m denotes the inverse of the mass of the aircraft, and c_7 is the inverse of inertia of the aircraft about its pitching axis.

The forces and the moments in (3.1) are in general nonlinear functions of the state and the deflections of the CFC (conventional flight control) surfaces i.e., the elevator and the throttle [10]. However, the SMC design technique has mainly been developed for systems that are input affine. Most of the FCS applications cited earlier are based on input affine or linearized models of the aircraft. Bartolini and Zolezzi [65] extended the SMC method to include the case of systems nonlinear in the input by redefining the equivalent control, based on the existence of a particular map. This approach has been used in this work through the FCA, which is discussed next.

If the forces F_x, F_z, and the pitching moment M can be independently varied, these may be treated as the pseudo input vector, and would render the governing system of equations in (3.1) input affine. Independent control of the 3-component force vector with the two CFC inputs is however not possible, and therefore, it becomes necessary to use additional control effectors. Smith and Meyer [23] treated the desired accelerations as pseudo-inputs. Hauser et al. [66] assumed that there exists a *one-to-one* mapping from the input space to the force vector. Snell et.al. [49] used TV (thrust vectoring) to augment the standard control surfaces. Franklin [39] used the forces as input for the translational longitudinal control problem. The TV concept is gaining increasing

popularity and in fact is going to be present in almost all of the next generation fighters [6, 8]. It has the advantage that its effectiveness does not vary much with the aircraft speed as opposed to the conventional aerodynamic surfaces. Hence, it may be used to advantage when the CFC surfaces are ineffective or are damaged in combat [46]. The TV-FCS has been flight tested on scaled aircraft models and is already equipping the front line USAF F-15,F-16, and YF-22 fighters [7], the X-31 experimental aircraft [45], and the Russian Sukhoi family of fighters [9]. With TV capability, the forces F_x, F_z and the pitching moment M, with the assumption that the thrust acts through the center of gravity, are given [46] as

$$\begin{aligned} F_x &= \bar{q}S\left[C_x(\alpha,\delta_{el}) + \frac{\bar{c}Q}{2V_t}C_{x_Q}(\alpha)\right] + T_x, \\ F_z &= \bar{q}S\left[C_z(\alpha,\delta_{el}) + \frac{\bar{c}Q}{2V_t}C_{z_Q}(\alpha)\right] + T_z, \text{ and} \\ M &= \bar{q}S\bar{c}\left[C_m(\alpha,\delta_{el}) + \frac{\bar{c}Q}{2V_t}C_{m_Q}(\alpha) + C_{m_{TV}}\delta_v\right], \end{aligned} \tag{3.2}$$

where, $\bar{q}$, S, α, δ_{el}, $\bar{c}$, V_t represent the dynamic pressure, the wing surface area, the angle of attack, the elevator deflection, the mean aerodynamic chord, and the total velocity. Also the δ_v represents the effective pitch thrust-vectoring angle. The various $C_i(\cdot,\cdot)$ give the functional relations of the i^{th} component of the non-dimensional force with its arguments (Refer [10] for further details). Also T_x and T_z are the components of the thrust vector in the directions specified by their subscripts, and are given as $T_x = \eta T_a \cos(\delta_v)$ and $T_z = \eta T_a \sin(\delta_v)$, where η is a dimensionless nozzle thrust coefficient, and T_a is the actual thrust of the engine [46]. Thus the force vector is seen to be a function of three variables δ_{el}, the T_a and the vectoring angle δ_v. Other more conventional alternatives, such as the air brakes, spoilers, flaps etc. may also be used. Thus using a suitable combination of the available effectors, it should be possible to control the 3-component force vector. Durham [48] considers the control allocation problem to generate a set of desired accelerations. In case, many solutions exist, a suitable combination of these alternatives may be used to perform other control configured vehicle (CCV) functions. For this work, it is assumed that the aircraft has sufficient number of control effectors so that the 3-component force vector may be used as pseudo-input.

With this, the governing equation (3 1) becomes input affine and can be seen to depend on parameters such as R_m and c_7 Depending on the mission objectives of the aircraft project, a fair estimate of these parameters can be made using data from other aircrafts of a similar category It is better to define these parameters as a range of values they are likely to take This would have to be taken as such even if the aircraft parameters were known, because fuel and armaments carried on-board vary with time and also from mission to mission These have been incorporated as time varying but bounded multiplicative uncertainties as

$$\begin{aligned} R_m &= (1+\delta_{b1})\hat{R}_m, \text{ and} \\ c_7 &= (1+\delta_{b2})\hat{c}_7 \end{aligned} \tag{3 3}$$

where $\hat{R}_m$ and $\hat{c}_7$ represent the nominal values of R_m and c_7 respectively The time varying multiplicative uncertainties represented by δ_{b1} and δ_{b2} are bounded as $|\delta_{b1}| \leq D_{b1}$, and $|\delta_{b2}| \leq D_{b2}$ In this section the aircraft longitudinal dynamics system, as considered in this work, has been explained As discussed in Chapter 1, a model-following approach has been used for this problem and is presented next

3.3 The Model-Following Control

A MF structure as shown in Fig 3 1 is used to achieve robust tracking performances The nonlinear aircraft state equations (3 1) have already been presented in the previous section The method also requires a model response trajectory This can be generated by the pilot with the inputs available to him namely the elevator, the throttle gear and the mode selector The mode selector specifies the outputs to be tracked Different models may be selected, for the various modes and with varying operating regimes, as specified by the HQ engineers and/or the pilots It suffices to assume, that one is provided with the state trajectory to be tracked and its time derivative The model used in the present study is given in the Appendix D

As can be seen from the figure, the controller gives as output the desired force vector F_{com} which should be applied to the aircraft An aerodynamic inversion is required

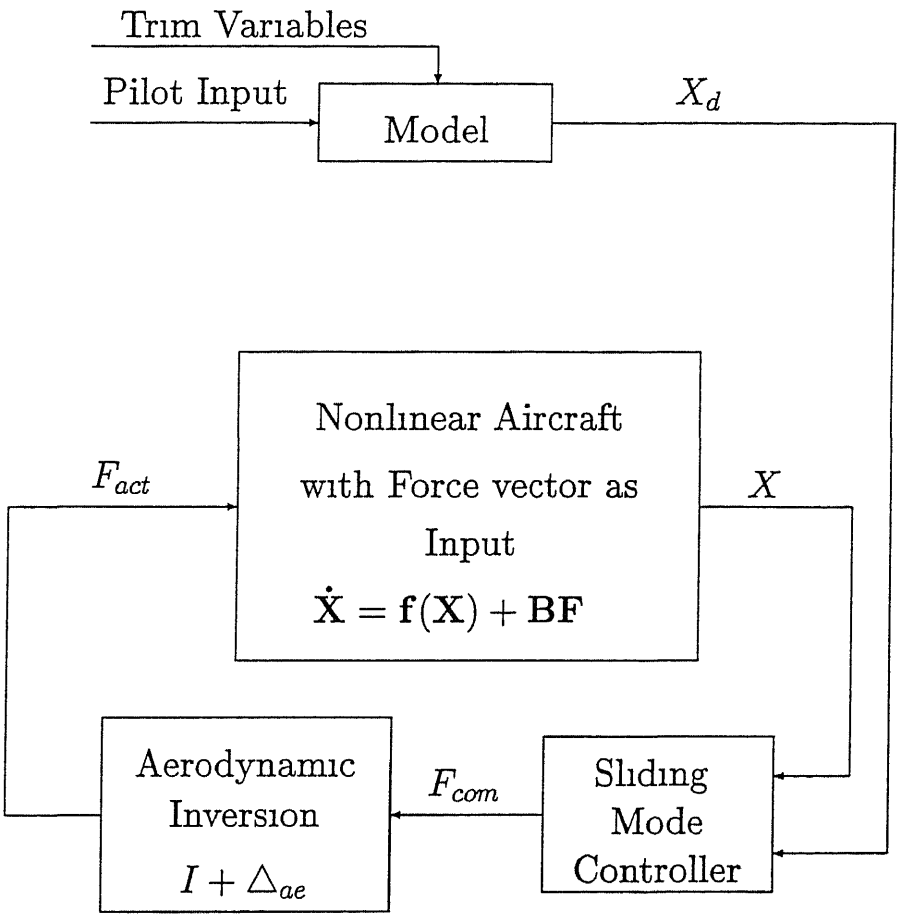

Fig. 3 1 Schematic Model-Following Control Scheme

to get the actual control surface deflections On applying these to the actual aircraft, the generated force vector F_{act} is likely to be different from the F_{com} as shown in Fig 3 1 Most of the works cited earlier [23, 39] assume that these signals are identical However, in practice this assumption is likely to lead to errors for the following reasons

1 **Uncertainties in the aerodynamic modeling and data:** The data used for control design is normally based on some models and/or observations from wind-tunnel experiments on the scaled models of the aircraft Also the aeroelastic effects are generally not considered

2 **Uncertainties in the aerodynamic inversion block:** The nonlinear inversion process itself may not be exact

3 **Unmodeled actuator dynamics** The actuator dynamics are generally neglected in a first level control design

4 **Uncertain position of the center of gravity (CG):** The moment M depends, besides other factors, on the actual position of the CG

5 **Uncertainty in the air velocity relative to the aircraft:** The forces and the moments vary proportionally with the square of the relative air velocity Errors in measurement and the presence of wind gusts can lead to this uncertainty

It is assumed that errors from the above sources are bounded and can be represented by time varying multiplicative uncertainties as

$$F_{act} = (I + \triangle_{ae})F_{com} \tag{3 4}$$

where $\triangle_{ae}$ is a 3×3 diagonal matrix with the diagonal entries being $\delta_{ae}(i)$, $i = 1, 2, 3$ all of which are bounded with $|\delta_{ae}(i)| \leq D_{ae}(i)$, a known quantity

The Section 3 2 and this section completely define the FCS design problem with the system equations in (3 1), the uncertainties involved in the aircraft inertia parameters and the inputs in (3 3) and (3 4), the desired model response (as in Appendix D), and the MF control structure used (as shown in Fig 3 1) The SMC design method for the MF problem of a MI nonlinear system as presented above is next discussed

3.4 Tracking in Multi-Input Nonlinear Systems

The aircraft system of equations in (3 1) with external disturbances can be expressed in a general form as

$$\begin{aligned} \mathbf{x} &= \mathbf{f}(\mathbf{x}) + \mathbf{G}(\mathbf{x})\mathbf{u} + \mathbf{d}, \text{ and} \\ \mathbf{y} &= \mathbf{y}(\mathbf{x}), \end{aligned} \tag{3 5}$$

where $\mathbf{x} \in \mathcal{R}^n$, $\mathbf{u}, \mathbf{y} \in \mathcal{R}^m$ represent the state, input and output vectors respectively, and $\mathbf{d}$ represents the external disturbance vector given bounded as $|d_i| \leq D_i$, $i = 1, \quad , n$ Since the number of trackable outputs equals the number of independent inputs, the number of outputs and inputs are assumed to be equal Also $\mathbf{G}(\mathbf{x})$ is assumed to be of rank m over the entire state space The number of differentiations of $\mathbf{y}(\mathbf{x})$ required for the input $\mathbf{u}$ to appear in its expression is called the relative degree of the system It is assumed without any loss of generality that all components of $\mathbf{y}$ have a relative degree '1'

Under a suitable coordinate transformation from $\mathbf{x}$ to $\mathbf{z} = [\mathbf{y}^{\mathrm{T}} \xi^{\mathrm{T}}]^{\mathrm{T}}$, where the superscript T denotes the transpose, and $\xi \in \mathcal{R}^{n-m}$, the above nonlinear system may be expressed in a reduced form [37, 52] as

$$\mathbf{y} = \mathbf{f}_1(\mathbf{z}) + \mathbf{B}_1(\mathbf{z})\mathbf{u} + \mathbf{d}_1, \text{ and} \tag{3 6}$$

$$\xi = \mathbf{f}_2(\mathbf{z}) + \mathbf{d}_2 \tag{3 7}$$

The (3 6) represents the matched dynamics and the disturbances and/or uncertainties, $\mathbf{d}_1$, entering this equation are called matched The (3 7) gives the unmatched portion of the dynamics and the disturbances and/or uncertainties, $\mathbf{d}_2$, entering this equation are said to be unmatched In this chapter, only matched disturbances/uncertainties are assumed since the SMC guarantees invariant performance in the presence of this class of uncertainties The case of unmatched uncertainties is considered in the next chapter. The matched disturbance vector $\mathbf{d}_1$ is given to be bounded with $|d_{1_i}| \leq D_{1_i}$, $i = 1, \quad , m$ Under the assumptions made above the matched dynamics represents a square system of m equations Also $\mathbf{B}_1(\mathbf{z})$ is an $m \times m$ matrix having full rank over

the state space z thus implying a strong relative degree '1' The arguments of the various functions defined above are dropped if no confusion is likely to arise Let $\hat{\mathbf{B}}_1$ represent the nominal $\mathbf{B}_1$ matrix It is assumed that the $\mathbf{B}_1$ may be expressed as $\mathbf{B}_1 = (I + \triangle_b)\hat{\mathbf{B}}_1$, in which all the matrices are appropriately dimensioned with I representing the identity matrix Also the matrix $\triangle_b$ is bounded by a known matrix D_b as $|\triangle_b(i,j)| \leq D_b(i,j)$

As explained earlier, $\mathbf{u}$ in (3 6) is the actually applied control signal, i e $\mathbf{u}_{\text{act}}$ With the uncertainty as modeled in (3 4), $\mathbf{u}_{\text{act}} = (I + \triangle_{ae})\mathbf{u}_{\text{com}}$, the system equations in (3 6) and (3 7) can be rewritten as

$$\mathbf{y} = \mathbf{f}_1 + (I + \triangle_b)\hat{\mathbf{B}}_1(I + \triangle_{ae})\mathbf{u}_{\text{com}} + \mathbf{d}_1, \text{ and} \tag{3 8}$$

$$\xi = \mathbf{f}_2 \tag{3 9}$$

The MF-SMC design for the case when $\triangle_{ae} = 0$ is reported in Slotine and Li [21] and Hedrick and Gopalswamy [42] In this chapter the method has been extended to a more general case with $\triangle_{ae} \neq 0$

Let the trajectory to be followed be specified as $\mathbf{y}_d$ and $\dot{\mathbf{y}}_d$ Define $\mathbf{S}$ as a vector consisting of the error function for the output vector as

$$\mathbf{S} = \mathbf{y} - \mathbf{y}_d \tag{3 10}$$

It is desired that $\mathbf{S} = 0$ To this end, taking time derivative of the above equation, and using (3 8) gives

$$\begin{aligned} \dot{\mathbf{S}} &= \dot{\mathbf{y}} - \dot{\mathbf{y}}_d \\ &= \mathbf{f}_1 + (I + \triangle_b)\hat{\mathbf{B}}_1(I + \triangle_{ae})\mathbf{u}_{\text{com}} + \mathbf{d}_1 - \dot{\mathbf{y}}_d \end{aligned} \tag{3 11}$$

The equivalent control [21] is defined as the input $\hat{\mathbf{u}}_{\text{com}}$, which makes $\dot{\mathbf{S}} = 0$, when $\mathbf{S} = 0$ for the nominal plant, i e $\triangle_b = 0$, $\triangle_{ae} = 0$, and $\mathbf{d}_1 = 0$ Thus the equivalent control becomes

$$\hat{\mathbf{u}}_{\text{com}} = \hat{\mathbf{B}}_1^{-1}(\dot{\mathbf{y}}_d - \mathbf{f}_1) \tag{3 12}$$

The applied input function should make the SS attractive in the presence of disturbances and uncertainties also This is achieved by selecting the applied control signal

as the sum of the equivalent control and a discontinuous function as

$$\mathbf{u}_{\text{com}} = \hat{\mathbf{B}}_1^{-1}(\mathbf{y}_d - \mathbf{f}_1 - \mathbf{k}\ \text{sgn}[\mathbf{S}]) \tag{3 13}$$

where, $\mathbf{k}$ sgn[S] is an $m \times 1$ column vector with all $k_i > 0$, $i = 1, \quad , m$ Let $(\mathbf{k}\ \text{sgn}[\mathbf{S}])_i = k_i \text{sgn}[S_i]$ represent the i^{th} component of the vector The real vector $\mathbf{k}$ has to be selected so that trajectories starting from nonzero values of $\mathbf{S}$ approach the SS Putting $\mathbf{u}_{\text{com}}$ from (3 13) in (3 11) gives

$$\mathbf{S} = \mathbf{f}_1 + (I + \triangle_b)\hat{\mathbf{B}}_1(I + \triangle_{ae})\hat{\mathbf{B}}_1^{-1}(\mathbf{y}_d - \mathbf{f}_1 - \mathbf{k}\ \text{sgn}[\mathbf{S}]) + \mathbf{d}_1 - \mathbf{y}_d \tag{3 14}$$

The above equation may be simplified by defining an $m \times m$ matrix $\triangle_t$, such that

$$(I + \triangle_t) = (I + \triangle_b)\hat{\mathbf{B}}_1(I + \triangle_{ae})\hat{\mathbf{B}}_1^{-1} \tag{3 15}$$

The bounds on the matrix $\triangle_t$ can be evaluated from the known bounds on $\triangle_b$ and $\triangle_{ae}$ as will be shown in the next section Let these be given as $|\triangle_t(i,j)| \leq D_t(i,j)$ With this, (3 14) can be rewritten as

$$\mathbf{S} = \mathbf{f}_1 + (I + \triangle_t)(\mathbf{y}_d - \mathbf{f}_1 - \mathbf{k}\ \text{sgn}[\mathbf{S}]) + \mathbf{d}_1 - \mathbf{y}_d, \tag{3 16}$$

which may further be simplified to

$$\mathbf{S} = \triangle_t(\mathbf{y}_d - \mathbf{f}_1) - (I + \triangle_t)\mathbf{k}\ \text{sgn}[\mathbf{S}] + \mathbf{d}_1 \tag{3 17}$$

The SS is made attractive by selecting $\mathbf{k}$ such that

$$S_i S_i < -\eta_i |S_i|, \tag{3 18}$$

where $\eta_i, i = 1, \quad , m$ is a positive scalar quantity to be selected, thus satisfying the reaching condition [21] The above equation guarantees (see Appendix A) that the S_i response will be better than the response of

$$S_i = -\eta_i \text{sgn}[S_i] \tag{3 19}$$

Following the algebraic manipulations along the lines of [21, 42], $\mathbf{k}$ can be obtained as the solution of the following system of linear algebraic equations

$$(I - D_t)\mathbf{k} = \Psi, \tag{3 20}$$

where, D_t is the matrix with $D_t(i,j)$ as its components, and Ψ is an $m \times 1$ vector with

$$\Psi_i = \Psi(i) = D_{1_i} + \eta_i + \sum_{j=1}^{m} D_t(i,j)|y_d(j) - f_1(j)|, \; i = 1, \quad , m \tag{3 21}$$

It is obvious that $\Psi(i) > 0$, $i = 1, \quad , m$ from the above equation The existence of a unique solution $\mathbf{k}$ with all $k_i \geq 0$ is easily established using the Forbenius-Perron Theorem [21] (See Theorem 1 in Appendix G) and requires that the largest positive eigenvalue of D_t be less than 1 0

The use of a sgn[ ] function in (3 13) gives rise to the chattering problem Various methods have been suggested in the literature for its alleviation [21, 56] In this study, the concept of a boundary layer as proposed by Slotine [21] has been used to approximate the discontinuity by a continuous control law Accordingly, for implementation purposes, the vector $\mathbf{k}$ sgn[$\mathbf{S}$] in (3 13) is replaced by $\mathbf{k}$ sat[$\mathbf{S}/\Phi$], whose i^{th} element is given as k_i sat[S_i/ϕ_i], where Φ is a $m \times 1$ column vector of appropriately selected boundary layer thickness, given as $[\phi_i]^{\mathrm{T}}$, $i = 1, \quad , m$ The control law in (3 13), then becomes

$$\mathbf{u}_{\text{com}} = \hat{\mathbf{B}}_1^{-1}(\mathbf{y}_d - \hat{\mathbf{f}} - \mathbf{k} \text{ sat}[\mathbf{S}/\Phi]) \tag{3 22}$$

The S_i dynamics then becomes

$$S_i = -\eta_i \text{sat}[S_i/\phi_i] \tag{3 23}$$

With the $\mathbf{u}_{\text{com}}$ as selected above, the motion in the sliding mode is guaranteed to be inside of thickness Φ of the SS [21] Thus,

$$|S_i| \leq \phi_i \tag{3 24}$$

Moreover, starting from a non-zero initial condition $\mathbf{S}_0$, the dynamics in (3 23) guarantees that its i^{th} component S_i reaches the boundary layer within a finite time (t_{0_i}) given by

$$t_{0_i} \leq \frac{S_{0_i} - \phi_i}{\eta_i} \tag{3 25}$$

Thus, a larger value of η leads to a smaller reaching time and larger control efforts

Thus, the above selection of $\mathbf{u}_{com}$ in (3 22) guarantees that the outputs are tracked with a desired accuracy, however, the stability properties of the unmatched dynamics in (3 9) need to be investigated It has been shown [21] that this can be determined by studying the stability of the zero dynamics (ZD), which is defined as the dynamics of the system when the outputs and all its time derivatives are kept at 0 (zero) by appropriate choice of the input The ZD for the system (3 5), with all outputs having a relative degree '1' is thus seen to be a special case of the unmatched dynamics in (3 9) as

$$\xi = \mathbf{f}_2([0^T \xi^T]^T) \tag{3 26}$$

The stability of the unmatched dynamics is proved if the ZD is at least bounded [21]

The SMC method as outlined here is applied to the design of control laws for the longitudinal dynamics of an aircraft using the MF structure as discussed in Section 3 3 Therefore, the method is termed as the MF-SMC The results of numerical simulation are presented next

3.5 Numerical Example and Simulation

MF-SMC laws are synthesized, following the steps outlined in the previous section, for the FCS design problem as presented in Sections 3 2 and 3 3 The numerical values of the time varying multiplicative parametric uncertainties and disturbances and their bounds as defined in the previous sections as also the mass and inertia parameters of the aircraft as used for simulation purposes are given in the Appendix D To show the applicability of the proposed method, controllers are designed for the following two cases

1 **C1:** In this case, the controller design is done assuming that the F_{com} and F_{act} are identical, i e $\triangle_{ae} = 0$

2 **C2:** Here, the controller design takes into account that $\triangle_{ae} \neq 0$

The controllers corresponding to the cases **C1** and **C2** will be called as the **M1** and **M2** respectively

As stated earlier, it is possible to track only three states or outputs using the 3-component force vector Thus various operational modes for the aircraft can be specified, depending on the variables which are of concern during a given flight phase However, any trajectory of interest can be tracked using a suitably generated velocity signal denoted by U_d, W_d, and Q_d where the subscript 'd' stands for desired trajectory Trimming of an aircraft at a level flight condition is of vital importance to the pilot The trim variables are also required to evaluate the desired trajectories as can be seen in the Appendix D The responses obtained by the two controllers (**M1** and **M2**) are then compared for the Tracking and Trimming modes The velocity tracking is considered first

3.5.1 Controller Design for Tracking Mode

In this case, the state equation (3 1) including the disturbances can be seen to be

$$\begin{pmatrix} U \\ W \\ Q \\ \theta \\ p_x \\ p_z \end{pmatrix} = \begin{pmatrix} -QW - g_0 \sin(\theta) \\ QU + g_0 \cos(\theta) \\ 0 \\ Q \\ U\cos(\theta) + W\sin(\theta) \\ U\sin(\theta) - W\cos(\theta) \end{pmatrix} + \begin{pmatrix} R_m F_x \\ R_m F_z \\ c_7 M \\ 0 \\ 0 \\ 0 \end{pmatrix} + \begin{pmatrix} d_U \\ d_W \\ d_Q \\ 0 \\ 0 \\ 0 \end{pmatrix} \tag{3 27}$$

where, d_i, $i = U, W, Q$ represent the external disturbances and uncertainties entering in the channels denoted by the subscript i and their magnitudes are bounded by $|d_i| < D_i$ It is seen that, with $\mathbf{y}^{\mathrm{T}} = [U\ W\ Q]$ as the output vector, the above equation is already in the reduced form, with the first three components forming the matched dynamics (3 6) and the remaining three the unmatched dynamics (3 7) The ZD (3 26) in this case is thus given by

$$\begin{pmatrix} \theta \\ p_x \\ p_z \end{pmatrix} = \begin{pmatrix} 0 \\ 0 \\ 0 \end{pmatrix} \tag{3 28}$$

Thus, the states of the ZD are in a neutral equilibrium, implying that the unmatched dynamics are bounded-input bounded-state (BIBS)

For both cases (**C1** and **C2**), the $\hat{\mathbf{B}}_1$ matrix is seen from (3 27 to be

$$\hat{\mathbf{B}}_1 = \text{diag}[\hat{R}_m,\ \hat{R}_m,\ \hat{c}_7], \tag{3 29}$$

where diag[ ] denotes a diagonal matrix Also, the $\triangle_b$ matrix is seen to be diag$[\delta_{b1},\ \delta_{b1},\ \delta_{b2}]$ The vector $\mathbf{S} = [S_U,\ S_W,\ S_Q]^{\mathrm{T}}$ is as defined in (3 10) Following the steps as outlined in the previous section, $I + \triangle_t$ in (3 15) can be simplified as

$$(I + \triangle_t) = \text{diag}[q_1,\ q_2,\ q_3], \tag{3 30}$$

where, $q_1 = (1+\delta_{b1})(1+\delta_{ae}(1))$, $q_2 = (1+\delta_{b1})(1+\delta_{ae}(2))$, and $q_3 = (1+\delta_{b2})(1+\delta_{ae}(3))$ The $\triangle_t$ matrix for the case **C1** can be obtained by putting $\delta_{ae}(i) = 0$ for $i = 1, 2, 3$ In this case the D_t matrix, which bounds the $\triangle_t$ matrix in (3 30), is seen to be given by the bounds on δ_{b1} and δ_{b2} (given in the Appendix D) as

$$D_t = \text{diag}[1/3,\ 1/3,\ 3/7] \tag{3 31}$$

For the case **C2**, the $I+\triangle_t$ matrix in (3 30) would attain its maximum (minimum) values when both the terms in the product individually take their maximum (minimum) values Using the bounds as given in Appendix D, the elements of the diagonal matrix $I + \triangle_t$ can be seen to vary within the following bounds

$$\begin{aligned} \frac{8}{15} &\leq 1 + \triangle_t(1,1) \leq \frac{8}{5} \\ \frac{8}{15} &\leq 1 + \triangle_t(2,2) \leq \frac{8}{5} \\ \frac{16}{35} &\leq 1 + \triangle_t(3,3) \leq \frac{12}{7} \end{aligned} \tag{3 32}$$

from which, the D_t matrix bounding $\triangle_t$ in (3 30) becomes

$$D_t = \text{diag}[3/5,\ 3/5,\ 5/7] \tag{3 33}$$

It is obvious that in both cases, all the eigenvalues of D_t are less than 1 0, thus guaranteeing the existence of k in (3 20) The positive scalar η_i in (3 18) has been taken to

be 1 0, $i = 1, \quad , 3$ With these choices, the 3×1 vector Ψ in (3 21) can be seen to be

$$\begin{aligned}
\Psi_1 &= \Psi(1) = \quad 1\,0 + D_U + D_t(1,1)|U_d - QW + g_0 \sin(\theta)|, \\
\Psi_2 &= \Psi(2) = \quad 1\,0 + D_W + D_t(2,2)|W_d - QU - g_0 \cos(\theta)|, \text{ and} \\
\Psi_3 &= \Psi(3) = \quad 1\,0 + D_Q + D_t(3,3)|Q_d| \qquad (3\,34)
\end{aligned}$$

Note that for the two cases **C1** and **C2**, different D_t as in (3 31) and (3 33) respectively have to be used

The 3×1 vector $\mathbf{k}$ in (3 20) can then be evaluated for the two cases as

1 **C1:** $\mathbf{k}^{\mathrm{T}} = [1\,5\Psi_1, \ 1\,5\Psi_2, \ 1\,75\Psi_3]$, and

2 **C2.** $\mathbf{k}^{\mathrm{T}} = [2\,5\Psi_1, \ 2\,5\Psi_2, \ 3\,5\Psi_3]$

The calculated values of $\mathbf{k}$ are then used in (3 22) to obtain the control law as

$$\begin{aligned}
F_{x_{\mathrm{com}}} &= \frac{1}{\hat{R}_m}\left(U_d + QW + g_0 \sin(\theta) - k_1 \mathrm{sat}[\frac{S_U}{\phi_U}]\right), \\
F_{z_{\mathrm{com}}} &= \frac{1}{\hat{R}_m}\left(W_d - QU - g_0 \cos(\theta) - k_2 \mathrm{sat}[\frac{S_W}{\phi_W}]\right), \text{ and} \\
M_{\mathrm{com}} &= \frac{1}{\hat{c}_7}\left(Q_d - k_3 \ \mathrm{sat}[\frac{S_Q}{\phi_Q}]\right) \qquad (3\,35)
\end{aligned}$$

The boundary layer thicknesses (ϕ_U, ϕ_W and ϕ_Q) for the three outputs as used in the simulation are specified in the Appendix D It can be seen that the state variables p_x and p_z are not used in the control law, however they constitute the ZD, and hence they have been included in the above development Simulation has been done using a fourth order Runge-Kutta algorithm with the time step of 0 25ms The aircraft is initially assumed to be in a trimmed level flight with a total velocity of 502 feet per second (fps) Till 0 5s, the elevator and throttle gear commands are maintained at their equilibrium values, and at this time instant the pilot increments the elevator by 15^0 and the throttle gear by 20 units and maintains them at a constant value till 2 0s

The responses were obtained for two sets of uncertainties (UC1 and UC2, as specified in the Appendix D) for the two cases (**C1** and **C2**) The tracking error of the

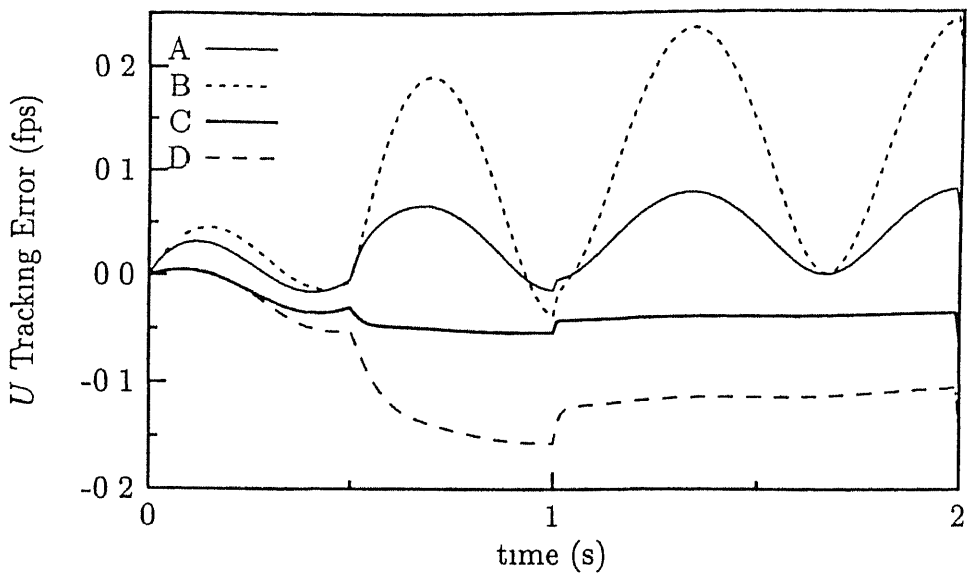

Fig. 3.2 Tracking error in U (fps)

outputs (U, W and Q) are shown in Figs 3 2, 3 3 and 3 4 respectively In these figures, the solid lines labeled 'A' and 'C' correspond to the responses using the M2 controller for the uncertainties UC1 and UC2 respectively Similarly the dashed lines 'B' and 'D' show the results using the controller M1 for UC1 and UC2 respectively It is observed from the figures, that the output tracking error stays well within the specified boundary layer thickness and good tracking of the desired trajectory is achieved. From the figures, it is clear that the tracking errors in the case C2 are smaller than those of the case C1 for all the outputs Although, θ is not a tracked output, in the absence of unmatched uncertainties, it was found to be well tracked with a similar trend Thus, the controller M2 clearly gives better performance as compared to the controller M1 Thus it is seen that ignoring the uncertainties involved in the force generation can lead to a degraded system performance

The desired force command and the actually applied force vector, with the assumed uncertainty in aerodynamic inversion /modeling is shown in Figs 3 5, 3 6, and 3 7 for the UC1 uncertainty and case C2

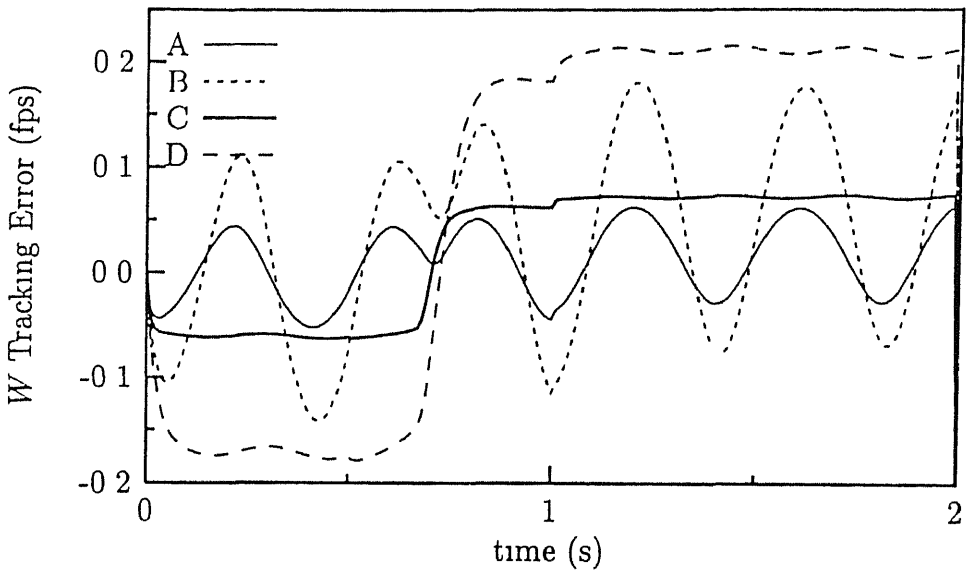

Fig 3.3 Tracking error in W (fps)

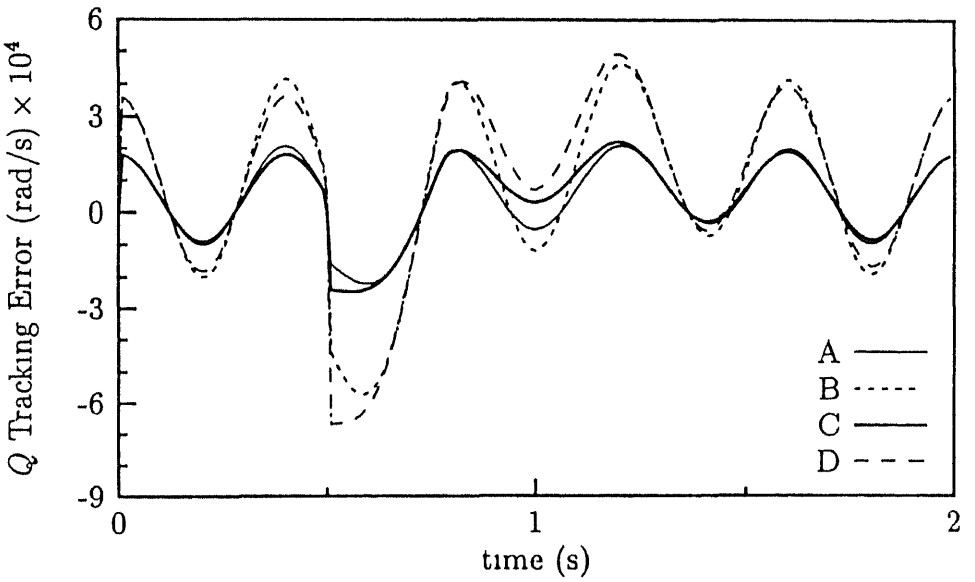

Fig. 3.4 Tracking error in Q (rad/s)

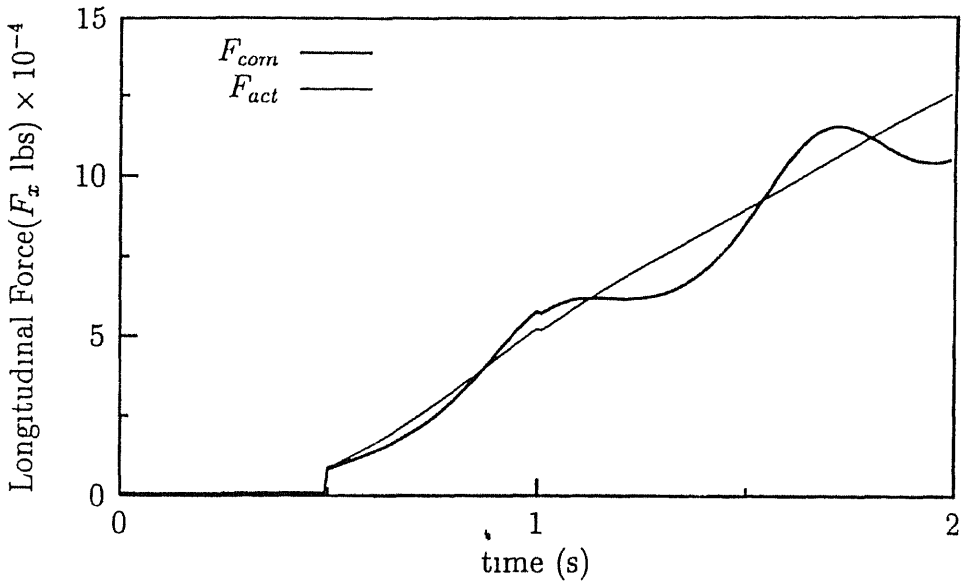

Fig 3.5 The command F_x (F_{com}) and the actually realized force (F_{act})

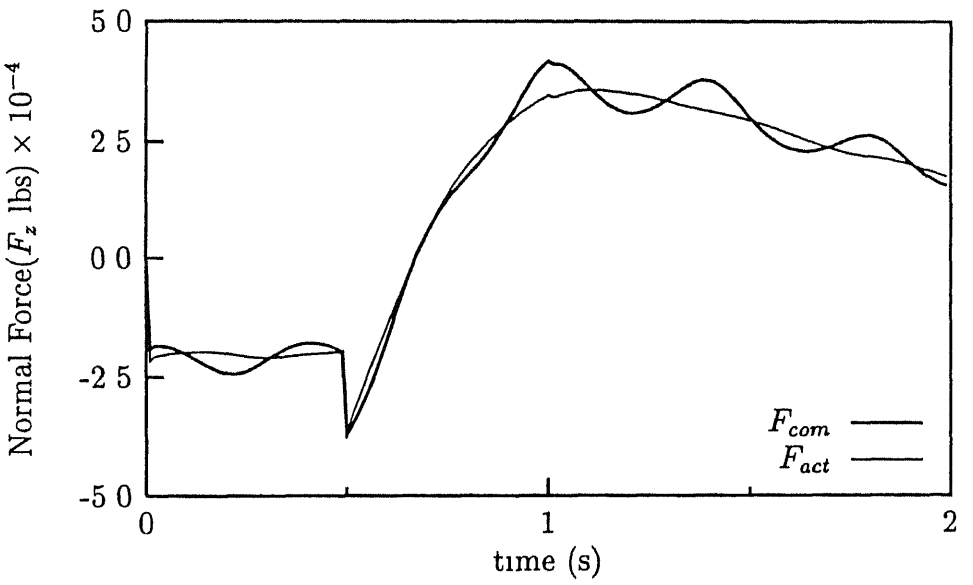

Fig. 3.6 The command F_z (F_{com}) and the actually realized force (F_{act})

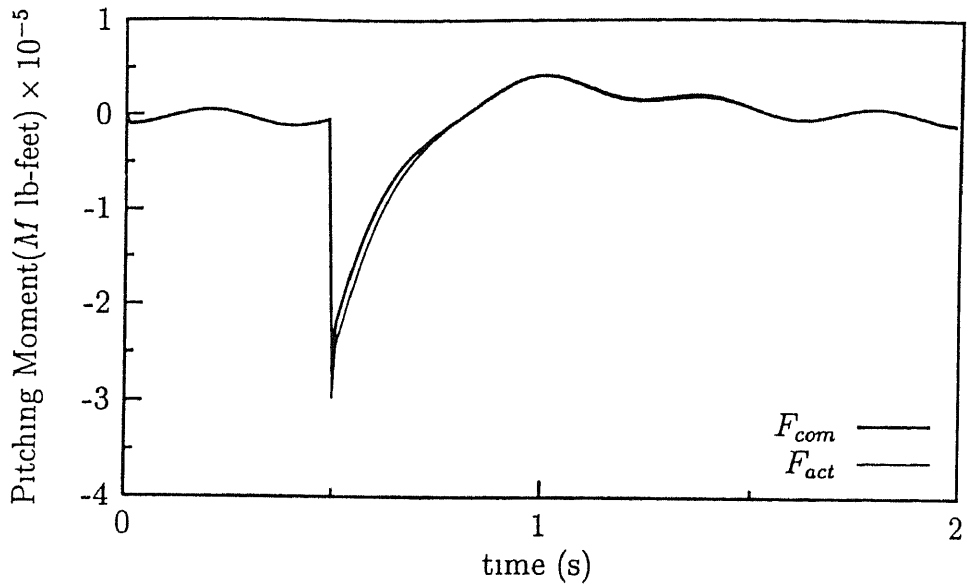

Fig. 3.7 The command M (M_{com}) and the actually realized force (M_{act})

3.5.2 Controller Design for Trim Mode

The trimming of an aircraft at a level flight condition requires that an equilibrium condition is reached at any given velocity Most earlier works require a trim map or some algorithm [23] to generate the trimming variables With the proposed design method this is not required Given the velocity at which the aircraft is to be trimmed, the control law leads the aircraft states to the desired trim variables The pilot is provided with a trim switch to trim the aircraft at the current value of the total forward velocity Continuing with the simulation results in the previous section, the pilot activates the trim switch at $t = 2\ 0$s The trimmed or the equilibrium state is defined as

$$\begin{pmatrix} V_t \\ \gamma \\ Q \end{pmatrix} = \begin{pmatrix} V_0 \\ 0 \\ 0 \end{pmatrix} \tag{3 36}$$

where, V_0 is the desired trim velocity In the above equation $V_t = (U^2 + W^2)^{1/2}$ represents the total velocity, $\alpha = \tan^{-1}(W/U)$ is called the angle of attack, and $\gamma =$

$\theta - \alpha$ is the flight path angle It is assumed that there are appropriate sensors to measure these quantities Also define $\mathbf{S} = [S_{V_t},\ S_\gamma,\ S_Q]^{\mathrm{T}}$ as the error function for the outputs as in (3 10) To track the outputs as defined in (3 36) the dynamic equations governing them need to be defined These are given in standard textbooks [10] or can be directly obtained from the definitions of the outputs as above, and using (3 27) The state equation in the new set of coordinates, $\mathbf{z}^{\mathrm{T}} = [V_t\ \gamma\ Q\ \theta\ p_x\ p_z]$, may be written as

$$\begin{pmatrix} V_t \\ \gamma \\ Q \\ \theta \\ p_x \\ p_z \end{pmatrix} = \begin{pmatrix} -g_0 \sin(\gamma) \\ -g_0 \cos(\gamma) \\ 0 \\ Q \\ V_t \cos(\gamma) \\ V_t \sin(\gamma) \end{pmatrix} + \begin{bmatrix} R_m \cos(\alpha) & R_m \sin(\alpha) & 0 \\ R_m \sin(\alpha) & -R_m \cos(\alpha) & 0 \\ 0 & 0 & c_7 \\ 0 & 0 & 0 \\ 0 & 0 & 0 \\ 0 & 0 & 0 \end{bmatrix} \begin{pmatrix} F_x \\ F_z \\ M \end{pmatrix} + \begin{pmatrix} d_{V_t} \\ d_\gamma \\ d_Q \\ 0 \\ 0 \\ 0 \end{pmatrix} \tag{3 37}$$

where, d_{V_t}, d_γ, and d_Q represent the matched external disturbances and can be evaluated as

$$\begin{aligned} d_{V_t} &= d_U \cos(\alpha) + d_W \sin(\alpha), \\ d_\gamma &= d_U \sin(\alpha) - d_W \cos(\alpha), \text{ and} \\ d_Q &= d_Q \end{aligned} \tag{3 38}$$

Their bounds change to

$$\begin{aligned} D_{V_t} &= D_U + D_W, \\ D_\gamma &= D_U + D_W, \text{ and} \\ D_Q &= D_Q \end{aligned} \tag{3 39}$$

It is seen that, with $\mathbf{y}^{\mathrm{T}} = [V_t\ \gamma\ Q]$ as the output vector, (3 37) is already in the reduced form as before with the first three equations defining the matched dynamics and the remaining unmatched dynamics Also the ZD in this case are the same as in (3 28) Thus the unmatched dynamics is BIBS

For the system (3 37) the input distribution matrix (denoted by $\mathbf{B}_1'$), corresponding to the $\mathbf{B}_1$ in (3 6), is defined in the first three equations in (3 37), and the nominal $\hat{\mathbf{B}}_1'$ matrix is seen to be given as

$$\hat{\mathbf{B}}_1' = \begin{bmatrix} \hat{R}_m \cos(\alpha) & \hat{R}_m \sin(\alpha) & 0 \\ \hat{R}_m \sin(\alpha) & -\hat{R}_m \cos(\alpha) & 0 \\ 0 & 0 & \hat{c}_7 \end{bmatrix} \tag{3 40}$$

for both the cases It is easily verified that $\hat{\mathbf{B}}_1'$ matrix above is invertible over the entire state space and the chosen parameter range The $\triangle_b$ matrix is the same as in the tracking mode Following the steps as in the previous section, $I + \triangle_t$ in (3 15), can be obtained as

$$(I + \triangle_t) = \begin{bmatrix} (1+\delta_{b1})q_1 & \frac{1}{2}(1+\delta_{b1})q_2 & 0 \\ \frac{1}{2}(1+\delta_{b1})q_2 & (1+\delta_{b1})q_3 & 0 \\ 0 & 0 & (1+\delta_{b2})(1+\delta_{ae}(3)) \end{bmatrix} \tag{3 41}$$

where, $q_1 = (1 + \delta_{ae}(1)\cos^2(\alpha) + \delta_{ae}(2)\sin^2(\alpha))$, $q_2 = (\delta_{ae}(1) - \delta_{ae}(2))\sin(2\alpha)$, and $q_3 = (1 + \delta_{ae}(1)\sin^2(\alpha) + \delta_{ae}(2)\cos^2(\alpha))$

Note that for the case **C1** with $\triangle_{ae} = 0$, $q_1 = q_3 = 1$ 0 and $q_2 = 0$ With this, the matrix D_t for this case is seen to be the same as in the tracking mode and is given in (3 31)

For the case **C2**, with $\triangle_{ae}(i) \neq 0$ using the bounds as given in the Appendix D, it is seen that the q_1, q_2 and q_3 as defined above are bounded as

$$\begin{aligned} \frac{4}{5} &\leq q_1 \leq \frac{6}{5} \\ \frac{-2}{5} &\leq q_2 \leq \frac{2}{5} \\ \frac{4}{5} &\leq q_3 \leq \frac{6}{5} \end{aligned} \tag{3 42}$$

Proceeding as in the previous section, the components of the symmetric $I + \triangle_t$ matrix in (3 41) are seen to assume values as given by

$$\frac{8}{15} \leq [I + \triangle_t](1,1) \leq \frac{8}{5}$$

$$\begin{aligned} \frac{-2}{15} &\leq [I + \Delta_t](1,2) \leq \frac{4}{15} \\ \frac{8}{15} &\leq [I + \Delta_t](2,2) \leq \frac{8}{5} \\ \frac{16}{35} &\leq [I + \Delta_t](3,3) \leq \frac{12}{7} \end{aligned} \tag{3 43}$$

From the above equation, a 3×3 bounding matrix D_t can be selected as

$$D_t = \begin{bmatrix} 3/5 & 4/15 & 0 \\ 4/15 & 3/5 & 0 \\ 0 & 0 & 5/7 \end{bmatrix} \tag{3 44}$$

It can be easily verified that for both the cases, all the eigenvalues of D_t are less than 1 0 The Ψ vector (3 21) in this mode becomes

$$\begin{aligned} \Psi_1 &= 1\,0 + D_{V_t} + g_0 D_t(1,1)|\sin(\gamma)| + g_0 D_t(1,2)|\cos(\gamma)|, \\ \Psi_2 &= 1\,0 + D_\gamma + g_0 D_t(2,1)|\sin(\gamma)| + g_0 D_t(2,2)|\cos(\gamma)|, \text{ and} \\ \Psi_3 &= 1\,0 + D_Q + D_t(3,3) \end{aligned} \tag{3 45}$$

with the time derivatives of the outputs (i e V_{t_d}, γ_d, and Q_d) taken to be zero Using the D_t in (3 31) and (3 44) for the cases **C1** and **C2** respectively, the $\mathbf{k}$ in (3 20) can be evaluated in the two cases as

1 **C1:** $\mathbf{k}^{\mathrm{T}} = [1\,5\Psi_1,\ 1\,5\Psi_2,\ 1\,75\Psi_3]$, and

2 **C2:** $\mathbf{k}^{\mathrm{T}} = [4\,5\Psi_1 + 3\,0\Psi_2,\ 3\,0\Psi_1 + 4\,5\Psi_2,\ 3\,5\Psi_3]$

Using the $\mathbf{k}$ as above and the inverse of the $\hat{\mathbf{B}}_1'$ matrix in (3 40) in (3 22) gives the control law as

$$\begin{aligned} F_{x_{\text{com}}} &= \frac{g_0}{\hat{R}_m}\sin(\theta) - \frac{1}{\hat{R}_m}\left[k_1\ \text{sat}[\frac{S_{V_t}}{\phi_{V_t}}]\cos(\alpha) + k_2\ \text{sat}[\frac{S_\gamma}{\phi_\gamma}]\sin(\alpha)\right], \\ F_{z_{\text{com}}} &= -\frac{g_0}{\hat{R}_m}\cos(\theta) - \frac{1}{\hat{R}_m}\left[k_1\ \text{sat}[\frac{S_{V_t}}{\phi_{V_t}}]\sin(\alpha) - k_2\ \text{sat}[\frac{S_\gamma}{\phi_\gamma}]\cos(\alpha)\right], \\ M_{\text{com}} &= -\frac{1}{\hat{c}_7}k_3 \text{sat}[\frac{S_Q}{\phi_Q}], \end{aligned} \tag{3 46}$$

where, the boundary layer thicknesses used are specified in the Appendix D It can be easily seen that the command forces ($F_{x_{\text{com}}}$ and $F_{z_{\text{com}}}$) consist of two terms, the first of which gives the equilibrium force component for the nominal aircraft, and the second term is a correction factor based on the errors in the output

At the end of the simulation as shown in the previous section, the trim switch is activated Simulation results are presented for an interval of 2 0s from 2 0 to 4 0s The tracking errors for the outputs (V_t and γ), the angle of attack α and the altitude variation are shown in Figs 3 8, 3 9, 3 10 and 3 11 respectively The labels 'A'-'D' are as explained for the tracking mode It was noticed that the pitch rate Q attains very small values almost instantaneously in both the cases and hence it is not presented here It can be seen from Fig 3 8 that the control law **M2** takes less than 1 0s to trim the aircraft for both uncertainty cases and that the error in V_t remains well inside the boundary layer However, the control law **M1** is seen to be unable to trim the aircraft even till 2 0 seconds, and in fact for the UC2 uncertainty, the error in V_t is seen to go outside the boundary layer This can also be seen from the slow response of γ (Fig 3 9) obtained in case **C1** as compared with **C2** Similarly the α variation (Fig 3 10) shows that fast responses are obtained in the case **C2** From, the altitude variation (Fig 3 11) it is seen that for the controller **M2**, the aircraft looses an altitude of about 70 and 58 feet for the uncertainty sets UC1 and UC2 respectively Comparatively the aircraft drops approximately 244 and 225 feet with the **M1** controller without achieving the trim state in the same time Thus, the **M2** controller is seen to give vastly improved performance over the **M1** controller

Thus it is observed that the MF-SMC gives fast and robust trimming performance It is evident from the simulation results that the proposed design method is robust to the uncertainties that can creep into the *aerodynamic inversion block* (see Fig 3 1). Moreover, the method does not require a trim map or an algorithm to find out the trim variables It eliminates the necessity of developing a dynamic trim map and reduces the pilot workload of actively trimming the aircraft, and thus represents considerable improvement over the prevailing practice

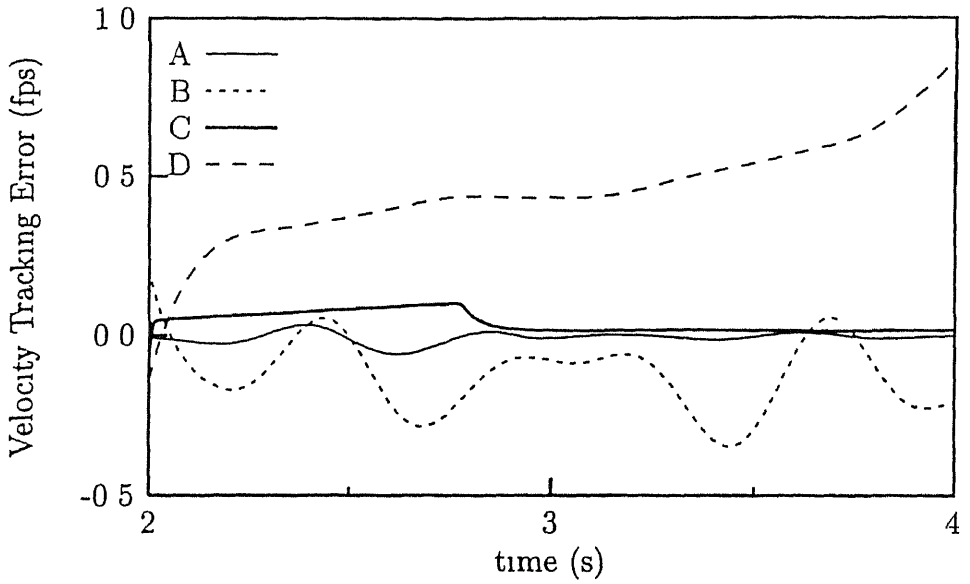

Fig. 3.8 V_t tracking error in the Trimming mode (fps)

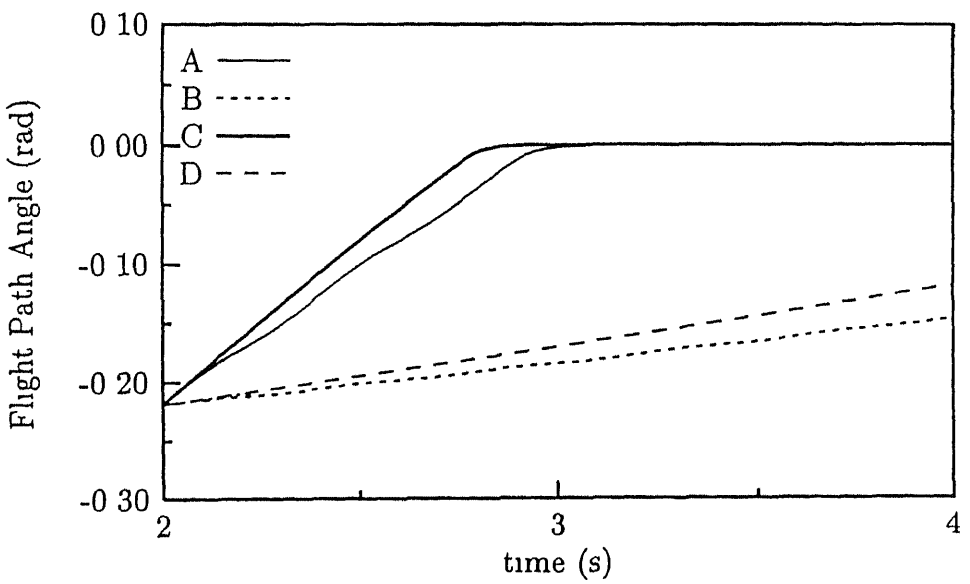

Fig. 3.9 Flight path angle (γ) response in the Trimming mode (rad)

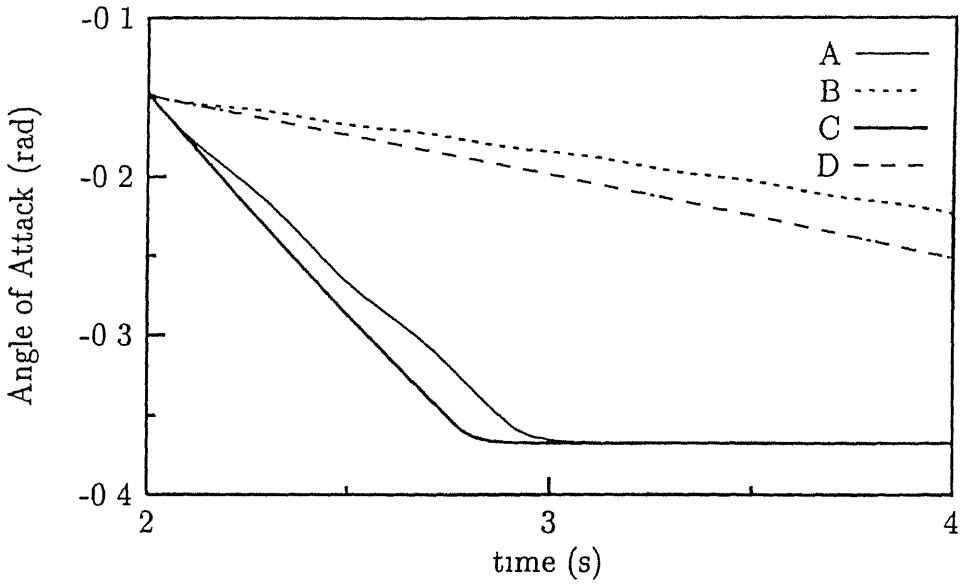

Fig. 3 10 Angle of attack (α) response in the Trimming mode (rad)

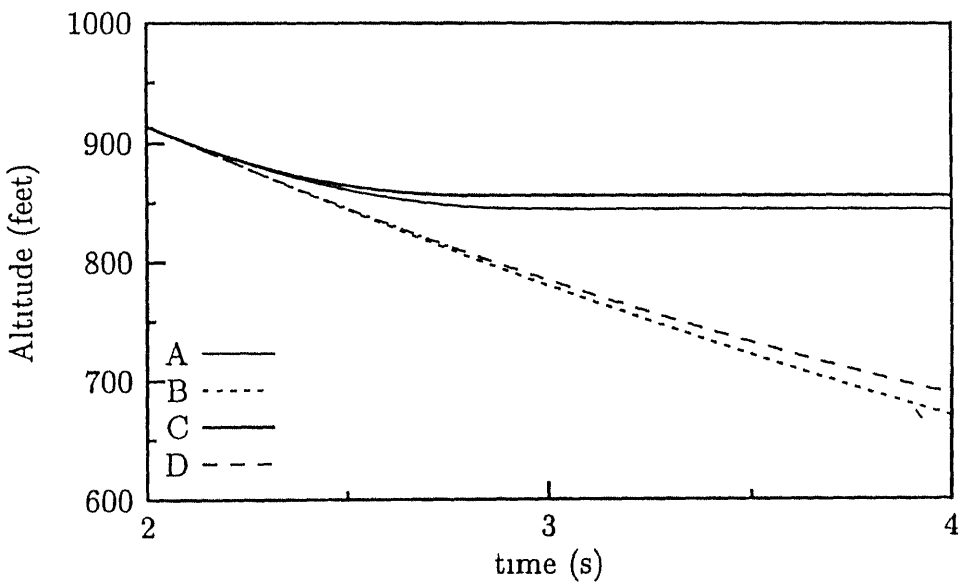

Fig. 3.11 Altitude (p_z (ft)) response in the Trimming mode

3.6 Conclusions

In this chapter, the robust nonlinear control law design for the nonlinear longitudinal dynamics of a fighter aircraft, based on a model following sliding mode approach and using a full state feedback, is presented The components of the force vector are considered as inputs to the aircraft, with the assumption that a desired force vector can be generated using appropriate control surface deflections An error between the commanded force vector and the actually obtained force vector is considered, which is in contrast to the assumptions made in the literature The MF-SMC method is extended to include this uncertainty Simulation results show that ignoring this uncertainty in the controller design may lead to substantial loss in performance All other uncertainties and disturbances are assumed to satisfy the matching conditions Analytical expressions for the control laws for two operational modes, namely the velocity tracking and the trimming are derived It can be seen from the developed control laws for the two modes in (3 35) and (3 46) that they depend on the estimated mass and inertia parameters and their expected range of variation only In a preliminary aircraft design project, these control laws can thus be used to generate the required forces and moments for some critical flight maneuvers which can be placed as targets to the aerodynamics and the propulsion groups This would enable the control group to have a more active role in such an exercise, and help in achieving the best possible performance from the airframe Numerical simulations on a fighter aircraft show the robustness of the control law An interesting feature of the trimming control law is that it does not require an algorithm or a trim map to specify the trim variables

Chapter 4

Multi-Loop SMC Laws for The Unmatched Uncertainty Case

4.1 Introduction

In the previous chapter, controller design for output tracking with matched uncertainty and disturbances was considered As seen there, the number of trackable outputs are limited by the number of independent inputs available This leaves out a portion of the dynamics, also called the internal dynamics, and is seen from (3 7) to be a function of the tracked outputs and the internal states An approach to control these internal states was to formulate the aircraft dynamics as a two time scale problem and use a multi-loop (ML) strategy The state vector was thus separated into fast and slow variables [49, 50] and a dynamic inversion based inner loop control law was then designed for the fast variables With the command signals for the fast variables as the input, an outer loop control law is designed to track the slow states, which gives the command signals to be tracked in the inner loop The inversion based control law was reported to give better responses as compared to a gain-scheduled linear law [49] Analysis for robustness was, however, not performed Azam and Singh [50] used an integral error feedback in the outer loop for robustness against parameter variations Both of the works cited above use conventional control surfaces as inputs and hence were limited to track the angular velocities in the inner loop and corresponding angular states in the outer loop However, with the force control approach (Section 3 2), control

of the entire state vector is possible, as is shown in this chapter

The presence of unmatched disturbances and uncertainties, $\mathbf{d}_2$ in (3 7) in the internal states, which was neglected in the works cited above, is a practical problem and leads to a degraded system performance This chapter deals with the design of SMC laws in the presence of unmatched uncertainties using the ML strategy A basic assumption used in this work is that the nominal unmatched dynamics are assumed to be acceptable Accordingly, tracking of the position state variables is accomplished in the outer loop considering the command velocity signals as the inputs A SMC law is designed in the inner loop so that the velocity states track these augmented velocity commands generated in the outer loops The ML strategy is shown to lead to a simpler propagation of disturbances in the outer loop to the inner loop using which robustness properties are evaluated in terms of the bounds on the tracking errors in the inner and the outer loops Simulation results for the nonlinear longitudinal dynamics of an aircraft are then presented The ML strategy is next applied to a higher order SISO system with unmatched disturbances and uncertainties The developments herein can be seen to be giving results similar to those of [67, 68] which uses the singular perturbation methods (SPMs) The SMC design method presented here requires the knowledge of the bounds as in the previous works [67, 68] It is shown that the conventional SMC design, with the modified way of selecting the switching gains, may be used to handle this problem

4.2 ML Strategy for Mechanical Systems

Many mechanical systems may be represented in the reduced form as in (3 6) and (3 7) as

$$\mathbf{V} = \mathbf{f}_1(\mathbf{X}, \mathbf{V}) + \mathbf{B}_1(\mathbf{X}, \mathbf{V})\mathbf{u} + \mathbf{d}_1, \tag{4 1}$$

$$\mathbf{X} = \mathbf{f}_2(\mathbf{X}, \mathbf{V}) + \mathbf{d}_2 \tag{4 2}$$

where $\mathbf{X}, \mathbf{V}$ and $\mathbf{u} \in \mathcal{R}^n$ represent the position and velocity state variables and the input vectors respectively, and $\mathbf{d}_1$ and $\mathbf{d}_2$ represent the combined influence of the exter-

nal disturbance and uncertainty vector and are given to be bounded d_{i_j} representing the j^{th} component of the disturbance vector $\mathbf{d}_i$ is bounded as $|d_{i_j}| \leq D_{i_j}$, $i = 1, 2$, $j = 1, \quad , n$ Let $\mathbf{Z} = [\mathbf{X}^T \ \mathbf{V}^T]^T$ Also $\mathbf{B}_1(\mathbf{Z})$ is assumed to be of full rank over the entire state space The other assumptions in Section 3 4 for matrix $\mathbf{B}_1$ hold in this chapter It is clear from the above system equation that with the velocity variables as the output, it has a strong relative degree of 1 Also, the above nonlinear system is seen to be in the reduced form [37, 52] The arguments of the various functions defined above are dropped if no confusion is likely to arise

As in the Section 3 4, (4 1) represents the matched dynamics and (4 2) gives the unmatched portion of the dynamics The ZD, for the class of systems defined above, were seen to be a special case of the unmatched dynamics (3 26) These equations in such systems generally are integrators of the velocity variables and as seen in the aircraft examples in Sections 3 5 1 and 3 5 2 are BIBS It is also seen from the system equation in (3 27) in Section 3 5 1 that the term $\mathbf{f}_2(\mathbf{X}, \mathbf{V})$ is actually separable in $\mathbf{X}$ and $\mathbf{V}$, i e it may be represented as $\mathbf{B}_2(\mathbf{X})\mathbf{V}$ Thus (4 2) may be rewritten as

$$\mathbf{X} = \mathbf{B}_2(\mathbf{X})\mathbf{V} + \mathbf{d}_2 \tag{4 3}$$

The earlier control laws (in Section 3 4) were designed neglecting the presence of $\mathbf{d}_2$ In this section, a ML strategy for the SMC is presented It is assumed that the desired trajectories for the velocity variables are specified $(\mathbf{V}_d, \mathbf{V}_d)$ and the associated desired position trajectories given by the nominal $\mathbf{X}$ dynamics (4 2) as

$$\mathbf{X}_d = \mathbf{B}_2(\mathbf{X}_d)\mathbf{V}_d \tag{4 4}$$

are acceptable For notational simplicity, $\mathbf{B}_{2d}$ will be taken to represent $\mathbf{B}_2(\mathbf{X}_d)$, and similarly $\mathbf{B}_2 = \mathbf{B}_2(\mathbf{X})$ from now on It is further required that $\mathbf{B}_2$ be nonsingular everywhere

The ML control scheme is shown in Fig 4 1 As can be seen from the figure an inner loop is used to synthesize $\mathbf{u}_{\text{com}}$ such that the velocity variables track an augmented signal $\mathbf{V}_a$ instead of the conventional $\mathbf{V}_d$ The outer loop is used to create the augmented signal for the inner loop such that the position tracking is within acceptable

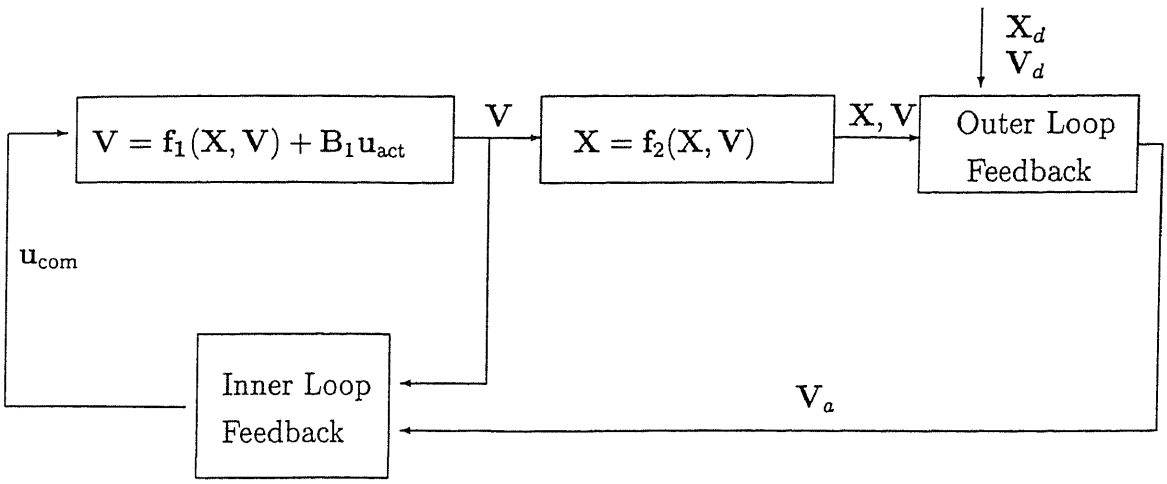

Fig. 4 1 Schematic Multi-Loop Control Scheme

bounds Accordingly bounds on the tracking errors in the inner and outer loops are developed as follows

Define $\mathbf{S}_x$ and $\mathbf{S}_v$ as vectors consisting of the error function for the position and velocity variables as

$$\mathbf{S}_x = \mathbf{X} - \mathbf{X}_d, \text{ and} \tag{4 5}$$

$$\mathbf{S}_v = \mathbf{V} - \mathbf{V}_a, \tag{4 6}$$

where, $\mathbf{V}_a$ is yet to be defined Taking the time derivative of $\mathbf{S}_x$ and using (4 3), $\mathbf{S}_x$ becomes

$$\mathbf{S}_x = \mathbf{B}_2\mathbf{V} + \mathbf{d}_2 - \mathbf{B}_{2d}\mathbf{V}_d \tag{4 7}$$

Using $\mathbf{V} = \mathbf{V}_a + \mathbf{S}_v$ from (4 6) in the above equation gives

$$\mathbf{S}_x = \mathbf{B}_2\mathbf{V}_a + \mathbf{B}_2\mathbf{S}_v + \mathbf{d}_2 - \mathbf{B}_{2d}\mathbf{V}_d \tag{4 8}$$

Note that the time derivative of $\mathbf{V}_a$ would be required for $\mathbf{V}$ to track $\mathbf{V}_a$ in the inner loop, therefore $\mathbf{V}_a$ should not have discontinuities and should be selected so as to make $\mathbf{S}_x$ as small as possible With the invertibility condition on $\mathbf{B}_2$, the command signal $\mathbf{V}_a$ for the inner loop is selected from (4 8) to cancel out the known terms and by

introducing a stabilizing feedback as

$$\mathbf{V}_a = \mathbf{B}_2^{-1}(\mathbf{B}_{2d}\mathbf{V}_d - \mathbf{K}_x\mathbf{S}_x), \tag{4 9}$$

where, $\mathbf{K}_x\mathbf{S}_x \in \mathcal{R}^n$ with its i^{th} component as $[\mathbf{K}_x\mathbf{S}_x]_i = K_{x_i}S_{x_i}$ and $K_{x_i} > 0$, $i = 1, \quad , n$ $\mathbf{K}_x$ is taken as a $n \times n$ real matrix as diag$[K_{x_1}, \quad , K_{x_n}]$

Using the $\mathbf{V}_a$ selected above in (4 8) gives $\mathbf{S}_x$ as

$$\mathbf{S}_x = -\mathbf{K}_x\mathbf{S}_x + \mathbf{B}_2\mathbf{S}_v + \mathbf{d}_2, \tag{4 10}$$

which is rewritten as

$$\mathbf{S}_x = \mathbf{T}_x + \mathbf{d}_2 \tag{4 11}$$

for simplicity, and $\mathbf{T}_x$ is obviously defined The S_{x_i} is thus seen to have the dynamics given by

$$S_{x_i} = -K_{x_i}S_{x_i} + [\mathbf{B}_2\mathbf{S}_v]_i + \mathbf{d}_{2_i} \tag{4 12}$$

The assumption of $\mathbf{f}_2 = \mathbf{B}_2\mathbf{V}$ has been used in the selection of $\mathbf{V}_a$ in (4 9) However, only the existence of the following map guarantees that there would exist a unique $\mathbf{V}_a$, such that

$$\mathbf{f}_2(\mathbf{X}, \mathbf{V}_a) = \mathbf{f}_2(\mathbf{X}_d, \mathbf{V}_d) - \mathbf{K}_x\mathbf{S}_x \tag{4 13}$$

From (4 12), it is seen that any bounds on the position error $\mathbf{S}_x$ depend on the velocity error $\mathbf{S}_v$ Hence, it is first necessary to check the $\mathbf{S}_v$ dynamics before any estimates of the $\mathbf{S}_x$ bounds can be made The time derivative of the $\mathbf{V}_a$ in (4 9) would be required for $\mathbf{V}$ to track $\mathbf{V}_a$ in the inner loop Snell et al [49] used a band limited filter to generate this time derivative Azam and Singh [50] used the nominal system equations (4 1) and (4 3) to evaluate the derivative However, the effect of disturbances and uncertainties was not directly considered in their study The time derivative of $\mathbf{V}_a$ is obtained from (4 9) as

$$\mathbf{V}_a = \frac{d}{dt}[\mathbf{B}_2^{-1}](\mathbf{B}_{2d}\mathbf{V}_d - \mathbf{K}_x\mathbf{S}_x) + \mathbf{B}_2^{-1}\frac{d}{dt}[\mathbf{B}_{2d}\mathbf{V}_d - \mathbf{K}_x\mathbf{S}_x] \tag{4 14}$$

The definitions and notations used in the present work to calculate the time derivatives of scalar, vector, and matrix functions of vectors are given in Appendix E A well

known result in matrix theory [69] gives that for a nonsingular matrix $\mathbf{B}_2$

$$\frac{d}{dt}[\mathbf{B}_2^{-1}] = -\mathbf{B}_2^{-1}[\frac{d}{dt}\mathbf{B}_2]\mathbf{B}_2^{-1} \tag{4 15}$$

Using the notation in (E 8) from Appendix E, the time derivative of $\mathbf{B}_2$ in the above equation is seen to be

$$\frac{d}{dt}[\mathbf{B}_2] = J_{B_2}[I_n \otimes \mathbf{X}], \tag{4 16}$$

where $\otimes$ represents the Kronecker product From (4 2), it is observed that $\mathbf{X} = \mathbf{f}_2 + \mathbf{d}_2$ Substituting this in the above equation gives

$$\frac{d}{dt}[\mathbf{B}_2] = J_{B_2}[I_n \otimes \mathbf{f}_2] + J_{B_2}[I_n \otimes \mathbf{d}_2] \tag{4 17}$$

Using (4 15) and (4 17) and $\mathbf{S}_x = \mathbf{T}_x + \mathbf{d}_2$ from (4 11), $\mathbf{V}_a$ in (4 14) becomes

$$\begin{aligned}
\mathbf{V}_a &= -\mathbf{B}_2^{-1}\frac{d}{dt}[\mathbf{B}_2]\mathbf{B}_2^{-1}(\mathbf{B}_{2d}\mathbf{V}_d - \mathbf{K}_x\mathbf{S}_x) + \mathbf{B}_2^{-1}(\frac{d}{dt}[\mathbf{B}_{2d}\mathbf{V}_d] - \mathbf{K}_x\mathbf{S}_x) \\
&= \mathbf{B}_2^{-1}[(\frac{d}{dt}[\mathbf{B}_{2d}\mathbf{V}_d] - \mathbf{K}_x\mathbf{T}_x - \mathbf{K}_x\mathbf{d}_2) \\
&\quad -(J_{B_2}[I_n \otimes \mathbf{f}_2] + J_{B_2}[I_n \otimes \mathbf{d}_2])\mathbf{B}_2^{-1}(\mathbf{B}_{2d}\mathbf{V}_d - \mathbf{K}_x\mathbf{S}_x)],
\end{aligned} \tag{4 18}$$

which may be rewritten as

$$\begin{aligned}
\mathbf{V}_a &= \mathbf{B}_2^{-1}\left(\frac{d}{dt}[\mathbf{B}_{2d}\mathbf{V}_d] - \mathbf{K}_x\mathbf{T}_x - J_{B_2}[I_n \otimes \mathbf{f}_2]\mathbf{B}_2^{-1}(\mathbf{B}_{2d}\mathbf{V}_d - \mathbf{K}_x\mathbf{S}_x)\right) \\
&\quad -\mathbf{B}_2^{-1}\left(\mathbf{K}_x\mathbf{d}_2 + J_{B_2}[I_n \otimes \mathbf{d}_2]\mathbf{B}_2^{-1}(\mathbf{B}_{2d}\mathbf{V}_d - \mathbf{K}_x\mathbf{S}_x)\right)
\end{aligned} \tag{4 19}$$

The above equation may be expressed as

$$\mathbf{V}_a = \mathbf{T}_a + \mathbf{d}_2', \tag{4 20}$$

where

$$\mathbf{T}_a = \mathbf{B}_2^{-1}\left(\frac{d}{dt}[\mathbf{B}_{2d}\mathbf{V}_d] - \mathbf{K}_x\mathbf{T}_x - J_{B_2}[I_n \otimes \mathbf{f}_2]\mathbf{B}_2^{-1}(\mathbf{B}_{2d}\mathbf{V}_d - \mathbf{K}_x\mathbf{S}_x)\right), \tag{4 21}$$

$$\text{and } \mathbf{d}_2' = -\mathbf{B}_2^{-1}\left(\mathbf{K}_x\mathbf{d}_2 + J_{B_2}[I_n \otimes \mathbf{d}_2]\mathbf{B}_2^{-1}(\mathbf{B}_{2d}\mathbf{V}_d - \mathbf{K}_x\mathbf{S}_x)\right) \tag{4 22}$$

It is seen from the above equation that $\mathbf{d}_2'$ contains the effects of disturbance terms $\mathbf{d}_2$, which was not considered in [50]

The dynamics of $\mathbf{S}_v$ may now be considered The time derivative of $\mathbf{S}_v$ in (4 6) is seen to be $\dot{\mathbf{S}}_v = \dot{\mathbf{V}} - \dot{\mathbf{V}}_a$, and using (4 1) and (4 20) it becomes

$$\dot{\mathbf{S}}_v = \mathbf{f}_1 + \mathbf{B}_1\mathbf{u} - \dot{\mathbf{T}}_a + \mathbf{d}_1 - \mathbf{d}_2' \tag{4 23}$$

Thus, it is seen that a ML strategy passes on the effect of the disturbances $\mathbf{d}_2$ in the outer loop to the inner loop as $\mathbf{d}_2'$ (4 22) as in the above equation, which can then be incorporated in the design process Using the augmented disturbance signal, the SMC as in (3 22) may still be designed by following the steps outlined in Section 3 4 S_{v_i} can thus be made to satisfy the reaching condition as in (3 18) and the S_{v_i} response is guaranteed to be better than

$$\dot{S}_{v_i} = -\eta_{v_i}\mathrm{sgn}[S_{v_i}] \tag{4 24}$$

as in (3 19) As in Section 3 4, the sgn[ ] term is replaced by a continuous term $\mathrm{sat}(S_{v_i}/\phi_{v_i})$, where ϕ_{v_i} represents the i^{th} component of the selected boundary layer thickness vector (Φ_v) With the reaching times t_{0_i} as given in (3 25), all the S_{v_i}'s will be bounded after some finite time t_{0_m} $(= \max[t_{0_i},\ i = 1,\ \ldots,n]$, where max[, .,] gives the maximum of its arguments) as

$$|S_{v_i}| \leq \phi_{v_i} \tag{4 25}$$

With the velocity error $\mathbf{S}_v$ bounded as above, the effect of the $[\mathbf{B}_2\mathbf{S}_v]_i$ term in the $\dot{S}_{x_i}$ dynamics in (4 12) is seen to be bounded by the sum $\sum_j(|\mathbf{B}_2|_{ij}\phi_{v_j})$ and may be considered as an additional disturbance term for all $t > t_{0_m}$ It can be shown that the error S_{x_i} is globally uniformly ultimately bounded (see Appendix F) as

$$|S_{x_i}| \leq \frac{[|\mathbf{B}_2|\Phi_v + \mathbf{D}_2]_i}{K_{x_i}} \tag{4 26}$$

Thus it is seen that the $\mathbf{S}_x$ and $\mathbf{S}_v$ errors defined in (4 5) and (4 6) remain within bounds as specified in (4 26) and (4 25) respectively The bounds on $\mathbf{S}_v$ (4 25) is directly governed by the choice of Φ_v The bound on $\mathbf{S}_x$ (4 26) may be lowered by choosing a higher value for the K_{x_i}, however, it is observed that the bound on $K_{x_i}S_{x_i}$ does not change It directly depends on the size of the unmatched uncertainties $\mathbf{D}_2$ and the selected boundary layer thicknesses Φ_v

Another point of interest is to find out the magnitude of the difference between the $\mathbf{V}_d$ and $\mathbf{V}_a$ signals From (4 9) it is seen that

$$\mathbf{V}_d - \mathbf{V}_a = [I - \mathbf{B}_2^{-1}\mathbf{B}_{2d}]\mathbf{V}_d + \mathbf{B}_2^{-1}\mathbf{K}_x\mathbf{S}_x \tag{4 27}$$

The difference $\mathbf{V}_d - \mathbf{V}_a$ is seen to be equal to 0 if and only if $\mathbf{S}_x = 0$, since it also implies that $\mathbf{B}_2^{-1}\mathbf{B}_{2d} = I$ However, as $\mathbf{S}_x$ is only guaranteed to be within some bounds, there will be a finite error between the two signals

Thus it is seen that the SMC method can be applied to the unmatched uncertainty case using a ML framework and bounds for the errors in the loops may be derived as shown here The method developed for a general mechanical system is next validated by applying it to the aircraft longitudinal dynamics

4.3 SMC Design for Aircraft Velocity Tracking

In this section, the ML controller design for the unmatched uncertainty case as discussed in the previous section is applied to the aircraft example in Section 3 5 1 The state equations for this case are already reported in (3 27) The matched dynamics representing the velocity dynamics in (4 1) remain the same as earlier Thus, the $\mathbf{V}$ in this chapter represents the velocity vector $[U, W, Q]^{\mathrm{T}}$ However, the unmatched uncertainties, which were not considered in Chapter 3, appear in the $\mathbf{X}$ dynamics as in (4 2) Rearranging the last three equations of (3 27) with the corresponding states being given by $\mathbf{X} = [p_x,\ p_z,\ \theta]^{\mathrm{T}}$, the governing equations may be rewritten as

$$\begin{pmatrix} p_x \\ p_z \\ \theta \end{pmatrix} = \begin{pmatrix} U\cos(\theta) + W\sin(\theta) \\ U\sin(\theta) - W\cos(\theta) \\ Q \end{pmatrix} + \begin{pmatrix} d_{2x} \\ d_{2z} \\ d_{2\theta} \end{pmatrix} \tag{4 28}$$

The $\mathbf{f}_2$ as defined in (4 2) is seen from the above equation as

$$\mathbf{f}_2 = \begin{bmatrix} \cos(\theta) & \sin(\theta) & 0 \\ \sin(\theta) & -\cos(\theta) & 0 \\ 0 & 0 & 1 \end{bmatrix} \begin{pmatrix} U \\ W \\ Q \end{pmatrix} = \mathbf{B}_2\mathbf{V} \tag{4 29}$$

From the above equation, it is seen that the position state dynamics $\mathbf{X}$ as given in (4 28) is in the form of (4 3) It is easily verified that the matrix $\mathbf{B}_2$ in the above equation is non-singular As in Section 3 5 1, the nominal ZD (3 28) is seen to be BIBS

The error $\mathbf{S}_x$ (4 5) in the position variables is defined as $[S_x,\ S_z,\ S_\theta]^{\mathrm{T}}$ and is given by

$$\begin{pmatrix} S_x \\ S_z \\ S_\theta \end{pmatrix} = \begin{pmatrix} p_x - p_{xd} \\ p_z - p_{zd} \\ \theta - \theta_d \end{pmatrix} \tag{4 30}$$

Note that $\mathbf{S}_x$ represents a vector quantity, whereas the S_x is a scalar quantifying the x position error Similarly, $\mathbf{K}_x$ represents diag$[K_x,\ K_z,\ K_\theta]$ While K_x is a scalar quantity representing the feedback gain of S_x, the $\mathbf{K}_x$ is a 3×3 matrix Similarly, the velocity error $\mathbf{S}_v = \mathbf{V} - \mathbf{V}_a$ in (4 6), where the augmented signal $\mathbf{V}_a = [U_a, W_a, Q_a]^{\mathrm{T}}$ will be chosen as in (4 9), represents the column vector $[S_U, S_W, S_Q]^{\mathrm{T}}$

With the $\mathbf{B}_2$ matrix as defined in (4 29), the $\mathbf{S}_x$ dynamics in (4 12) may be evaluated to get

$$\begin{aligned} \dot{S}_x &= -K_x S_x + S_U \cos(\theta) + S_W \sin(\theta) + d_{2x}, \\ \dot{S}_z &= -K_z S_z + S_U \sin(\theta) - S_W \cos(\theta) + d_{2z}, \text{and} \\ \dot{S}_\theta &= -K_\theta S_\theta + S_Q + d_{2\theta}, \end{aligned} \tag{4 31}$$

and the augmented signal $\mathbf{V}_a$ in this case can be derived from (4 9) as

$$\begin{pmatrix} U_a \\ W_a \\ Q_a \end{pmatrix} = \begin{pmatrix} U_d \cos(S_\theta) - W_d \sin(S_\theta) - K_x S_x \cos(\theta) - K_z S_z \sin(\theta) \\ U_d \sin(S_\theta) + W_d \cos(S_\theta) - K_x S_x \sin(\theta) + K_z S_z \cos(\theta) \\ Q_d - K_\theta S_\theta \end{pmatrix} \tag{4 32}$$

Its derivative $\dot{\mathbf{V}}_a$ in (4 19) may be evaluated as shown below As $\mathbf{B}_2$ in (4 29) for this problem is a function of θ only, it is seen that for a column vector $C = [C_x,\ C_z,\ C_\theta]^{\mathrm{T}}$,

$J_{B_2}[I \otimes C]$ as required in (4 21) and (4 22) may be evaluated as

$$J_{B_2}[I \otimes C] = C_\theta M_{1\theta} = C_\theta \begin{bmatrix} -\sin(\theta) & \cos(\theta) & 0 \\ \cos(\theta) & \sin(\theta) & 0 \\ 0 & 0 & 0 \end{bmatrix} \tag{4 33}$$

Moreover, the following result may be easily established by matrix multiplication for the system under study

$$-\mathbf{B}_2^{-1} M_{1\theta} \mathbf{B}_2^{-1} = M_{1\theta} \tag{4 34}$$

Combining (4 33) and (4 34), it is seen that

$$-\mathbf{B}_2^{-1} J_{B_2}[I_n \otimes C]\mathbf{B}_2^{-1} = C_\theta M_{1\theta} \tag{4 35}$$

From (4 15) and (4 16), it is seen that $\frac{d}{dt}[\mathbf{B}_2^{-1}] = -\mathbf{B}_2^{-1} J_{B_2}[I_n \otimes \mathbf{X}]\mathbf{B}_2^{-1}$ Here $C = \mathbf{X}$ Thus, using $C_\theta = \theta = Q + d_{2\theta}$ from (4 28), the above equation gives $\frac{d}{dt}[\mathbf{B}_2^{-1}]$ as

$$\frac{d}{dt}[\mathbf{B}_2^{-1}] = -\mathbf{B}_2^{-1} J_{B_2}[I_n \otimes \mathbf{X}]\mathbf{B}_2^{-1} = (Q + d_{2\theta}) M_{1\theta} \tag{4 36}$$

The quantity $\mathbf{T}_a$ in (4 21) and $\mathbf{d}_2'$ in (4 22) may be simplified using the equality in (4 35) to get

$$\begin{aligned} \mathbf{T}_a &= \mathbf{B}_2^{-1}\left(\frac{d}{dt}[\mathbf{B}_{2d}\mathbf{V}_d] - \mathbf{K}_x\mathbf{T}_x\right) + QM_{1\theta}(\mathbf{B}_{2d}\mathbf{V}_d - \mathbf{K}_x\mathbf{S}_x), \text{ and} \\ \mathbf{d}_2' &= -\mathbf{B}_2^{-1}\mathbf{K}_x\mathbf{d}_2 + d_{2\theta}M_{1\theta}(\mathbf{B}_{2d}\mathbf{V}_d - \mathbf{K}_x\mathbf{S}_x) \end{aligned} \tag{4 37}$$

The various terms in $\mathbf{T}_a$ may now be evaluated as follows

$$\mathbf{B}_2^{-1}\frac{d}{dt}[\mathbf{B}_{2d}\mathbf{V}_d] = \begin{pmatrix} U_d\cos(S_\theta) - W_d\sin(S_\theta) + \theta_d U_d\sin(S_\theta) + \theta_d W_d\cos(S_\theta) \\ U_d\sin(S_\theta) + W_d\cos(S_\theta) - \theta_d U_d\cos(S_\theta) + \theta_d W_d\sin(S_\theta) \\ Q_d \end{pmatrix} \tag{4 38}$$

From the $\mathbf{S}_x$ dynamics in (4 31), and the definition of $\mathbf{T}_x$ (4 11), one can obtain

$$-\mathbf{B}_2^{-1}\mathbf{K}_x\mathbf{T}_x = \begin{pmatrix} K_x^2 S_x\cos(\theta) + K_z^2 S_z\sin(\theta) - K_x S_U cos^2(\theta) - K_z S_U sin^2(\theta) \\ -K_x S_W\sin(\theta)\cos(\theta) + K_z S_W\sin(\theta)\cos(\theta) \\ K_x^2 S_x\sin(\theta) - K_z^2 S_z\cos(\theta) - K_x S_W sin^2(\theta) - K_z S_W cos^2(\theta) \\ -K_x S_U\sin(\theta)\cos(\theta) + K_z S_U\sin(\theta)\cos(\theta) \\ K_\theta^2 S_\theta - K_\theta S_Q \end{pmatrix} \tag{4 39}$$

The third term of $\mathbf{T}_a$ is obtained as

$$QM_{1\theta}(\mathbf{B}_{2d}\mathbf{V}_d - \mathbf{K}_x\mathbf{S}_x) = Q\begin{pmatrix} -U_d\sin(S_\theta) - W_d\cos(S_\theta) + K_xS_x\sin(\theta) - K_zS_z\cos(\theta) \\ U_d\cos(S_\theta) - W_d\sin(S_\theta) - K_xS_x\cos(\theta) - K_zS_z\sin(\theta) \\ 0 \end{pmatrix} \quad (4\ 40)$$

The complete $\mathbf{T}_a$ in (4 21) may be obtained by summing up the contributions of the three terms given in (4 38), (4 39), and (4 40) above The $\mathbf{T}_a$ is seen to be a 3×1 vector whose components will be represented as $[T_a^U, T_a^W, T_a^Q]^{\mathrm{T}}$

Similarly the two terms in $\mathbf{d}_2'$ in (4 37) may be evaluated as

$$-\mathbf{B}_2^{-1}\mathbf{K}_x\mathbf{d}_2 = \begin{pmatrix} -K_xd_{2x}\cos(\theta) - K_zd_{2z}\sin(\theta) \\ -K_xd_{2x}\sin(\theta) + K_zd_{2z}\sin(\theta) \\ -K_\theta d_{2\theta} \end{pmatrix}, \text{ and} \quad (4\ 41)$$

$$d_{2\theta}M_{1\theta}(\mathbf{B}_{2d}\mathbf{V}_d - \mathbf{K}_x\mathbf{S}_x) = d_{2\theta}\begin{pmatrix} -U_d\sin(S_\theta) - W_d\cos(S_\theta) + K_xS_x\sin(\theta) - K_zS_z\cos(\theta) \\ U_d\cos(S_\theta) - W_d\sin(S_\theta) - K_xS_x\cos(\theta) - K_zS_z\sin(\theta) \\ 0 \end{pmatrix} \quad (4\ 42)$$

A conservative bound $\mathbf{D}_2'$ on the disturbance term $\mathbf{d}_2'$ can be obtained, by taking the sum of the absolute values of the two contributing terms in (4 41) and (4 42), as

$$\mathbf{D}_2' = \begin{pmatrix} K_xD_{2x}|\cos(\theta)| + K_zD_{2z}|\sin(\theta)| \\ +D_{2\theta}\left[|U_d\sin(S_\theta)| + |W_d\cos(S_\theta)| + K_x|S_x| + K_z|S_z|\right] \\ K_xD_{2x}|\sin(\theta)| + K_zD_{2z}|\sin(\theta)| \\ +D_{2\theta}\left[|U_d\cos(S_\theta)| + |W_d\sin(S_\theta)| + K_x|S_x| + K_z|S_z|\right] \\ K_\theta D_{2\theta} \end{pmatrix} \quad (4\ 43)$$

The time derivative of the augmented signal $\mathbf{V}_a$ in (4 32) may be obtained using the above developments and $\mathbf{V}_a = \mathbf{T}_a + \mathbf{d}_2'$ from (4 20) With $\mathbf{d}_2'$ and its bound $\mathbf{D}_2'$ (4 43) as obtained above, the total disturbance term in $\mathbf{S}_v$ dynamics (4 23) is seen to be bounded by $\mathbf{D}_1 + \mathbf{D}_2'$ The Ψ_i, $i = 1, 2, 3$ (3 34) would now include the terms

arising due to $\mathbf{D}_2'$ also However, the gains k_i, $i = 1, 2, 3$ will have the same functional dependence on Ψ_i as in the Section 3 5 1 Thus the control law in (3 35) is modified with the new $\mathbf{V}_a$ signals, and gives the new control law as

$$\begin{aligned} F_{x_{\text{com}}} &= \frac{1}{\hat{R}_m}\left(T_a^U + QW + g_0 \sin(\theta) - k_1 \text{sat}(\frac{S_U}{\phi_U})\right), \\ F_{z_{\text{com}}} &= \frac{1}{\hat{R}_m}\left(T_a^W - QU - g_0 \cos(\theta) - k_2 \text{sat}(\frac{S_W}{\phi_W})\right), \text{ and} \\ M_{\text{com}} &= \frac{1}{\hat{c}_7}\left(T_a^Q - k_3 \text{sat}(\frac{S_Q}{\phi_Q})\right) \end{aligned} \tag{4 44}$$

With the above control law, the associated tracking errors $\mathbf{S}_v$ are guaranteed to stay bounded inside the boundary layers $\Phi_v = [\phi_U,\ \phi_W,\ \phi_Q]^{\mathrm{T}}$ as discussed earlier The results obtained from the simulation using the parameters of the aircraft problem considered in Section 3 5 1 are next presented

4.3.1 Simulation Results

The numerical values of the unmatched uncertainties and disturbances and their bounds are given in Appendix D The variation in the reciprocal of aircraft mass R_m and inverse of the pitching moment of inertia c_7 as considered for the simulation are as shown in Fig 4 2 The pilot maintains the equilibrium value of the control inputs till 0 5s and then applies an elevator doublet of magnitude $\pm 15^0$ and a simultaneous throttle doublet of ± 25 units with a total time period of 1 0s The inputs are then restored to the equilibrium values at 1 5s and maintained thereafter The $\triangle ae$ uncertainty as given for the case UC1 in the Appendix D is used in the simulation For comparison purposes, responses were obtained using the control law in (3 35) which was designed under the assumption of $\mathbf{d}_2 = 0$, to show the effect of the presence of these disturbances These responses are termed as R_0 in the following discussion The responses were obtained for four sets of $K_i, i = 1,$, 4 (the corresponding responses obtained are accordingly termed R_i) to find out the effect of variation of the individual feedback gains in the outer loop Note that K_i's are vectors given as $[K_x,\ K_z,\ K_\theta]_i^{\mathrm{T}}$ The gain values are taken as $K_1 = [0\ 1,\ 0\ 1,\ 10\ 0]^{\mathrm{T}}$, $K_2 = [1\ 0,\ 1\ 0,\ 1\ 0]^{\mathrm{T}}$, $K_3 = [5\ 0,\ 5\ 0,\ 5\ 0]^{\mathrm{T}}$, and

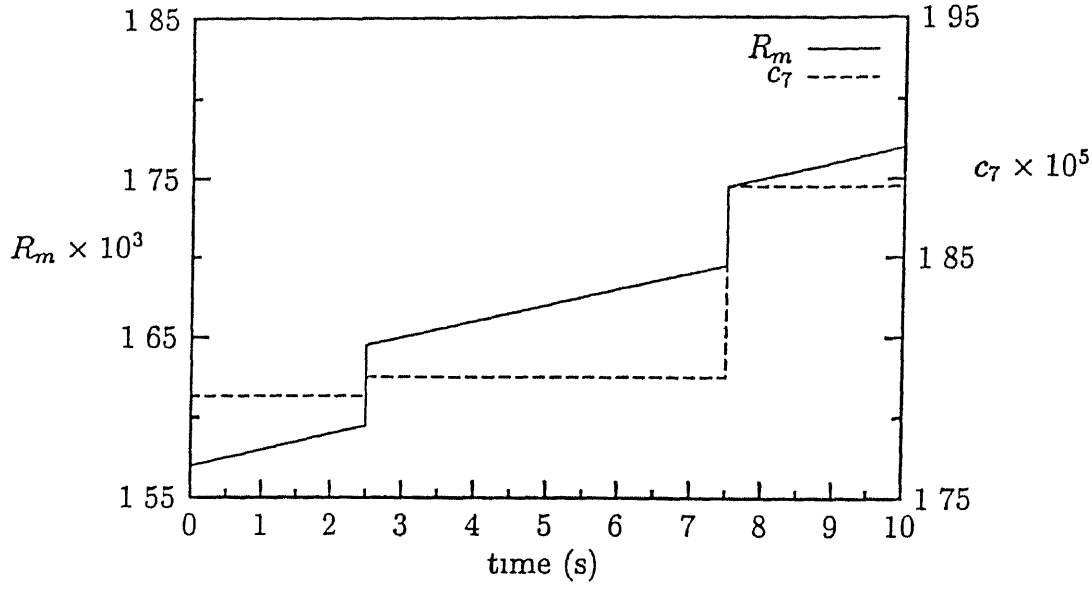

Fig. 4.2 Variation in the R_m and the c_7 parameters of the aircraft

$K_4 = [1\,0,\ 1\,0,\ 10\,0]^{\mathrm{T}}$ Also, Φ_v is taken as $[0\,5,\ 0\,5,\ 5\,0 \times 10^{-4}]^{\mathrm{T}}$ and $\eta_{v_i} = 1\,0$ Numerical simulation was done using the fourth order Runge-Kutta algorithm with a time step of 50μs

With the boundary layers for S_v selected as Φ_v and B_2 as defined in (4 29), a conservative estimate of the bounds on $|\mathrm{S}_x|$ may be derived from (4 26) as

$$\begin{aligned} |S_x| &\leq \frac{\phi_U + \phi_W + D_{2x}}{K_x}, \\ |S_z| &\leq \frac{\phi_U + \phi_W + D_{2z}}{K_z}, \text{ and} \\ |S_\theta| &\leq \frac{\phi_Q + D_{2\theta}}{K_\theta}. \end{aligned} \tag{4.45}$$

Using numerical values, the bounds on S_x, S_z, and S_θ may be seen to be 20 0, 20 0, and 0 03 respectively for the gains in case R_1, 2 0, 2 0, and 0 3 in case R_2, 0 4, 0.4, and 0 06 for R_3, and 2 0, 2 0, and 0 03 for R_4 Note that R_0 does not satisfy any such bounds

From (4 45) it is clear that the S_x can be made arbitrarily small by an appropriate choice of K_x This improvement in position tracking is obtained at the cost of a decreased velocity tracking performance in the sense that the controller is tracking V_a

(4 32) instead of the desired $\mathbf{V}_d$ Therefore, it is important to look at the difference between the two signals It follows directly from (4 27) that

$$\begin{pmatrix} U_d - U_a \\ W_d - W_a \\ Q_d - Q_a \end{pmatrix} = \begin{pmatrix} U_d[1 - \cos(S_\theta)] + W_d \sin(S_\theta) + K_x S_x \cos(\theta) + K_z S_z \sin(\theta) \\ -U_d \sin(S_\theta) + W_d[1 - \cos(S_\theta)] + K_x S_x \sin(\theta) - K_z S_z \cos(\theta) \\ K_\theta S_\theta \end{pmatrix} \tag{4 46}$$

Although the $\mathbf{S}_x$ can be made small as discussed earlier, the $[\mathbf{K}_x \mathbf{S}_x]_i$ terms as in the above equation are seen from (4 45) to be bounded Under the condition of small S_θ ($\cos(S_\theta) = 1$, and $\sin(S_\theta) = S_\theta$) for an appropriately large K_θ, and using the bounds on the $\mathbf{S}_x$ from (4 45), $\mathbf{V}_d - \mathbf{V}_a$ in the above equation can be simplified and approximate bounds on its variations are obtained as

$$\begin{pmatrix} |U_d - U_a| \\ |W_d - W_a| \\ |Q_d - Q_a| \end{pmatrix} = \begin{pmatrix} |W_d||S_\theta| + 2(\phi_U + \phi_W) + D_{2x} + D_{2z} \\ |U_d||S_\theta| + 2(\phi_U + \phi_W) + D_{2x} + D_{2z} \\ \phi_Q + D_{2\theta} \end{pmatrix} \tag{4 47}$$

For aircraft trajectories in the low angle of attack regimes $U_d >> W_d$, and hence the above equation indicates that the error $W_d - W_a$ is expected to be larger than $U_d - U_a$ Note that even if $S_\theta = 0\ 0$, there will be a finite error between the desired and the augmented velocity signals leading to a compromised velocity tracking The magnitude of this error is seen from the above equation to depend on the selected boundary layer thicknesses Φ_v and the bounds on the unmatched disturbances and uncertainties as given by $\mathbf{D}_2$

The tracking error with respect to the desired response $\mathbf{V}_d$ of the velocity outputs (U, W and Q) are shown in Figs 4 3, 4 4, and 4 5 respectively for the five responses (R_0 to R_4) With the inner loop control law, the velocities were seen to be tracking the augmented signals $\mathbf{V}_a$ within the specified boundary layers (Φ_v) Thus the tracking errors $\mathbf{V} - \mathbf{V}_d$ are presented in these figures instead of the $\mathbf{S}_v$ in (4 6), as the actual tracking errors are of direct interest It is observed from these figures that velocity tracking in R_0 has the best response in all these figures However, as the augmented velocity signals are tracked for the various gain cases all the other cases show a com-

promised velocity tracking As discussed earlier the errors $W - W_d$ ($\approx W_a - W_d$) in Fig 4 4 are seen to be much larger than the $U - U_d$ ($\sim U_a - U_d$) signal in Fig 4 3

Figs 4 6, 4 7, and 4 8 show the errors in θ, p_x and p_z from their desired values $\mathbf{X}_d$ Here, as expected, it was found that R_0 shows the worst response In fact the errors in the θ, p_x, and p_z at $t = 10$ 0s are seen to be about 0 4rad, 161ft, and 1048ft respectively Responses for the other cases are a lot better, and as would be expected the best responses are obtained for the higher feedback gains The position variable responses for the R_0 case are not shown in the figures as errors in these variables are very large

It is seen from Fig 4 6 that increasing the gain K_θ results in better θ tracking and smaller S_θ as is also evident from (4 45) As the K_θ gain is increased from 1 0 in K_2 to 5 0 in K_3 and finally to 10 0 in cases K_1 and K_4, better responses are obtained Also seen from the figure is the fact that the responses R_1 and R_4 with the same value of $K_\theta = 10$ 0 almost overlap An increase in K_θ would give smaller deviations $|\mathbf{V}_d - \mathbf{V}_a|$ for the translational velocity signals (U and W) as would be expected from (4 47) This is also seen from the $\mathbf{V} - \mathbf{V}_d$ plots for the two translational velocities in Figs 4 3 and 4 4 The responses R_1 and R_4 in these figures are seen to be much better than the others and are almost overlapping However, the better θ tracking would be achieved only with an associated increase in the $Q_a - Q_d$ error Since $S_Q = Q - Q_a$ is guaranteed to be smaller than $\phi_Q = 5 \times 10^{-4}$, this may be seen from the $Q - Q_d$ response in Fig 4 5 also The figure shows larger deviations from the Q_d as the K_θ gains are increased from K_2 to K_3 to the maximum value of 10 0 in the gains K_1 and K_4 Here also, the R_1 and R_4 responses are seen to be coinciding The $|Q_d - Q_a|$ in (4 47) is bounded by $\phi_Q + D_{2\theta} = 0$ 3005 from the numerical values used All the responses in Fig 4 5 are seen to satisfy this bound

Also as the K_x and K_z feedback gains are increased from K_1 to K_2 to K_3, a better position tracking of the remaining variables, i e the p_x and p_z is seen from the Figs 4 7 and 4 8 It is observed in these figures also that as the corresponding K_x and K_z gains are same in the gain sets K_2 and K_4, the responses R_2 and R_4 are seen to be

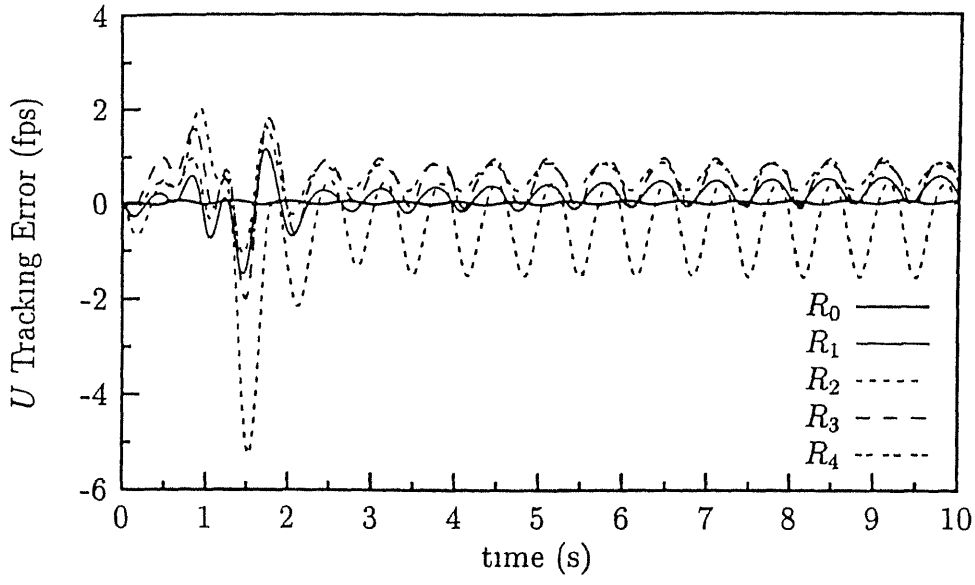

Fig. 4.3 Tracking error $U - U_d$ (fps).

almost same, with their curves almost overlapping Thus it is seen that, the gains have a decoupled effect on the related position tracking error, i e a change only in K_θ effects almost primarily the S_θ, similarly a change in K_x changes the S_x, and so on In all cases an increase in the gains is seen to lead to better position tracking as was expected However, it is observed that as the gain K_θ is increased to a maximum in the gain sets K_1 and K_4 with the corresponding gains K_x and K_z remaining the same, the deviation of the actual translational velocities from their desired signals are minimized as is expected from the discussions above Thus, a feasible choice of the gains would have a large K_θ, with K_x and K_z selected possibly smaller to have an acceptably large S_x and S_z position errors The high value of K_θ would lead to a lesser deviation in the generated U_a and W_a signals from their desired values and still achieve an acceptably small S_θ error, by marginally higher errors between the Q_a and Q_d signals, while allowing for slightly larger errors in the p_x and p_z

In all the cases the bounds on the position errors estimated using the (4 45) are seen to be satisfied in the Figs 4 6, 4.7 and 4 8 Thus, it is seen that with the outer loop feedback, better position tracking may be obtained at the cost of velocity

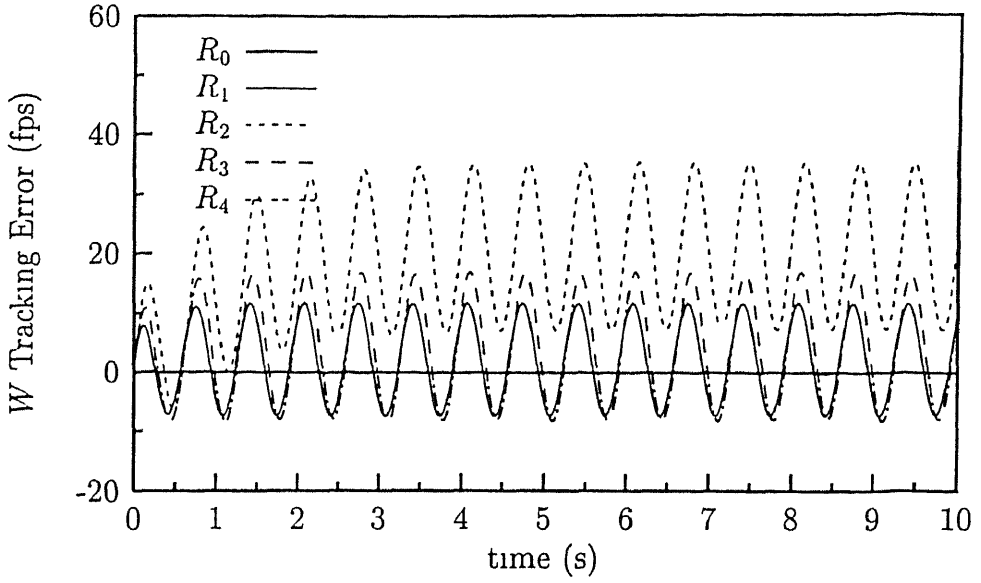

Fig. 4.4 Tracking error $W - W_d$ (fps) Note that responses R_1 and R_4 overlap

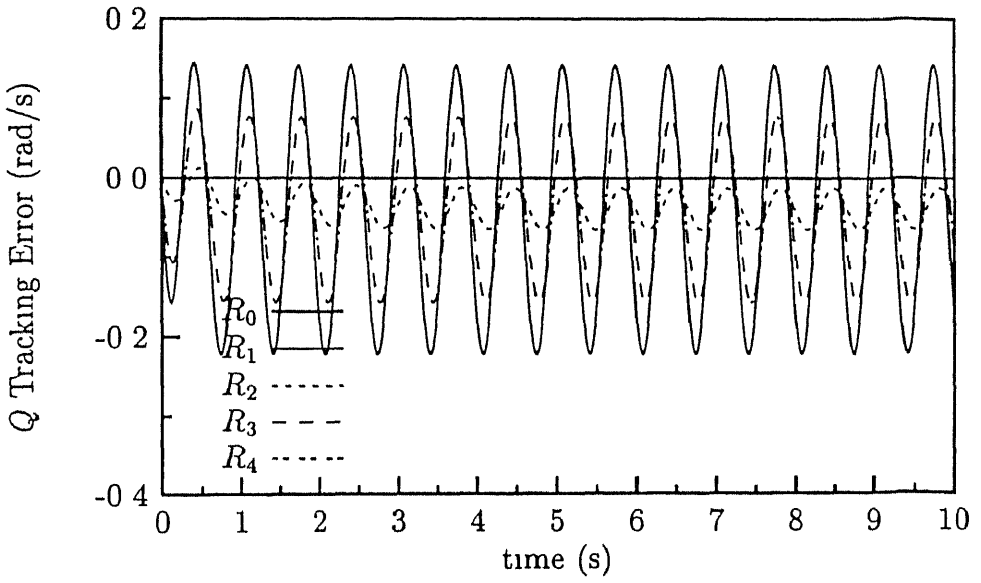

Fig. 4.5 Tracking error $Q - Q_d$ (rad/s) Note that responses R_1 and R_4 are overlapping

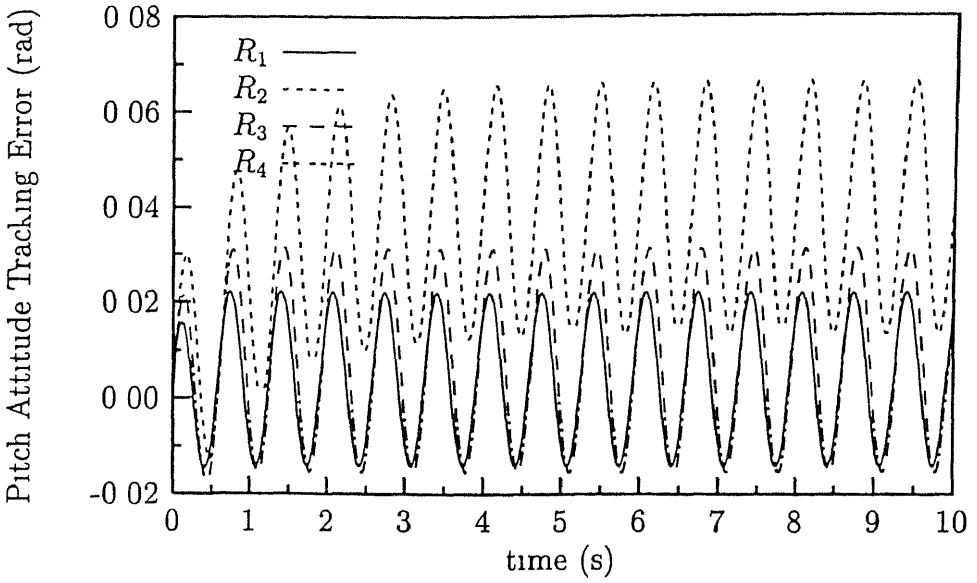

Fig. 4.6 The position tracking error $S_\theta = \theta - \theta_d$ (rad) Responses R_1 and R_4 are overlapping

tracking accuracy This then sets up a tradeoff for the control law designer, and the actual gain values may be appropriately selected for the various operational regimes and requirements

The commanded forces and moments along with their actually achieved values in the R_4 case are shown in Figs 4 9, 4 10, and 4 11 respectively Thus, the results of the numerical simulation show that the error bounds, as calculated using (4 45), are satisfied and validate the the SMC control laws in (4 44) For the general mechanical systems and the aircraft problem, as considered in Sections 4 2 and 4 3, with velocities as the primary outputs, the method has essentially been applied to systems with a strong relative degree of 1 The method is next extended for systems having higher relative degrees

4.4 ML Analysis for Higher Order SISO Systems

In this section, the ML strategy is applied to a higher order single input (SI) system with unmatched uncertainties The controller design for the unmatched uncertainty case

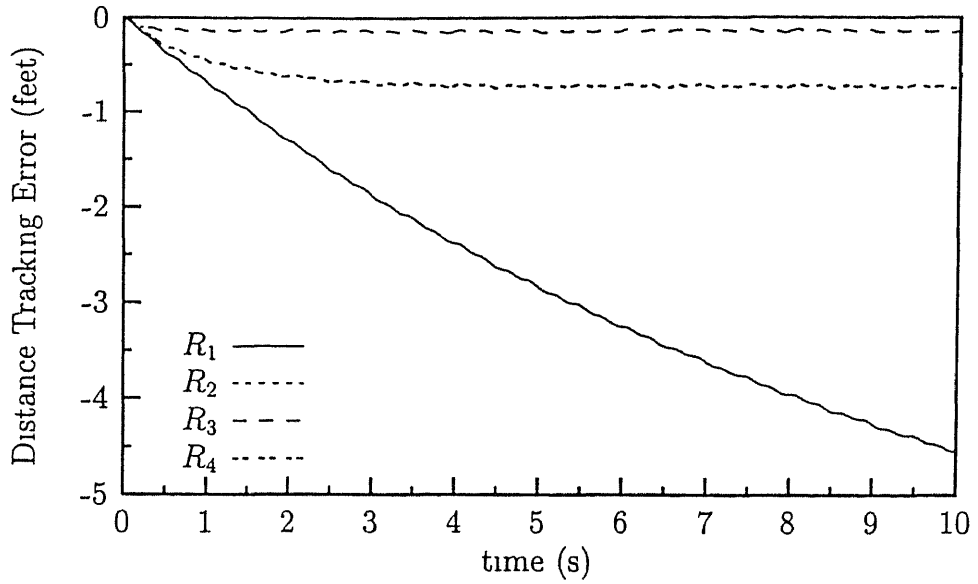

Fig. 4.7 The position tracking error $S_x = p_x - p_{x_d}$ (ft) Responses R_2 and R_4 overlap

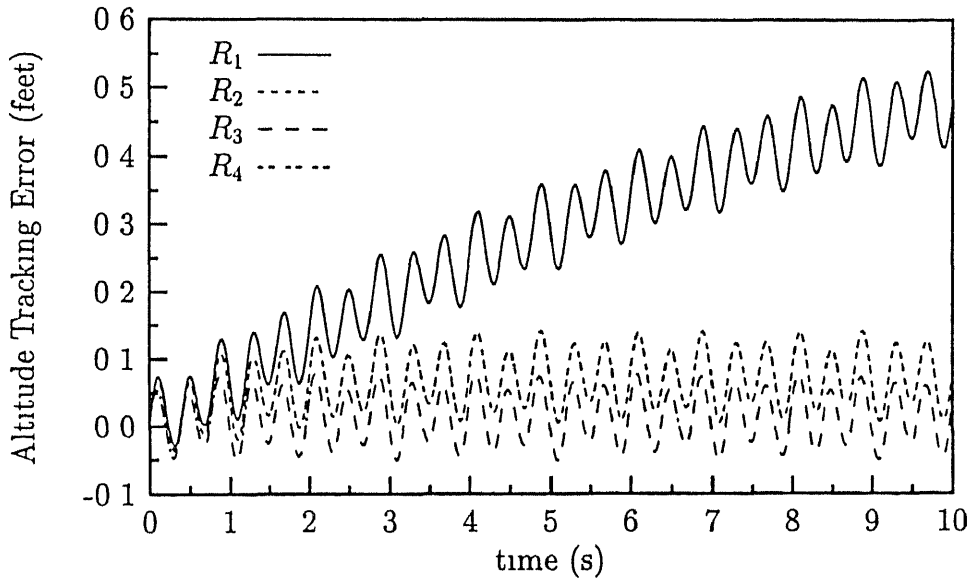

Fig. 4.8 The position tracking error $S_z = p_z - p_{z_d}$ (ft) Note that R_2 and R_4 are overlapping

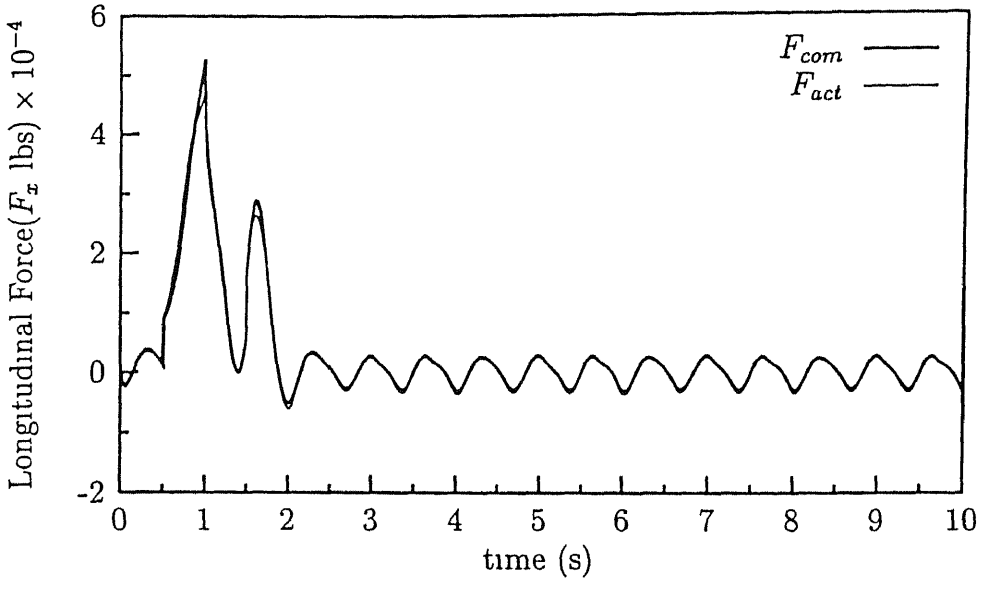

Fig 4.9 The command and achieved F_x

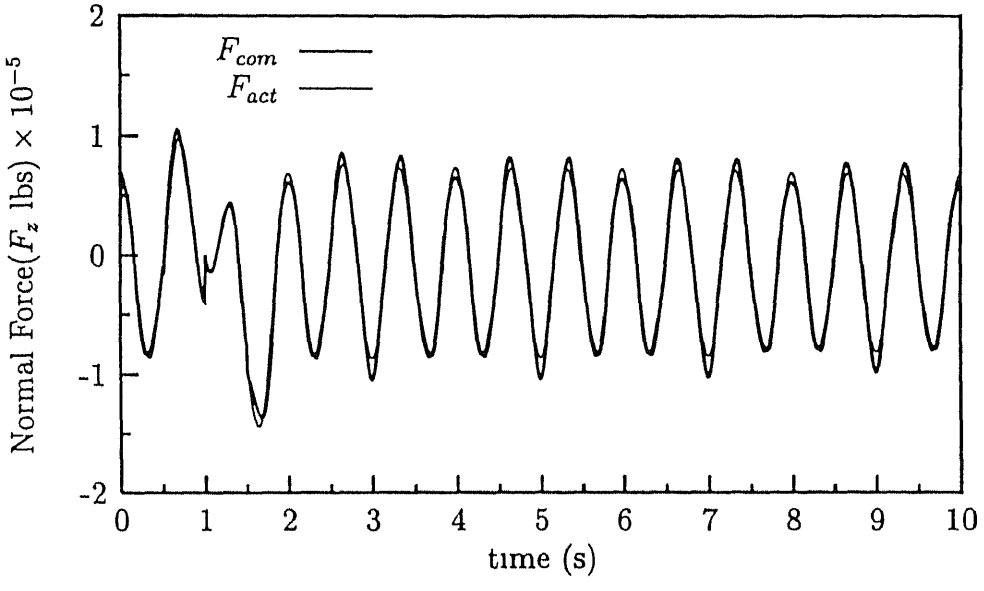

Fig. 4.10 The command and achieved F_z

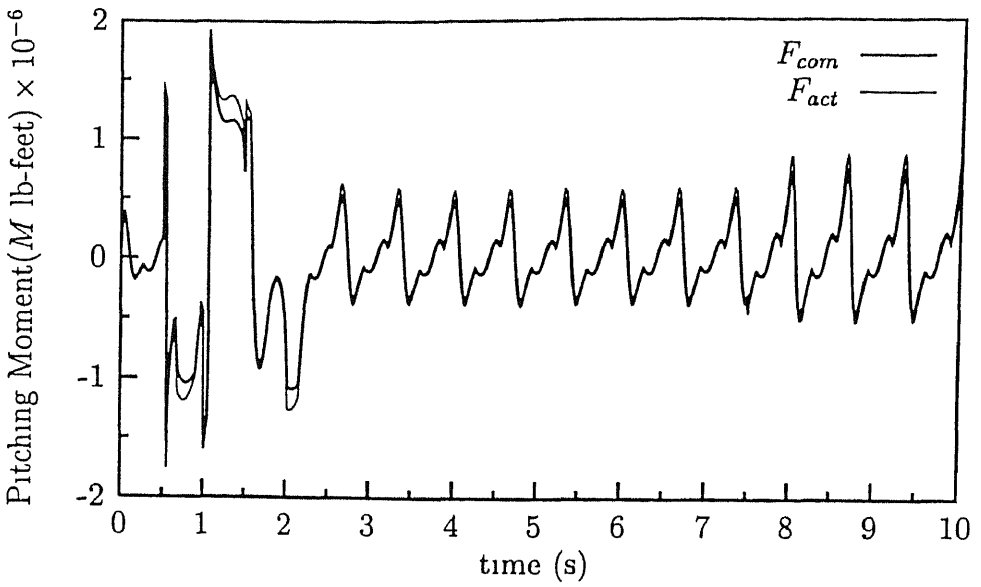

Fig. 4.11 The command and achieved M

has been considered by many researchers Spurgeon [51] and Spurgeon and Davies [52] however fail to address the effect of the disturbances and uncertainties on the ZD of the system They also require an assumption on the decomposability of uncertainty into matched and unmatched portions Hui and Zak [70] using similar assumptions show the practical stability of the system using both state and estimator feedback Under the above condition on the uncertainties Liao et al. [53] design continuous control laws to guarantee global stability and uniform boundedness of the tracking error The effect of the disturbances on the ZD is considered However, the verification of some of the assumptions on the disturbances is not trivial Qu [71] introduced equivalently matched uncertainties which satisfy some Lyapunov related bounds and designed continuous control laws to achieve global asymptotic stabilization Qu [72] relaxed the standard matching conditions to generalized matching conditions and a recursive procedure to design a continuous control law was proposed Cong and Landers [73] design control laws under some conditions to be satisfied by the input distribution matrix The effect on the ZD is not considered though Li et al [68], using singular perturbation methods (SPMs) design a high gain control law using stable combinations of variables, which

they call the stable combined variable perturbation method (SCVPM),under conditions to be met by the disturbance terms affecting the ZD They relax the requirement of the decomposability assumption Li et al [67] generalize the results of their earlier work to give more results about the types of Lyapunov stability achievable under varying conditions Wu and Chou [74] use a time varying singular perturbation method In the next section, a ML framework is applied to higher order nonlinear systems and a SMC law is developed It is shown that the method degenerates to a conventional SMC design, and bounds on the tracking errors in the various loops are obtained The proposed method differs in the selection of the gain of the switching term

4.4.1 ML Analysis

The system under consideration is given as [68]

$$\begin{aligned} \mathbf{x} &= \mathbf{f}(\mathbf{x}) + \mathbf{g}(\mathbf{x})u + \triangle\mathbf{f}(\mathbf{x}) + \triangle\mathbf{g}(\mathbf{x})u, \text{ and} \\ y &= h(\mathbf{x}), \end{aligned} \tag{4 48}$$

where, $\mathbf{x} \in \mathcal{R}^n$ and $u, y \in \mathcal{R}$ The functions in the above equations are smooth vector fields with appropriate dimensions The arguments of the functions are dropped for brevity The nominal system is the system defined above with the uncertain terms $\triangle\mathbf{f}$, and $\triangle\mathbf{g}u = 0$ The relative degree of the output, or equivalently the control characteristic index is assumed to be ρ Under a suitable coordinate transformation from $\mathbf{x}$ to $\mathbf{z} = [\xi^{\mathrm{T}}\eta^{\mathrm{T}}]^{\mathrm{T}}$, where $\xi = [y_1, y_2, \quad , y_\rho]^{\mathrm{T}} \in \mathcal{R}^\rho$, and $\eta \in \mathcal{R}^{n-\rho}$, the nominal system in (4 48) may be expressed in a reduced form as

$$\begin{aligned} y_i &= y_{i+1}, \; i = 1, 2, \quad \rho - 1 \\ y_\rho &= a(\xi, \eta) + b(\xi, \eta)u, \text{ and} \\ \eta &= q(\xi, \eta), \end{aligned} \tag{4 49}$$

with y_1 as the scalar output The functions a, b, q are as defined in standard text-books [21] b is assumed to be invertible for all z In the presence of uncertainties in (4 48), some uncertain terms will be present in the above set of equations Li et al [67,

68] require the knowledge of the characteristic indices of the uncertainties in the actual system as their design procedure is based on it For the following analysis uncertain terms are assumed present in all the equations, and the actual system is then given as

$$\begin{aligned} y_i &= y_{i+1} + d_i, \ i = 1, 2, \quad , \rho - 1 \\ y_\rho &= a(z) + b(z)u + d_\rho + \beta(z)u, \text{ and} \\ \eta &= q(z) + q_1(z, u), \end{aligned} \tag{4 50}$$

where, d_i, $i = 1, \quad , \rho$ are taken to represent the disturbances as well as the functional uncertainties This may also include the effect of $\triangle g u$ Their bounds are assumed to be known and are given as $|d_i| < D_i$ Similarly $|\beta| < B$ q and q_1 are assumed to satisfy conditions as specified in [67, 68] Specifically, it is assumed that the system is minimum phase, q is Lipschitz in ξ and the effect of the disturbances on the ZD (q_1) is bounded Note that Li et al [67, 68] assume that $d_i = 0$, $i = 1, \quad , \sigma$, where $\sigma > 1$ represents the characteristic index of the uncertainty $\triangle f$ Their control design procedure depends on the value of σ In the method proposed here, this assumption is not required Since all other assumptions on the ZD are taken as in [67, 68], the corresponding results hold true here also Therefore in the following analysis, the ZD has not been considered Thus only the first ρ equations of the system dynamics (4 50) are used

The desired tracking signal is assumed to be given as $\xi_d = [y_{1d}, y_{2d}, \quad , y_{\rho d}]^T$ Following the ML structure as shown in Fig 4 1, augmented signals y_{ia} and its time derivative y_{ia}, $i = 1, \quad , \rho$ will be defined as was done in the Section 4 2 Conventionally the errors are defined as

$$\bar{e}_i = y_i - y_{id}, \ i = 1, \quad , \rho \tag{4 51}$$

New tracking errors with respect to the augmented signals are defined as

$$e_i = y_i - y_{ia}, \ i = 1, \quad , \rho \tag{4 52}$$

The analysis for the case of $\rho = 3$ is presented here It can however be similarly

extended for $\rho > 3$ From (4 50), the ξ dynamics in this case becomes

$$y_1 = y_2 + d_1, \tag{4 53}$$

$$y_2 = y_3 + d_2, \text{ and} \tag{4 54}$$

$$y_3 = a(z) + b(z)u + d_3 + \beta(z)u \tag{4 55}$$

Define $y_{1a} = y_{1d}$ and $y_{1a} = y_{1d} = y_{2d}$

Consider the dynamics in (4 53) The error is $e_1 = y_1 - y_{1a}$ Note that $e_1 = \bar{e}_1$ Taking its time derivative $e_1 = y_2 + d_1 - y_{2d}$ Using $y_2 = y_{2a} + e_2$ from (4 52) it becomes

$$e_1 = y_{2a} + e_2 + d_1 - y_{2d} \tag{4 56}$$

The command signal y_{2a} for the inner loop is selected, following the method of selection of V_a (4 9) as in Section 4 2, to cancel out the known terms and introducing a stabilizing feedback term as

$$y_{2a} = y_{2d} - K_1 e_1, \tag{4 57}$$

where K_1 is a positive real number With y_{2a} as chosen above, e_1 in (4 56) becomes

$$e_1 = -K_1 e_1 + e_2 + d_1 \tag{4 58}$$

The time derivative of y_{2a} may be derived using the above equation as

$$\begin{aligned} y_{2a} &= y_{3d} - K_1 e_1, \text{ or} \\ &= y_{3d} + K_1^2 e_1 - K_1 e_2 - K_1 d_1 \end{aligned} \tag{4 59}$$

The above equation may be rewritten as

$$y_{2a} = y_2' + d_{2c} \tag{4 60}$$

where, $d_{2c} = -K_1 d_1$ represents the disturbance terms and y_2' includes all the remaining terms in (4 59) The inner loop will be designed so that y_{2a} and its time derivative are tracked

Next consider the dynamics in (4 54) The error e_2 is defined as $e_2 = y_2 - y_{2a}$ Using $y_3 = y_{3a} + e_3$ from (4 52), the time derivative of e_2 is obtained using (4 54) and (4 60) as

$$\begin{aligned} e_2 &= y_{3a} + e_3 + d_2 - y_{2a} \\ &= y_{3a} + e_3 + d_2 - y_2' - d_{2c} \end{aligned} \tag{4 61}$$

The command signal y_{3a} for the next inner loop is selected as was done in the case of y_{2a} as

$$\begin{aligned} y_{3a} &= y_2' - K_2 e_2, \text{ or} \\ &= y_{3d} + K_1^2 e_1 - (K_1 + K_2) e_2, \end{aligned} \tag{4.62}$$

where K_2 is a positive real number With y_{3a} as chosen above, e_2 in (4 61) becomes

$$e_2 = -K_2 e_2 + e_3 + d_2 + K_1 d_1 \tag{4 63}$$

The time derivative of y_{3a} may be derived using the above equation and (4 58) as

$$\begin{aligned} y_{3a} &= y_{4d} + K_1^2 e_1 - (K_1 + K_2) e_2, \text{ or} \\ y_{3a} &= y_{4d} - K_1^3 e_1 + (K_1^2 + K_1 K_2 + K_2^2) e_2 - (K_1 + K_2) e_3 \\ &\quad -(K_1 + K_2) d_2 - K_1 K_2 d_1 \end{aligned} \tag{4 64}$$

The above equation is rewritten as

$$y_{3a} = y_3' + d_{3c} \tag{4.65}$$

where, d_{3c} denotes all d_1, d_2 terms and the remaining terms represented by y_3' Using y_{2a} from (4 57) and the definition of $\bar{e}_i$ from (4 51), e_2 may be rewritten as

$$\begin{aligned} e_2 &= y_2 - y_{2d} + K_1 e_1, \text{ or} \\ &= \bar{e}_2 + K_1 \bar{e}_1 \end{aligned} \tag{4 66}$$

The y_{3a} (4 62) and its time derivative in (4 64) should be tracked by the next inner loop For $i = 3$, the y_3 dynamics (4 55) is considered next Here e_3 is defined as

$e_3 = y_3 - y_{3a}$ Its time derivative $y_3 - y_{3a}$ is obtained using (4 55) and (4 64) as

$$\begin{aligned} e_3 &= a(z) + b(z)u + d_3 + \beta(z)u - y_{3a}, \text{ or} \\ &= a + bu + d_3 + \beta u - y_3' - d_{3c} \end{aligned} \tag{4 67}$$

From (4 64), it is seen that $d_3 - d_{3c} = d_3 + (K_1 + K_2)d_2 + K_1K_2d_1 = d_3'$ Let the bound on d_3' be represented as D_3' Note that d_3' includes the effect of disturbances and uncertainties in the outer loops, i e d_1 and d_2 Also, let $|\beta b^{-1}| < \alpha < 1$ This condition guarantees that $b + \beta$ is invertible over the entire z space Then a SMC law may be designed as in Section 2 2 as

$$u = b^{-1}[y_3' - a - K_3e_3 - K_4\text{sgn}[e_3]], \tag{4 68}$$

where $K_3, K_4 > 0$ can be appropriately selected With u as selected above, e_3 in (4 67) becomes

$$e_3 = -K_3e_3 - (1 + \beta b^{-1})K_4\text{sgn}[e_3] + \beta b^{-1}(y_3' - a - K_3e_3) + d_3' \tag{4 69}$$

Following the developments in Section 2 2, K_4 is selected as

$$K_4 \geq \frac{\alpha|y_3' - a - K_3e_3| + D_3' + \eta_K}{1 - \alpha} \tag{4 70}$$

where $\eta_K > 0$ With this choice, the e_3 dynamics in (4 69) can be guaranteed (using developments in Appendix A) to have a decay response better than

$$e_3 = -K_3e_3 - \eta_K\text{sgn}[e_3] \tag{4 71}$$

The choice of u in (4 68) is thus seen to give a proportional plus constant rate reaching law and the time to reach $e_3 = 0$ starting from a non-zero initial condition $e_3(0)$ can be evaluated as in (A 7)

Using y_{3a} from (4 62) and e_2 from (4 66) and noting that $e_1 = \bar{e}_1$, e_3 may be simplified as

$$e_3 = \bar{e}_3 + (K_1 + K_2)\bar{e}_2 + K_1K_2\bar{e}_1 \tag{4 72}$$

This is the conventionally chosen SS with the poles at $-K_1, -K_2$ The newly defined tracking errors e_i are obtained as in (4 66) and (4 72) These are rewritten collectively to get

$$\begin{aligned} e_1 &= \bar{e}_1, \\ e_2 &= \bar{e}_2 + K_1\bar{e}_1, \text{ and} \\ e_3 &= \bar{e}_3 + (K_1 + K_2)\bar{e}_2 + K_1K_2\bar{e}_1 \end{aligned} \tag{4 73}$$

The e_i's are seen to be stable combinations of the conventional errors Note that [68] also uses stable combinations of variables with SPMs The e_i dynamics here is seen from (4 58), (4 63), and (4 69) as

$$\begin{aligned} e_1 &= -K_1e_1 + e_2 + d_1, \\ e_2 &= -K_2e_2 + e_3 + d_2 + K_1d_1, \text{ and} \\ e_3 &= -K_3e_3 - (1 + \beta b^{-1})K_4\text{sgn}[e_3] + \beta b^{-1}(y_3' - a - K_3e_3) + d_3', \end{aligned} \tag{4 74}$$

where the e_3 dynamics is shown to have a decay characteristic better than (4 71)

Using y_3' as defined in (4 64) and (4 65), and e_i as defined in (4 73), the $y_3' - K_3e_3$ term in u in (4 68) may be simplified to get

$$y_3' - K_3e_3 = y_{4d} - K_1K_2K_3\bar{e}_1 - (K_1K_2 + K_2K_3 + K_3K_1)\bar{e}_2 - (K_1 + K_2 + K_3)\bar{e}_3 \tag{4 75}$$

which is seen to be the error and its derivatives feedback term in the conventional SMC design (as in Section 2 2) Thus it is observed that the ML approach applied to the unmatched uncertainty case leads to the conventional SMC law in (4 68), while incorporating the effect of the unmatched disturbances and uncertainties through the $d_3' = d_3 - d_{3c}$ term in (4 67) which is bounded by D_3', which is reflected in the selection of the gain of the switching term K_4 in (4 70)

Note that the analysis can be continued for $i > 3$ in a similar fashion with similar results Hence the analysis has been shown up to $i = 3$ Also the e_3 dynamics is known to be better than the dynamics specified in (4 71), and hence, it is obvious that $e_3 \to 0$ as it satisfies a sliding condition To alleviate chattering, a sat$[e_3/\phi]$ term is

used instead of the sgn[e_3] term, where ϕ is a selected boundary layer thickness With this $|e_3|$ is ultimately bounded by ϕ, and once e_3 reaches the boundary layer, the e_2 can be shown to decay and be ultimately bounded with $|e_2| \leq \frac{\phi+D_2+K_1D_1}{K_2}$ (refer Appendix F) With e_3 and e_2 bounded as above, e_1 is also seen to be ultimately bounded with $|e_1| \leq \frac{|e_2|+D_1}{K_1}$ Thus it is seen that

$$\begin{aligned} |e_3| &\leq \phi, \\ |e_2| &\leq \frac{\phi + D_2 + K_1 D_1}{K_2}, \text{ and} \\ |e_1| &\leq \frac{\phi + D_2 + (K_1 + K_2) D_1}{K_1 K_2} \end{aligned} \tag{4 76}$$

From the definition of the e_i, $i = 1, 2, 3$ in (4 73) and its dynamics in (4 74), it becomes clear that first the SS e_3 is reached, then the trajectory starts moving along surfaces with lower dimensions in the $\bar{e}$ space in a sequential manner, i e a representative point would first try to reach $e_3 = 0$, when it is sufficiently small then e_2 is made small and so on

The bounds for higher order systems $\rho > 3$ can be similarly derived From the above analysis, it is seen that if the conventional SMC design is performed, with K_4 as selected in (4 70), then the output tracking error $e_1 = \bar{e}_1$ will be ultimately bounded as in (4 76) for the unmatched uncertainty case Given positive real numbers K_1 and K_2, there is a unique surface $e_3 = 0$ (4 72) which satisfies the sliding condition, however conversely, given a surface $e_3 = 0$ with poles at $-K_1$ and $-K_2$, the corresponding e_i dynamics (4 74) cannot be uniquely defined as it depends on the order of choice of K_1 and K_2 The output tracking error bound however remains the same The choice of K_1 and K_2 can be done so as to keep the $|e_1|$ under some desired value For example, in the case of $\rho = 3$, it is seen from (4 76) that a smaller $|e_1|$ will be achieved when K_1 and K_2 are sufficiently large and $K_1 + K_2 < K_1 K_2$ The area above the curve in Fig 4 12 gives the region of the $K_1 - K_2$ space in which these conditions are satisfied Similar results may be obtained for the higher order systems too

Under the assumptions made on the η dynamics in (4 50), and the fact that the e_i errors are ultimately bounded as in (4 76), the ultimate boundedness of the states and

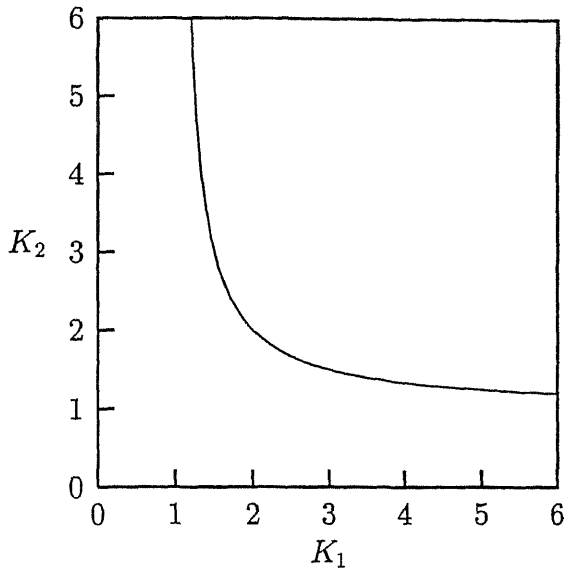

Fig 4.12 The $K_1 - K_2$ space

thus the practical stability [70] of the complete system (4 50) may be easily established using Lyapunov method as is reported in [21, 67, 68] Thus it is concluded that, the conventional SMC design can be done for the general uncertainty case with a new method of switching gain selection as in (4 70), and the tracking error bounds can be derived as above The method developed here is applied to an example problem in the next section

4.4.2 Numerical Example and Simulation

The example considered here is taken from Li et al [67] It is a four state problem with the functions in (4 48) given as

$$f(x) = \begin{pmatrix} x_3 \\ x_1^2 - x_2 + 2x_1^2 x_3 \\ x_1^2 - x_3 \\ x_1 + x_4 \end{pmatrix}, \quad g(x) = \begin{pmatrix} 0 \\ 2x_3 \\ 1 \\ 0 \end{pmatrix}, \text{ and} \qquad (4\,77)$$

$$\triangle f(x) = \begin{pmatrix} 0\,5\exp(x_1) \\ 0\,5\exp(x_3) \\ 0\,5\exp(x_4) \\ 0 \end{pmatrix}, \quad \triangle g(x) = \begin{pmatrix} 0 \\ 0\,5\sin(x_2) \\ 0\,5\cos(x_3) \\ 0 \end{pmatrix} \tag{4 78}$$

The output $y = x_4$ The above set of equations may be rewritten in a reduced form in the new set of coordinates [67] given by $\xi = [x_4,\ x_1+x_4,\ x_1+x_3+x_4]^{\mathrm{T}}$ and $\eta = x_2 - x_3^2$ as in (4 50) The control characteristic index of the nominal system is seen to be $\rho = 3$ The resulting disturbance vector is obtained as

$$\mathbf{d} = \begin{pmatrix} 0 \\ 0\,5\exp(x_1) \\ 0\,5\exp(x_1) + 0\,5\exp(x_4) + 0\,5\cos(x_3)u \end{pmatrix} \tag{4 79}$$

The SS was selected to have both of its poles at -10, i e $e_3 = \bar{e}_3 + 20\bar{e}_2 + 100\bar{e}_1$ Also ϕ, K_3, and η_K were taken as 0 05, 5, and 1 0 respectively The initial condition was $\mathrm{x} = [2\,0,\ 2\,0,\ 2\,0,\ 2\,0]^{\mathrm{T}}$ and the desired output was taken to be $\sin(\pi t)$ It is easily established that $\alpha < 1$ for this example $e_3(0)$ is calculated to be 223 17 With the choices of K_3 and η_K as above the reaching time may be evaluated from (A 8) as 1 359s

Simulation was done using the fourth order Runge-Kutta algorithm with a time varying step size This was necessary as the system equations were found to be ill conditioned and application of a constant step Runge-Kutta algorithm required a prohibitively small time step These issues and an adaptive step selection procedure are discussed in Zhao and Utkin [75] In the present work, a simpler method involving the doubling and halving of step sizes was used The e_3 is seen to go inside the selected boundary layer in a very small time, approximately 0 076s which is well smaller than the estimated reaching time, and then stays there Note that $d_1 = 0$ from (4 79) Since $\xi_1 = x_4$ should track $\sin(\pi t)$, and $\xi_2 = x_1 + x_4$ should track $\pi\cos(\pi t)$, an estimate of the bound on the magnitude of $x_1 = \pi\cos(\pi t) - \sin(\pi t)$ was taken as $\pi + 1$ and is used to evaluate the bound on d_2 in (4 79) as $D_2 = 31.45$ approximately Once sliding begins, the error e_2 is expected to decay and be bounded as specified in (4 76) by 3 15 This

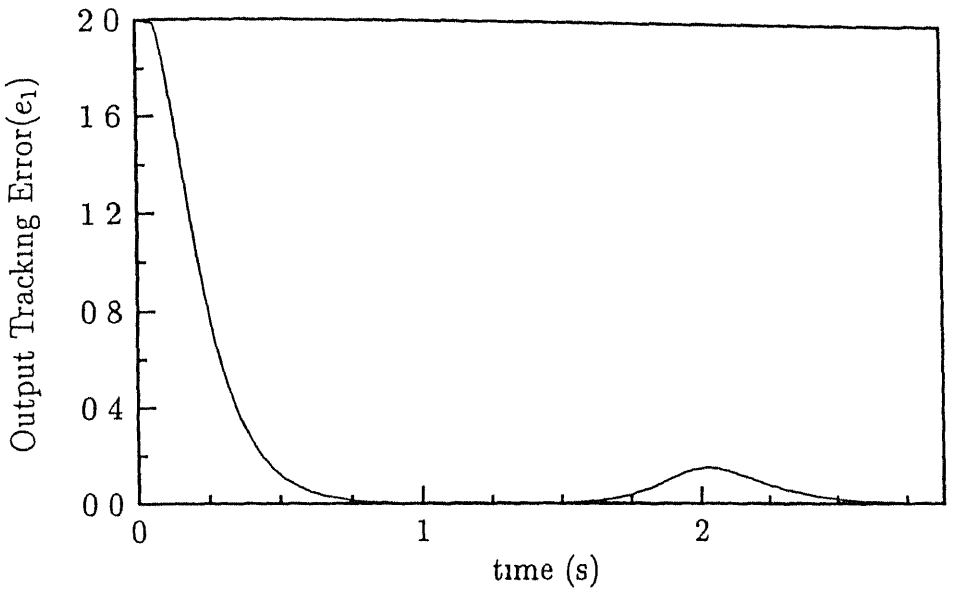

Fig. 4.13 Output tracking error $e_1(= \bar{e}_1)$

is achieved by $t = 0\ 23283$s, following which the e_1 should decay and remain bounded by 0 315 This bound is seen to be satisfied for all $t > 0\ 38127$s Fig 4 13 shows the time variation of the conventional error signal $\bar{e}_1$ It is seen that e_1 decays and stays within its bounds. The variation of e_2 signal defined in (4 73) is shown in Fig 4 14 Thus, all the error signals are seen to be varying between specified bounds

4.5 Conclusions

In this chapter, robust nonlinear control law design using a ML strategy for the unmatched uncertainty case is studied The outer loop tracking errors are used to augment the command signals for the inner loop dynamics A SMC law is used in the inner loop to track the augmented signals The method is directly applicable to almost all mechanical systems with velocities as the primary outputs The ultimate boundedness of the tracking errors in the two loops is established Control laws are derived for the aircraft longitudinal dynamics and simulation results for the velocity tracking mode are presented. The choice of parameters may be done based on a tradeoff between the errors in the inner and outer loops The ML method is then applied to higher order

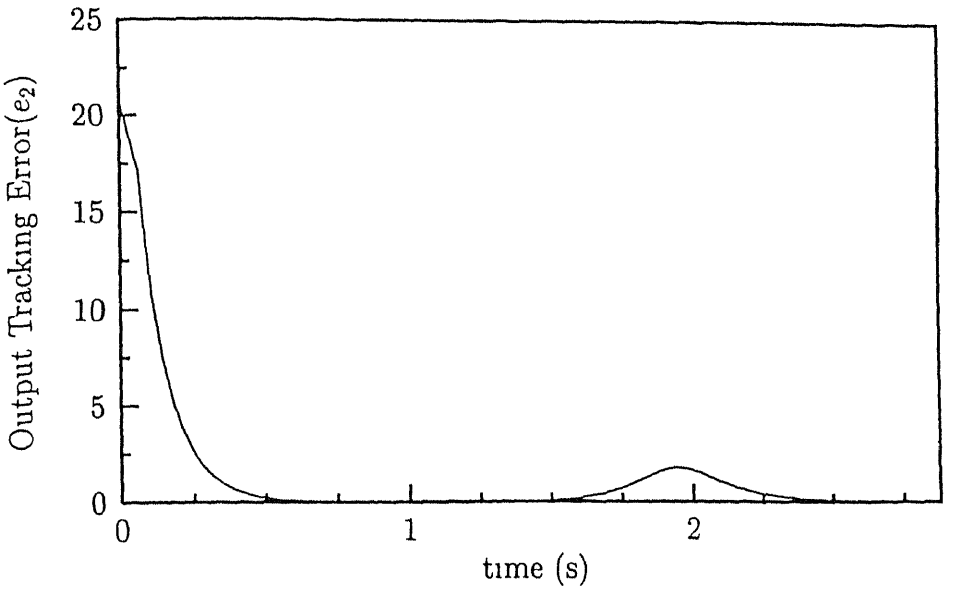

Fig. 4.14 Output tracking error e_2

single input systems (with relative degree > 1) with unmatched uncertainties The ML analysis is seen to give control laws equivalent to the conventional SMC design, however, the selection of the switching term gain is slightly modified Bounds on the defined tracking errors are developed Thus, it is concluded that a conventional SMC design can be implemented for the case of unmatched uncertainty also and the bounds for the tracking errors may be obtained Minimization of these bounds and the method proposed in Chapter 2 can guide the selection of the SMC parameters The method is verified by applying it to an example problem taken from published literature.

Chapter 5

SMC for Systems with Input Dynamics

5.1 Introduction

As discussed earlier, the SMC uses a discontinuous/switching control law, because of the sgn[ ] term in (2 9), and the associated invariance to matched disturbances and uncertainties accrue because of the assumption of exact switching The SMC method can therefore not be applied to systems where discontinuities in the input are not permissible, as in chemical systems where the inputs such as flow rates cannot be varied discontinuously Also, any practical system will have its inherent delays and a finite bandwidth, which rules out the possibility of an infinite switching frequency in practice Thus it is not possible to ensure that motion will be restricted to the SS (ideal sliding), however motion close to the SS (real sliding) may be guaranteed [54, 55] This was done by using continuous approximations to the discontinuous control laws [56] The use of a boundary layer [21] as in the earlier chapters is one such method and the motion is guaranteed to lie within a boundary layer of the SS An adaptive method of alleviation of chattering was proposed by Chang et al [76]

Elmali and Olgac [77] used a first order filter to smoothen out the response of the switching function (s) and then used the *signum* of the filter output to design SMC laws The method using a second order sliding mode results in less frequent switchings than the conventional method Emel'yanov et al [54] and Levant [55] used higher

order sliding modes for this problem Chiacchiarini et al [60] using a similar approach obtained a continuous control action which is the output of a series of integrators Ramirez [57, 58] using a differential algebraic approach, expressed the system in a generalized controller canonical form involving the inputs, the states and their higher order derivatives, and synthesized SMC laws with applications to nonlinear chemical processes [57] Ramirez et al [59] augmented the system equations with the input dynamic equations and represented the extended system in a canonical form This method was applied to the vertical flight regulation of a nonlinear helicopter model Most of these works require higher order derivatives of the outputs or the x-dynamics (5 2), which involves derivatives of the uncertainty or disturbance terms present therein Thus, the analysis of robustness properties becomes rather involved and has been addressed in very few works [60]

In this chapter, the ML strategy as outlined in the previous chapter, is applied to this problem As seen earlier in Section 4 2, the effect of disturbances in the outer loop is easily passed on to the inner loop, and thus the propagation of disturbances and as a result the robustness studies are more easily done in this procedure, as will be shown in this chapter The method however requires higher order derivatives of the desired response signals The inputs applied to any system are generally outputs of an actuator system with a finite bandwidth This is modeled in the present work as a first order dynamic system This dynamic system is added to the original dynamic system forming an augmented state space Following the developments in Chapter 4, the tracking of position variables is done in the outer loop by generating augmented velocity command signals, which are tracked in the inner loop by synthesizing augmented input signals, which are tracked in the innermost loop The resulting control law uses the full augmented state feedback, and has a discontinuity in the first derivative of the input It thus gives a continuous response in the system state space and the discontinuity is limited to the controller state space Control law is synthesized for a general SI mechanical system and applied to the nonlinear spring mass problem, considered earlier in Section 2 4 1, and simulation results are presented Time domain

bounds for the state and input errors are developed The method is then extended to the MI aircraft longitudinal dynamics problem of Section 4 3 Bounds on the position, velocity, and input errors are derived Simulation results using the developed control laws are presented The effect of the feedback gains is studied qualitatively

5.2 ML Analysis for a SI Mechanical System

The specified first order actuator dynamics are added to the general SI mechanical system in (2 1) The complete system, may then be expressed as

$$\begin{aligned} u &= f_1(x, x, u) + b_1(x, x, u)w + d_u, \text{ and} && (5\ 1) \\ x &= f_2(x, x) + b_2(x, x)u + d_x, && (5\ 2) \end{aligned}$$

where, w represents the actuator input Let the state vector be represented as $\mathbf{x} = [x_1,\ x_2]^{\mathrm{T}} = [x,\ x]^{\mathrm{T}}$ As a general case the input dynamics have been taken to be functions of the system states $(\mathbf{x})$ also The d_x, d_u denote the disturbances and uncertainties in the channels specified by their subscripts and are known to be bounded by D_x, D_U respectively Let $b_i = \hat{b}_i(1+\delta b_i)$, where $\hat{b}_i$ represents the nominal input function and $|\delta b_i| < \beta_i,\ i = 1, 2$ Moreover, b_1 and b_2 are assumed to be invertible Also x is supposed to track $x_{1d}, x_{2d} = x_{1d}$ and $x_{3d} = x_{2d}$ The above set of system equations is seen to be similar in structure to (4 1) and (4 2) The ML scheme as shown in Fig 4 1 is applied to this problem In the outer loop the x dynamics (5 2) is used to generate a signal u_a and u_a which should be tracked by the inner loop, which in this case is the u dynamics (5 1)

Define $e = x - x_{1d}$ and $e = x - x_{1d}$ Appropriate error functions in x and u are defined as in (2 5) and (4 6) as

$$\begin{aligned} s_x &= e + \lambda e, \text{ and} && (5.3) \\ s_u &= u - u_a && (5.4) \end{aligned}$$

where, $\lambda > 0$ and u_a is yet to be defined It is assumed that the input u is available for feedback Following the steps in Section 2 2, $\dot{s}_x = e + \lambda e$ and using (5 2), it may be

rewritten as

$$\begin{aligned} s_x &= f_2 + b_2 u + d_x - x_{3d} + \lambda e, \text{ or} \\ &= f_2 + b_2 u_a + b_2 s_u + d_x - x_{3d} + \lambda e, \end{aligned} \tag{5 5}$$

using $u = u_a + s_u$ from (5 4) As in Section 4 2, u_a would be required for the inner loop control law design, the control signal u_a is required to be continuous Thus, it is selected by replacing the *signum* term in (2 7) by a $k_x s_x$ term as in (4 9) and is of the form

$$u_a = \hat{b}_2^{-1}(x_{3d} - f_2 - ae - be - k_x s_x), \tag{5 6}$$

where, $a, b > 0$ are selected as in Section 2 3 with the poles selected as $-\lambda, -\epsilon$ Thus, $a = \lambda\epsilon$ and $b = \lambda + \epsilon$ from (2 8) Thus, the $-ae - be - k_x s_x$ term in the above equation may be written as $-(k_x + \epsilon)s_x - \lambda e$ Using u_a, as chosen in the above equation, s_x in (5 5) becomes

$$s_x = \delta b_2(x_{3d} - f_2 + \lambda e) - (1 + \delta b_2)(k_x + \epsilon)s_x + b_2 s_u + d_x \tag{5.7}$$

It is seen that from the above equation that calculation of bounds for s_x requires knowledge about the s_u bounds, and that is developed next

The inner loop control law is to be designed so that u tracks u_a, i e , $s_u \to 0$ As in the Section 4 2, the time derivative of u_a in (5 6) is required It may be derived as

$$u_a = \frac{d}{dt}[\hat{b}_2^{-1}](x_{3d} - f_2 - ae - be - k_x s_x) + \hat{b}_2^{-1}\frac{d}{dt}[x_{3d} - f_2 - ae - be - k_x s_x] \tag{5 8}$$

From the above equation it is seen that a higher order derivative of x_{3d} would be required The remaining terms, i e $\hat{b}_2, f_2, s_x$ and their derivatives are functions of the state vector x and x Accelerometers in mechanical systems are quite commonly used Hence the assumption of x being available for feedback is quite justified and will be used in the following developments However, this is not a necessary condition. In case the acceleration signals are not available for feedback, the above derivation of u_a would have a disturbance term as was the case in Section 4 2 (4 20) This disturbance term would then be passed on to the inner loop as was done in the previous chapter The

control law design for both the cases is outlined in the example problem considered in the next section For the rest of this section, it is assumed that the accelerometer signals are available for feedback

Since $x_{3d} - ae - be - k_x s_x = x_{3d} - ae - be - k_x e - k_x \lambda e = x_{3d} - (k_x\lambda + a)e - (k_x + b)e$, its time derivative may be easily obtained as

$$\frac{d}{dt}[x_{3d} - ae - be - k_x s_x] = x_{4d} - (k_x + b)(x - x_{3d}) - (k_x\lambda + a)e \tag{5 9}$$

Using (E 3) and the notations in Appendix E, the derivative $\frac{d}{dt}[\hat{b}_2^{-1}]$ in (5 8) may be expressed as $-\hat{b}_2^{-2} R_{b_2}\mathbf{x}$ Similarly $\frac{d}{dt}[f_2]$ may be expressed as $R_{f_2}\mathbf{x}$ Using these time derivatives and (5 9), u_a in (5 8) may be obtained as

$$\begin{aligned} u_a &= -\hat{b}_2^{-2}(x_{3d} - f_2 - ae - be - k_x s_x)R_{b_2}\mathbf{x} \\ &\quad +\hat{b}_2^{-1}[x_{4d} - (k_x + b)(x - x_{3d}) - (k_x\lambda + a)e - R_{f_2}\mathbf{x}], \text{ or} \\ u_a &= \hat{b}_2^{-1}[x_{4d} - (k_x + b)(x - x_{3d}) - (k_x\lambda + a)e \\ &\quad -R_{f_2}\mathbf{x} - \hat{b}_2^{-1}(x_{3d} - f_2 - ae - be - k_x s_x)R_{b_2}\mathbf{x}] \end{aligned} \tag{5 10}$$

Thus with the signals u_a and u_a synthesized in the outer loop as defined in (5 6) and (5 10), the design of the inner loop control law is done so as to make s_u in (5 4) go to 0 Taking the time derivative of s_u, it follows from (5 1) that

$$s_u = f_1 + b_1 w + d_u - u_a \tag{5 11}$$

The input w is selected as was done in Section 2 2 to satisfy a constant plus proportional rate reaching law as

$$w = \hat{b}_1^{-1}(u_a - f_1 - k_u s_u - k_d \text{sgn}[s_u]) \tag{5 12}$$

where, $k_u, k_d > 0$ The control law thus requires that all the states $\mathbf{x}$ and the input u be available for feedback With w as selected above, the s_u in (5 11) becomes

$$s_u = \delta b_1(u_a - f_1 + k_u s_u) - k_u s_u - (1 + \delta b_1)k_d \text{sgn}[s_u] + d_u \tag{5 13}$$

If k_d is selected following (4 70) as

$$k_d = \frac{\beta_1|u_a - f_1 + k_u s_u| + D_u + \eta_u}{1 - \beta_1}, \tag{5 14}$$

with $\eta_u > 0$, then following developments in Section 2 2, s_u can be shown to have decay characteristics better than

$$\dot{s}_u = -k_u s_u - \eta_u \mathrm{sgn}[s_u] \tag{5 15}$$

Thus $s_u \to 0$ in a finite time which may be derived using (A 7) and will then stay there For implementation purposes, the sgn[ ] term is replaced by a sat$[s_u/\phi_u]$ as in Section 3 4, where ϕ_u is an appropriately selected boundary layer thickness Note that this leaves w as a continuous signal with discontinuities in its first derivative only Thus, using a continuous w makes the actually applied u continuous up to its second derivative In this case, s_u will be ultimately bounded with

$$|s_u| \leq \phi_u \tag{5 16}$$

within a finite time which may be evaluated as in (A 8)

Then the $b_2 s_u$ term in (5 7) will be bounded by $|b_2|\phi_u$ With the further assumption that $\delta b_2(x_{3d} - f_2 + \lambda e)$ in (5 7) is bounded as $\beta_2|x_{3d} - f_2 + \lambda e|$, it can be shown as in Appendix F that s_x will be ultimately bounded with

$$|s_x| \leq \frac{\beta_2|(x_{3d} - f_2 + \lambda e)| + |b_2|\phi_u + D_x}{(1-\beta_2)(k_x + \epsilon)} \tag{5 17}$$

Thus, the errors defined in (5 3) and (5 4) are ultimately bounded as shown above The designed control law is applied to the nonlinear spring mass problem considered in Section 2 4 1.

5.2.1 A Nonlinear Spring Mass Damper System

The system equations are as given in Section 2 4 1 The u dynamics is assumed to be a first order actuator system with a bandwidth of 10rad/s, i e $\dot{u} = -10u + 10w + d_u$ d_u is taken as $0\ 15 + 0\ 09\cos(3\pi t)$ bounded by $D_u = 0\ 25$ The controller parameters were taken as follows: $\lambda = 6$, $\epsilon = 2$, and $k_x, k_u = 10$ $\phi_u = 0\ 1$ and $\eta_u = 1\ 0$ were used in the simulation. With this $a = 12$ and $b = 8$ As $\hat{b}_2 = 1$ and $\beta_2 = 0$, u_a in (5 6) becomes

$$u_a = x_{3d} - f_2 - 6e - 12 s_x \tag{5 18}$$

u_a is next calculated from (5 10) as

$$\begin{aligned} u_a &= x_{4d} - 18e - 72e - R_{f_2}\mathrm{x} \\ &= x_{4d} - 18(x - x_{3d}) - 72(x - x_{2d}) - R_{f_2}\mathrm{x} \end{aligned} \tag{5 19}$$

$R_{f_2}\mathrm{x}$ can be evaluated from the functions given in Section 2 4 1 as $(\mu_0 - 3\mu_1 x^2)x - (\nu_0 + 2\nu_1|x|\mathrm{sgn}[x])x$ Thus, u_a becomes

$$u_a = x_{4d} + 18x_{3d} + 72x_{2d} - (\mu_0 - 3\mu_1 x^2 + 72)x + (\nu_0 + 2\nu_1|x|\mathrm{sgn}[x] - 18)x \tag{5 20}$$

Note that if the accelerometer is not available for feedback, the x term in the above equation may instead be written using (5 2) as $x = f_2 + \hat{b}_2 u + \hat{b}_2 \delta b_2 u + d_x$ In this the first two terms are exactly known and the remaining two terms being uncertain will be passed onto the inner loop as a disturbance term (as in Section 4 2) The u_a may then be expressed as

$$\begin{aligned} u_a &= [x_{4d} + 18x_{3d} + 72x_{2d} - (\mu_0 - 3\mu_1 x^2 + 72)x \\ &\quad +(\nu_0 + 2\nu_1|x|\mathrm{sgn}[x] - 18)(f_2 + \hat{b}_2 u)] \\ &\quad +(\nu_0 + 2\nu_1|x|\mathrm{sgn}[x] - 18)(\hat{b}_2 \delta b_2 u + d_x) \end{aligned} \tag{5 21}$$

The u_a as derived in (5 20) or (5 21) in the presence and absence of accelerometers respectively may be rewritten as $T_u + d'_u$, where T_u is the term in the above equations not having any uncertainties or disturbances, and the d'_u contains the effect of the disturbances and uncertainties Thus it is seen that for the case of acceleration signals being present, $d'_u = 0$, and the right hand side of (5 20) gives T_u For the other case, d'_u is seen to be the last term in (5 21). It is assumed that a bound on d'_u may be estimated as D'_u. Thus for the case where the accelerometers are absent, s_u in (5.11) becomes

$$\dot{s}_u = f_1 + b_1 w + (d_u - d'_u) - T_u \tag{5.22}$$

The input w for this may be designed as in (5 12) Note that this approach requires higher switching gains, because of the presence of two disturbance terms This is expected to give rise to more chattering effects

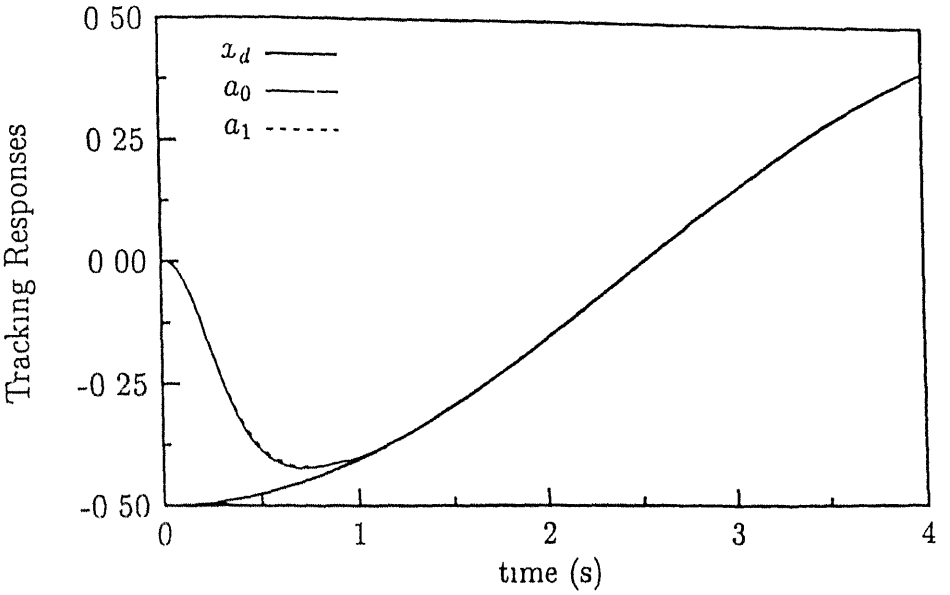

Fig. 5.1 The tracking responses for Cases a_0 and a_1

Simulation was done using the fourth order Runge-Kutta algorithm with a time step of 1ms In the following figures, the responses labeled a_0 are obtained in the case of accelerometers being not used The other case is labeled a_1 Fig 5 1 shows the tracking response obtained for the selected tracking signal A good tracking performance is seen in both the cases The bound on the tracking error as given in (5 17) is seen to depend on the functional like $(x_{3d} - f_2 + \lambda\dot{e})$, and thus numerical values of these bounds are difficult to be evaluated The figure qualitatively shows that these are indeed bounded and quite small. Figs 5.2 and 5 3 show the u dynamics (5 1) with the signal u_a to be tracked for cases a_0 and a_1 respectively It is observed that u in both the cases starts tracking u_a within about 0 5s. In both cases the input error was seen to lie inside the specified boundary layer. It was however observed from the two figures that the input tracking in the case a_0 is slightly faster than the a_1 response This may be attributed to the fact that higher switching gain in this case leads to better u_a tracking Thus it is seen that the ML strategy can be used to design continuous SMC laws In the next section, the method developed for SI systems is extended to MI systems

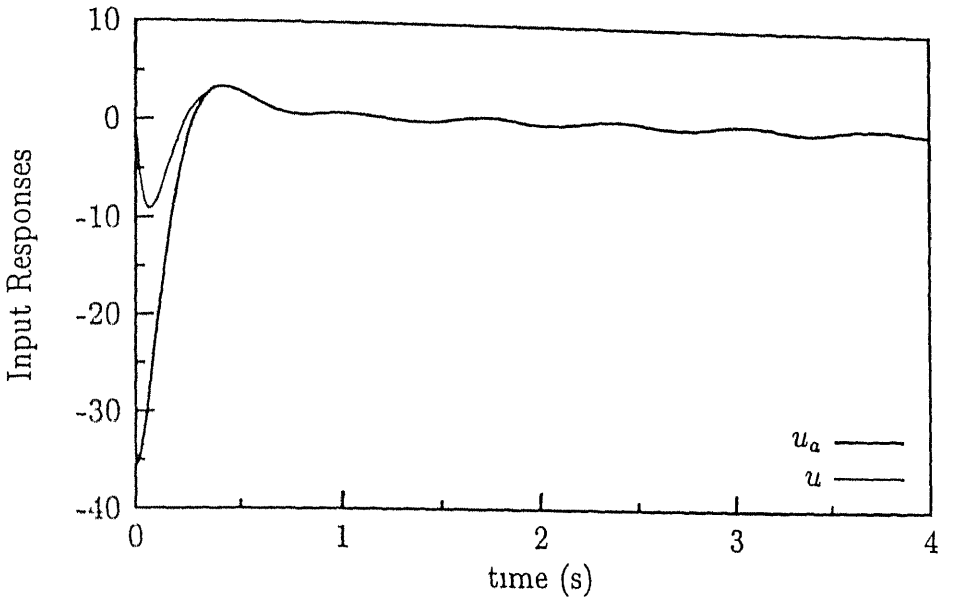

Fig. 5 2 The u dynamics for the a_0 case

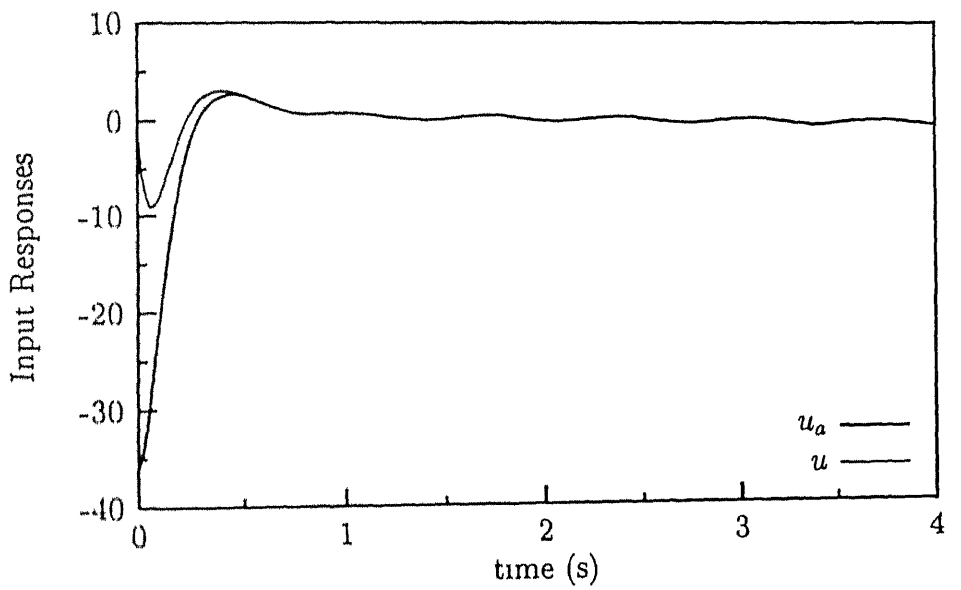

Fig. 5.3: The u dynamics for the a_1 case

5.3 Aircraft Longitudinal Control with First Order Input Dynamics

The method applied to a SI system in the previous section is extended to a MI aircraft control problem considered in Section 4 3 In this section it is assumed that accelerometers to measure the V vector are present, i e U, W, Q are available for feedback It is also assumed that the dynamics of the force vector is decoupled Augmenting the input dynamics equations to the MI aircraft system of equations in (4 1) and (4 3), the complete set of governing equations becomes

$$\mathbf{u} = \mathbf{g}(\mathbf{u}, \mathbf{X}, \mathbf{V}) + \mathbf{B}_0(\mathbf{u}, \mathbf{X}, \mathbf{V})\mathbf{w} + \mathbf{d}_0, \tag{5 23}$$

$$\mathbf{V} = \mathbf{f}_1(\mathbf{X}, \mathbf{V}) + \mathbf{B}_1(\mathbf{X}, \mathbf{V})\mathbf{u} + \mathbf{d}_1, \text{ and} \tag{5 24}$$

$$\mathbf{X} = \mathbf{B}_2(\mathbf{X})\mathbf{V} + \mathbf{d}_2 \tag{5 25}$$

Here $\mathbf{w} \in \mathcal{R}^n$ represents the actuator input, and the matrices $\mathbf{B}_i$, $i = 0, 1, 2$ are assumed to be invertible over the domain of interest, and $\mathbf{d}_0$ represents the disturbances and uncertainties in the input dynamics and is given to be bounded by $\mathbf{D}_0$ Let $\mathbf{Z} = [\mathbf{V}^T \ \mathbf{X}^T]^T$ The other assumptions/bounds in Section 4 2 are taken to be valid

Proceeding as in Section 4 2, the error functions for the position, velocity and input variables are defined as $\mathbf{S}_x$, $\mathbf{S}_v$ and $\mathbf{S}_u$ as

$$\mathbf{S}_x = \mathbf{X} - \mathbf{X}_d, \tag{5 26}$$

$$\mathbf{S}_v = \mathbf{V} - \mathbf{V}_a, \text{ and} \tag{5 27}$$

$$\mathbf{S}_u = \mathbf{u} - \mathbf{u}_a \tag{5 28}$$

where, $\mathbf{V}_a$, $\mathbf{u}_a$ are yet to be defined The procedure is developed using the ML strategy as outlined in Section 5 2 The control law for an inner loop is therefore designed based on the error dynamics of the immediate outer loop Thus $\mathbf{S}_x$ dynamics is set by synthesizing $\mathbf{V}_a$ and its time derivative $\mathbf{V}_a$ for tracking in the inner loop Similarly to obtain a desirable $\mathbf{S}_v$ dynamics, $\mathbf{u}_a$ and $\mathbf{u}_a$ signals will be generated as shown in the sequel. The actuator input $\mathbf{w}$ for the input dynamics (5 23) is designed so that $\mathbf{u}$ tracks $\mathbf{u}_a$ in the inner most loop

Following the developments in Section 4.2, $\mathbf{V}_a$ may be derived as in (4.9). For this choice, $\mathbf{S}_x$ has been earlier shown to satisfy the dynamics in (4.10) as

$$\mathbf{S}_x = -\mathbf{K}_x\mathbf{S}_x + \mathbf{B}_2\mathbf{S}_v + \mathbf{d}_2, \tag{5.29}$$

$\mathbf{V}_a$ is required for tracking in the inner loop as in Section 4.2 and is derived as in (4.19). The $\mathbf{S}_v$ dynamics can be obtained using (5.27) and (5.24) as

$$\begin{aligned} \mathbf{S}_v &= \mathbf{V} - \mathbf{V}_a, \text{ or} \\ &= \mathbf{f}_1 + \mathbf{B}_1\mathbf{u} + \mathbf{d}_1 - \mathbf{V}_a \end{aligned} \tag{5.30}$$

From (5.28), $\mathbf{u} = \mathbf{u}_a + \mathbf{S}_u$, and using $\mathbf{V}_a = \mathbf{T}_a + \mathbf{d}_2'$ from (4.20), the above equation may be rewritten as

$$\mathbf{S}_v = \mathbf{f}_1 + \mathbf{B}_1\mathbf{u}_a + \mathbf{B}_1\mathbf{S}_u + \mathbf{d}_1 - \mathbf{T}_a - \mathbf{d}_2' \tag{5.31}$$

The command signal $\mathbf{u}_a$ should be selected so as to make the $\mathbf{S}_v$ errors small. Therefore, it is selected to cancel out the known terms and introduce a stabilizing feedback as in Section 3.4. Since $\mathbf{u}_a$ would be required for tracking in the inner loop, the discontinuous sgn[ ] term in (3.13) is replaced by a $\mathbf{K}_v\mathbf{S}_v$ term as in (4.9). $\mathbf{u}_a$ is thus selected as

$$\mathbf{u}_a = \hat{\mathbf{B}}_1^{-1}(\mathbf{T}_a - \mathbf{f}_1 - \mathbf{K}_v\mathbf{S}_v), \tag{5.32}$$

where, $\mathbf{K}_v = \text{diag}[K_U,\ K_W,\ K_Q]$, all of which are positive real numbers. $\hat{\mathbf{B}}_1$ represents the nominal $\mathbf{B}_1$ matrix as defined in Section 3.4. Note that $\mathbf{u}_a$ represents the desired command forces which is different from the actually applied forces as discussed in Section 3.3. The effect of this uncertainty is incorporated into the design procedure (by defining the Δ_t matrix in 3.15) as was done in Section 3.4. Using $\mathbf{u}_a$ as chosen in (5.32), $\mathbf{S}_v$ in (5.31) may be obtained as in (3.17) as

$$\dot{\mathbf{S}}_v = -[I + \Delta_t]\mathbf{K}_v\mathbf{S}_v + \Delta_t(\mathbf{T}_a - \mathbf{f}_1) + \mathbf{B}_1\mathbf{S}_u + \mathbf{d}_1 - \mathbf{d}_2' \tag{5.33}$$

The $\mathbf{S}_v$ dynamics thus involves the $\mathbf{B}_1\mathbf{S}_u$ term, and thus the dynamics of $\mathbf{S}_u$ need to be considered before any bounds on the $\mathbf{S}_v$ errors can be developed. For this, the

time derivative of $\mathbf{u}_a$ in (5 32) is next developed For the tracking mode, since $\hat{\mathbf{B}}_1$ in (3 29) is a constant matrix (Section 3 5 1), $\mathbf{u}_a$ is seen to be

$$\begin{aligned} \mathbf{u}_a &= \hat{\mathbf{B}}_1^{-1}\frac{d}{dt}[\mathbf{T}_a - \mathbf{f}_1 - \mathbf{K}_v\mathbf{S}_v], \text{ or} \\ &= \hat{\mathbf{B}}_1^{-1}[\mathbf{T}_a - M_{f_1}\mathbf{Z} - \mathbf{K}_v\mathbf{S}_v], \end{aligned} \tag{5 34}$$

where $\frac{d}{dt}[\mathbf{f}_1] = M_{f_1}\mathbf{Z}$, using the notation given in (E 3) in Appendix E Note that $\mathbf{S}_v = \mathbf{V} - \mathbf{V}_a$ from (5 27) Thus, using $\mathbf{V}_a$ from (4 20), $\mathbf{S}_v = \mathbf{V} - \mathbf{T}_a - \mathbf{d}_2'$ Putting this in the above equation, $\mathbf{u}_a$ may be rewritten as

$$\mathbf{u}_a = \hat{\mathbf{B}}_1^{-1}[\mathbf{T}_a - M_{f_1}\mathbf{Z} - \mathbf{K}_v(\mathbf{V} - \mathbf{T}_a) + \mathbf{K}_v\mathbf{d}_2'] \tag{5 35}$$

Now it remains to evaluate $\mathbf{T}_a$ This may be derived starting from the definition of $\mathbf{T}_a$ in (4 37) Its time derivative may be evaluated as

$$\begin{aligned} \mathbf{T}_a &= \frac{d}{dt}[\mathbf{B}_2^{-1}](\frac{d}{dt}[\mathbf{B}_{2d}\mathbf{V}_d] - \mathbf{K}_x\mathbf{T}_x) + \mathbf{B}_2^{-1}(\frac{d^2}{dt^2}[\mathbf{B}_{2d}\mathbf{V}_d] - \mathbf{K}_x\mathbf{T}_x) \\ &\quad + \frac{d}{dt}[QM_{1\theta}](\mathbf{B}_{2d}\mathbf{V}_d - \mathbf{K}_x\mathbf{S}_x) + QM_{1\theta}(\frac{d}{dt}[\mathbf{B}_{2d}\mathbf{V}_d] - \mathbf{K}_x\mathbf{S}_x) \end{aligned} \tag{5 36}$$

$\frac{d}{dt}[\mathbf{B}_2^{-1}]$ is already derived in (4 36) Also $\mathbf{S}_x = \mathbf{T}_x + \mathbf{d}_2$ from (4 11) In the above equation $\frac{d}{dt}[QM_{1\theta}]$ may be evaluated as $QM_{1\theta} + QJ_{M_{1\theta}}[I_n \otimes \mathbf{X}]$ From $M_{1\theta}$ as defined in (4 33), it is easily obtained for the column vector C as used in (4 33), that

$$J_{M_{1\theta}}[I \otimes C] = C_\theta M_{2\theta} = C_\theta \begin{bmatrix} -\cos(\theta) & -\sin(\theta) & 0 \\ -\sin(\theta) & \cos(\theta) & 0 \\ 0 & 0 & 0 \end{bmatrix} \tag{5 37}$$

Thus, $J_{M_{1\theta}}[I_n \otimes \mathbf{X}]$ becomes $(Q + d_{2\theta})M_{2\theta}$ as C here is $\mathbf{X}$ and $C_\theta = \theta = Q + d_{2\theta}$ from (4 28) Thus, $\frac{d}{dt}[QM_{1\theta}] = QM_{1\theta} + Q^2M_{2\theta} + (d_{2\theta}Q)M_{2\theta}$ Using these equalities in (5 36), $\mathbf{T}_a$ may be obtained as

$$\begin{aligned} \mathbf{T}_a &= (2QM_{1\theta} + d_{2\theta}M_{1\theta})(\frac{d}{dt}[\mathbf{B}_{2d}\mathbf{V}_d] - \mathbf{K}_x\mathbf{T}_x) + \mathbf{B}_2^{-1}(\frac{d^2}{dt^2}[\mathbf{B}_{2d}\mathbf{V}_d] - \mathbf{K}_x\mathbf{T}_x) \\ &\quad + (QM_{1\theta} + Q^2M_{2\theta} + (d_{2\theta}Q)M_{2\theta})(\mathbf{B}_{2d}\mathbf{V}_d - \mathbf{K}_x\mathbf{S}_x) - QM_{1\theta}\mathbf{K}_x\mathbf{d}_2, \text{ or} \end{aligned} \tag{5 38}$$

$$
\begin{aligned}
= \; & 2QM_{1\theta}(\frac{d}{dt}[\mathrm{B}_{2d}\mathrm{V}_d] - \mathrm{K}_x\mathrm{T}_x) + \mathrm{B}_2^{-1}(\frac{d^2}{dt^2}[\mathrm{B}_{2d}\mathrm{V}_d] - \mathrm{K}_x\mathrm{T}_x) \\
& +(QM_{1\theta} + Q^2M_{2\theta})(\mathrm{B}_{2d}\mathrm{V}_d - \mathrm{K}_x\mathrm{S}_x) - QM_{1\theta}\mathrm{K}_x\mathbf{d}_2 \\
& +d_{2\theta}M_{1\theta}(\frac{d}{dt}[\mathrm{B}_{2d}\mathrm{V}_d] - \mathrm{K}_x\mathrm{T}_x) + (d_{2\theta}Q)M_{2\theta}(\mathrm{B}_{2d}\mathrm{V}_d - \mathrm{K}_x\mathrm{S}_x) \qquad (5\ 39)
\end{aligned}
$$

Also needed in the above equation is $-\mathrm{K}_x\mathrm{T}_x$ From its definition $\mathrm{T}_x = -\mathrm{K}_x\mathrm{S}_x + \mathrm{B}_2\mathrm{S}_v$ in (4 11), $\mathrm{T}_x = -\mathrm{K}_x\mathrm{S}_x + \frac{d}{dt}[\mathrm{B}_2]\mathrm{S}_v + \mathrm{B}_2\mathrm{S}_v$ Since $\mathrm{V}_a = \mathrm{T}_a + \mathrm{d}_2'$ from (4 20), S_v may be obtained from (5 27) as $\mathrm{V} - \mathrm{T}_a - \mathrm{d}_2'$ Also, using (4 16) and (4 33), $\frac{d}{dt}[\mathrm{B}_2]$ may be written as $(Q + d_{2\theta})M_{1\theta}$ Using this, S_v as developed, and S_x from (4 11), T_x may be expressed as

$$
\begin{aligned}
\mathrm{T}_x \; = \; & -\mathrm{K}_x(\mathrm{T}_x + \mathrm{d}_2) + (Q + d_{2\theta})M_{1\theta}\mathrm{S}_v \\
& +\mathrm{B}_2(\mathrm{V} - \mathrm{T}_a - \mathrm{d}_2') \qquad (5\ 40)
\end{aligned}
$$

Using the definition of d_2' from (4 20), $\mathrm{B}_2\mathrm{d}_2' = -\mathrm{K}_x\mathrm{d}_2 + d_{2\theta}\mathrm{B}_2M_{1\theta}(\mathrm{B}_{2d}\mathrm{V}_d - \mathrm{K}_x\mathrm{S}_x)$ Using the reverse equality from (4 34), i e replacing $M_{1\theta}$ by $-\mathrm{B}_2^{-1}M_{1\theta}\mathrm{B}_2^{-1}$ in this equation $\mathrm{B}_2\mathrm{d}_2'$ becomes equal to $-\mathrm{K}_x\mathrm{d}_2 - d_{2\theta}M_{1\theta}\mathrm{B}_2^{-1}(\mathrm{B}_{2d}\mathrm{V}_d - \mathrm{K}_x\mathrm{S}_x)$, which simplifies to $-\mathrm{K}_x\mathrm{d}_2 - d_{2\theta}M_{1\theta}\mathrm{V}_a$ from the definition of V_a in (4 9) Using this in (5 40) and substituting $\mathrm{V}_a + \mathrm{S}_v$ by V, as is evident from (5 27), gives

$$
\mathrm{T}_x = -\mathrm{K}_x\mathrm{T}_x + QM_{1\theta}\mathrm{S}_v + \mathrm{B}_2(\mathrm{V} - \mathrm{T}_a) + d_{2\theta}M_{1\theta}\mathrm{V} \qquad (5\ 41)
$$

Using T_x as above in (5 39) gives T_a as

$$
\begin{aligned}
\mathrm{T}_a \; = \; & 2QM_{1\theta}(\frac{d}{dt}[\mathrm{B}_{2d}\mathrm{V}_d] - \mathrm{K}_x\mathrm{T}_x) + \mathrm{B}_2^{-1}[\frac{d^2}{dt^2}[\mathrm{B}_{2d}\mathrm{V}_d] + \mathrm{K}_x^2\mathrm{T}_x \\
& -Q\mathrm{K}_xM_{1\theta}\mathrm{S}_v] - \mathrm{B}_2^{-1}\mathrm{K}_x\mathrm{B}_2(\mathrm{V} - \mathrm{T}_a) + (QM_{1\theta} + Q^2M_{2\theta})(\mathrm{B}_{2d}\mathrm{V}_d - \mathrm{K}_x\mathrm{S}_x) \\
& -QM_{1\theta}\mathrm{K}_x\mathrm{d}_2 + d_{2\theta}M_{1\theta}(\frac{d}{dt}[\mathrm{B}_{2d}\mathrm{V}_d] - \mathrm{K}_x\mathrm{T}_x) \\
& +(d_{2\theta}Q)M_{2\theta}(\mathrm{B}_{2d}\mathrm{V}_d - \mathrm{K}_x\mathrm{S}_x) - d_{2\theta}\mathrm{B}_2^{-1}\mathrm{K}_xM_{1\theta}\mathrm{V} \qquad (5\ 42)
\end{aligned}
$$

The term $\mathbf{B}_2^{-1}\frac{d^2}{dt^2}[\mathbf{B}_{2d}\mathbf{V}_d]$ in the above equation may be evaluated as

$$\mathbf{B}_2^{-1}\frac{d^2}{dt^2}[\mathbf{B}_{2d}\mathbf{V}_d] = \begin{pmatrix} \cos(S_\theta)[U_d + 2W_dQ_d - U_dQ_d^2 + W_dQ_d] - \sin(S_\theta)[W_d - 2U_dQ_d - W_dQ_d^2 - U_dQ_d] \\ \cos(S_\theta)[W_d - 2U_dQ_d - W_dQ_d^2 - U_dQ_d] + \sin(S_\theta)[U_d + 2W_dQ_d - U_dQ_d^2 + W_dQ_d] \\ Q_d \end{pmatrix} \tag{5 43}$$

Note that the second derivative terms U_d and so on as required in the above equation are evaluated as in (D 9) in the Appendix D These signals are seen to include higher order derivatives of the pilot inputs U_p Thus the so designed control law will be sensitive to the rate of application of pilot inputs However, this must be passed through a low pass filter to avoid any pilot induced oscillations

Thus $\mathbf{T}_a$ may be completely evaluated using (5 43) in (5 42) Using $\mathbf{f}_1$ as defined in (3 27), the term $M_{f_1}\mathbf{Z}$ in $\mathbf{u}_a$ (5 35) may be obtained as

$$\begin{aligned} M_{f_1}\mathbf{Z} &= \begin{pmatrix} -QW - QW - g_0\cos(\theta) \\ QU + QU - g_0\sin(\theta) \\ 0 \end{pmatrix} - d_{2\theta}\begin{pmatrix} g_0\cos(\theta) \\ g_0\sin(\theta) \\ 0 \end{pmatrix}, \text{ or} \\ &= \mathbf{f}_{1a} - d_{2\theta}\mathbf{f}_{1d} \end{aligned} \tag{5 44}$$

Using (5 42) and the above equation in (5 35), $\mathbf{u}_a$ may be evaluated For simplicity, it is rewritten as

$$\mathbf{u}_a = \mathbf{T}_u + \mathbf{d}'_u, \tag{5 45}$$

where, the first term is completely known and the $\mathbf{d}'_u$ contains the effect of all the disturbances present Thus, the term $\mathbf{T}_u$ may be obtained as

$$\begin{aligned} \mathbf{T}_u &= \hat{\mathbf{B}}_1^{-1}[2QM_{1\theta}(\frac{d}{dt}[\mathbf{B}_{2d}\mathbf{V}_d] - \mathbf{K}_x\mathbf{T}_x) + \mathbf{B}_2^{-1}(\frac{d^2}{dt^2}[\mathbf{B}_{2d}\mathbf{V}_d] \\ &\quad +\mathbf{K}_x^2\mathbf{T}_x - Q\mathbf{K}_xM_{1\theta}\mathbf{S}_v) - [\mathbf{B}_2^{-1}\mathbf{K}_x\mathbf{B}_2 + \mathbf{K}_v](\mathbf{V} - \mathbf{T}_a) \\ &\quad +(QM_{1\theta} + Q^2M_{2\theta})(\mathbf{B}_{2d}\mathbf{V}_d - \mathbf{K}_x\mathbf{S}_x) - \mathbf{f}_{1a}] \end{aligned} \tag{5 46}$$

Similarly, the total disturbance component of $\mathbf{u}_a$ is evaluated from (5 35), (5 42), and

(5 44) as

$$\mathbf{d}'_u = \hat{\mathbf{B}}_1^{-1}[-QM_{1\theta}\mathbf{K}_x\mathbf{d}_2 + d_{2\theta}M_{1\theta}(\frac{d}{dt}[\mathbf{B}_{2d}\mathbf{V}_d] - \mathbf{K}_x\mathbf{T}_x) + (d_{2\theta}Q)M_{2\theta}(\mathbf{B}_{2d}\mathbf{V}_d - \mathbf{K}_x\mathbf{S}_x) - d_{2\theta}\mathbf{B}_2^{-1}\mathbf{K}_xM_{1\theta}\mathbf{V} + d_{2\theta}\mathbf{f}_{1d} + \mathbf{K}_v\mathbf{d}'_2] \quad (5\ 47)$$

A conservative bound ($\mathbf{D}'_u$) on this term may be found as in Section 4 3

Now that $\mathbf{u}_a$ (5 32) and its time derivative $\mathbf{u}_a$ (5 45) have been evaluated, consider the $\mathbf{S}_u$ (5 28) dynamics Its time derivative may be expressed as $\mathbf{S}_u = \mathbf{u} - \mathbf{u}_a$, and using (5 23) and $\mathbf{u}_a$ as defined in (5 45), it is rewritten as $\mathbf{S}_u = \mathbf{g} + \mathbf{B}_0\mathbf{w} + \mathbf{d}_0 - \mathbf{T}_u - \mathbf{d}'_u$ The input $\mathbf{w}$ may be selected, following the procedure in Section 3 4 to ensure that $\mathbf{S}_u$ satisfies a constant rate reaching law, as

$$\mathbf{w} = \mathbf{B}_0^{-1}(\mathbf{T}_u - \mathbf{g} - \mathbf{K}_\eta \mathrm{sgn}[\mathbf{S}_u]), \quad (5\ 48)$$

where $\mathbf{K}_\eta\mathrm{sgn}[\mathbf{S}_u]$ is a n vector with its i^{th} component as $K_{\eta_i}\mathrm{sgn}[S_{u_i}]$ as in Section 3 4 K_{η_i} is selected as $D_{0_i} + D'_{u_i} + \eta_i$, where all $\eta_i > 0$ With this, the S_{u_i} response can be shown (as in Section 3 4) to be better than the response of

$$S_{u_i} = -\eta_i \mathrm{sgn}[S_{u_i}] \quad (5\ 49)$$

The sgn[ ] term in the control law (5 48) is replaced by an equivalent $\mathrm{sat}[S_{u_i}/\phi_{u_i}]$ term as in (3 22) Also let Φ_u represent the vector of boundary layer thicknesses as $[\phi_{u_i}]^{\mathrm{T}}$, $i = 1, \quad , n$ Thus as in Section 3 4, the S_{u_i} is guaranteed to be inside a boundary layer of thickness ϕ_{u_i}, i e

$$|S_{u_i}| \leq \phi_{u_i} \quad (5\ 50)$$

within a finite time as given in (3 25)

With $\mathbf{S}_u$ shown to be bounded by Φ_u, the bounds for the $\mathbf{S}_v$ and $\mathbf{S}_x$ errors may now be derived Note that the $\mathbf{S}_v$ dynamics in (5 33) involves $\mathbf{d}'_2$ which is bounded by $\mathbf{D}'_2$ (4 43) This bound is seen to depend on $\mathbf{S}_x$ Also, the $\mathbf{S}_x$ dynamics as derived in (5 29) depends on $\mathbf{S}_v$ Thus, the $\mathbf{S}_v$ and $\mathbf{S}_x$ dynamics are seen to be inter-dependent on one other Under the assumption that $\mathbf{S}_x$ can be shown to be bounded, and $(\mathbf{T}_a - \mathbf{f}_1)$ term

is bounded, and noticing that D_t is a diagonal matrix as given in (3 33), it follows from the S_v dynamics (5 33) that the S_{v_i} error satisfies

$$|S_{v_i}| \leq \frac{[|\mathbf{B}_1|\Phi_u + \mathbf{D}_1 + \mathbf{D}_2' + D_t(|\mathbf{T}_a - \mathbf{f}_1|)]_i}{K_{v_i}(1 - D_t(i,i))} \tag{5 51}$$

With $|\mathbf{S}_v|$ bounded as above, the $\mathbf{S}_x$ error can be shown to be bounded, as in (4 26), by

$$|S_{x_i}| \leq \frac{[|\mathbf{B}_2|\mathbf{S}_v + \mathbf{D}_2]_i}{K_{x_i}} \tag{5 52}$$

The velocity and the position tracking errors $\mathbf{S}_v$ and $\mathbf{S}_x$ errors are expected to be bounded as shown above As discussed above, the $|\mathbf{S}_v|$ and $|\mathbf{S}_x|$ are dependent on each other, resulting in simultaneous linear equations as shown in (G 5) with the bounds as variables These bounds should be positive to be practically meaningful It is shown in the Appendix G that this requires that $\mathbf{K}_v$ should be sufficiently large, or more specifically $K_U, K_W >> 2D_{2\theta}$ The actual bounds may be derived by solving the linear equation set in (G 5) It may be easily shown that these errors are uniformly ultimately bounded as in Appendix F with respect to these bounds However, the $|S_{v_i}|$ depends on functionals like $[|\mathbf{T}_a - \mathbf{f}_1|]_i$, which cannot be easily estimated and hence the numerical values of these bounds cannot be derived, and thus detailed derivations are not presented It suffices to know that these quantities are bounded Thus, the ML strategy is easily applicable to a MI problem as shown here Simulation results for the aircraft longitudinal dynamics is presented next The qualitative nature of variation of the error bounds for different sets of gains are also studied

5.3.1 Simulation Results

Simulation was done on the aircraft example considered in Section 4 3 In this example, the pilot maintains the equilibrium values of throttle gear and elevator till 0 5s, and then applies one complete cycle of the sinusoid elevator and throttle gear commands simultaneously The elevator command is assumed to be $\Delta U_p(1) = \delta_{el} = 20\sin(2t - 1\ 0)$ while the throttle command is taken as $\Delta U_p(2) = \delta_{tg} = 8\sin(2t - 1\ 0)$ The pilot then maintains the control inputs at the equilibrium values after $\pi + 0\ 5$s Note that

the U_p commands are continuous, however, U_p is not The input dynamics (5 23) for each component of the force vector was taken to be a first order system as $\mathbf{u}_i = -20\mathbf{u}_i + 20\mathbf{w}_i + \mathbf{d}_{0_i}$ The disturbance vector $\mathbf{d}_0$ was taken to be

$$\begin{aligned} d_{F_x} &= 10\,5 + 8\,5\cos(7\pi t), \\ d_{F_z} &= 10\,5 - 8\,5\cos(6\pi t), \text{ and} \\ d_M &= 10\,5 + 5\,5\cos(5\pi t), \end{aligned} \tag{5 53}$$

with the bound $D_u = 20\,0$ K_4 used for R_4 in Section 4 3 was taken as $\mathbf{K}_x = [1\,0,\ 1\,0,\ 10\,0]^{\mathrm{T}}$ η_i and ϕ_{u_i} were taken as 1 0 and 50 0 respectively For comparison purposes, the response that would be obtained by neglecting the presence of the input dynamics, i e by using the control law in (4 44), is obtained and is labeled as R_0 in the following discussions and figures The responses for different choices of $\mathbf{K}_v = [K_U, K_W, K_Q]^{\mathrm{T}}$ are presented next $\mathbf{K}_{v_1}$ is chosen as $[10\,0,\ 10\,0,\ 10\,0]^{\mathrm{T}}$, $\mathbf{K}_{v_2} = [10\,0,\ 30\,0,\ 20\,0]^{\mathrm{T}}$, and $\mathbf{K}_{v_3} = [20\,0,\ 30\,0,\ 20\,0]^{\mathrm{T}}$ The corresponding responses are termed R_1, R_2, and R_3 respectively From $\hat{\mathbf{B}}_1$ as defined in (3 29) and the nominal parameters as given in Appendix D, it is clear that $\hat{\mathbf{B}}_1^{-1}$ will have large diagonal entries leading to a large $\mathbf{d}'_u$, as can be seen from (5 47), and thus the gains $\mathbf{K}_\eta$ are expected to be quite large Thus a smaller time step for the Runge-Kutta algorithm needs to be taken Here it was selected as 50μs for R_0, 5μs for R_1, and R_2, and $2\,5\mu$s for the higher gain case of $\mathbf{K}_{v_3}$

Figs 5 4, 5 5, and 5 6 present the $\mathbf{S}_v = \mathbf{V} - \mathbf{V}_a$ responses obtained for the various gain cases $\mathbf{K}_v$ for the velocity variables U, W, and Q respectively Note that with the ML strategy, the velocities $\mathbf{V}$ are supposed to track the $\mathbf{V}_a$ signals as discussed in the previous section For the R_0 response, which is the case where no input dynamics are present, the $\mathbf{S}_v$ errors should be bounded by the boundary layer thicknesses $\Phi_v = [0\,5,\ 0\,5,\ 5\,0\times10^{-4}]^{\mathrm{T}}$ as selected in Section 4 2 That this condition is actually satisfied is easily seen from the R_0 response in these figures The $\mathbf{S}_v$ responses for the gain cases $\mathbf{K}_{v_i}$, $i = 1,2,3$ in the Figs 5 4, 5 5, and 5 6 show that, with the specified input dynamics, larger deviations are seen at the smaller gain values $\mathbf{K}_{v_1}$, and these are seen to decrease with higher $\mathbf{K}_v$ gains as is seen from the R_2 and R_3 responses These errors

creep into the system because of the additional input dynamics Thus, it is observed from the figures that an increase of the $\mathbf{K}_v$ gains leads to smaller $\mathbf{S}_v$ as was expected from (5 51)

It is also clear from the figures that an increase in K_U leads to a smaller value of S_U only This is seen in the $U - U_a$ response in Fig 5 4 The K_U gain has the same value in the gain sets $\mathbf{K}_{v_1}$ and $\mathbf{K}_{v_2}$ while the other K_W and K_Q gains are increased The $U - U_a$ response for these cases are seen to be almost same as from responses R_1 and R_2 as in Fig 5 4 and are found to overlap However, as the K_W and K_Q gains are increased from $\mathbf{K}_{v_1}$ to $\mathbf{K}_{v_2}$, the corresponding R_2 responses in the Figs 5 5 and 5 6 show a marked improvement over the R_1 responses, with almost no effect on the S_U Similarly, as the K_U gain is increased from $\mathbf{K}_{v_2}$ to $\mathbf{K}_{v_3}$, R_3 in Fig 5 4 shows a distinct improvement over the R_1 and R_2 responses Here, the gains K_W and K_Q are the same and the R_2 and R_3 responses for the associated velocity variables W and Q show almost no improvement with these responses almost overlapping as in Figs 5 5 and 5 6 Thus the feedback gains $\mathbf{K}_v$ have a decoupled effect on the related velocity errors It is thus observed from the figures that as the magnitudes of the gain $\mathbf{K}_v$ are increased, the system performance approaches the R_0 performance in the limit, as would have been expected, since the R_0 effectively has 'unity' as the specified input dynamics ($\mathbf{u}_{\text{com}} = \mathbf{w}$), implying a infinity bandwidth dynamic system

As discussed earlier, as the K_Q gains are increased, better Q_a tracking is expected and this would result in better θ tracking Similarly, for the higher K_U and K_W gains better U and W tracking of the augmented signals are observed This implies that larger $\mathbf{K}_v$ gains should result in better position tracking performances The obtained position error ($\mathbf{S}_x$ responses are shown in Figs 5 7, 5 8, and 5 9 for the considered gain cases A distinct improvement in the tracking performances is observed as the gains are increased due to the better velocity tracking performance and is seen to approach the R_0 response The $\mathbf{S}_x$ errors in the high gain cases of R_2 and R_3 are seen to be almost overlapping in these figures The effect of the $\mathbf{K}_x$ gains on the $\mathbf{S}_x$ errors has been discussed in Section 4 3 1 However, as discussed in the previous section, the $\mathbf{S}_x$

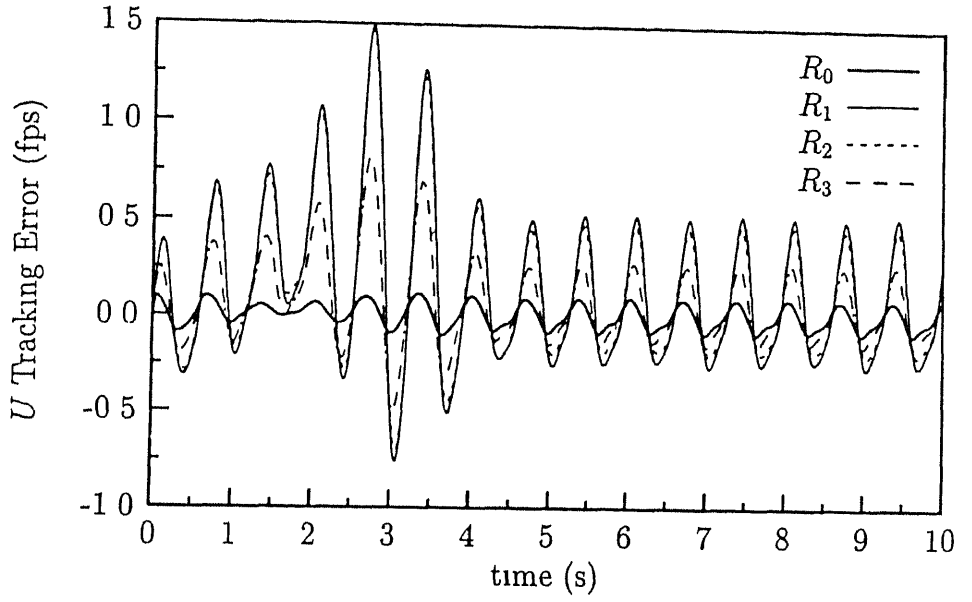

Fig. 5.4 The $S_U = U - U_a$ response Note that responses R_1 and R_2 overlap

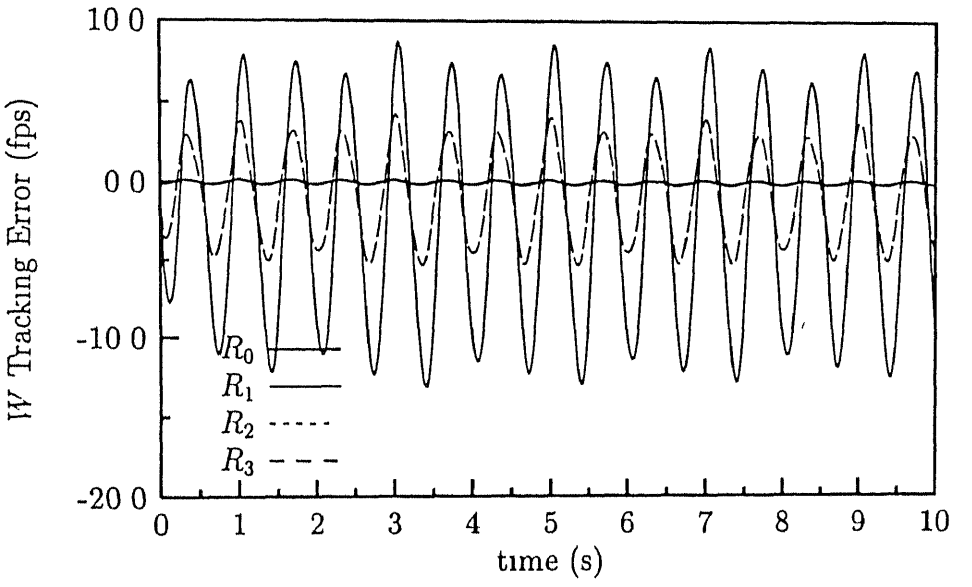

Fig. 5.5 The $S_W = W - W_a$ response The R_2 and R_3 are seen to be overlapping

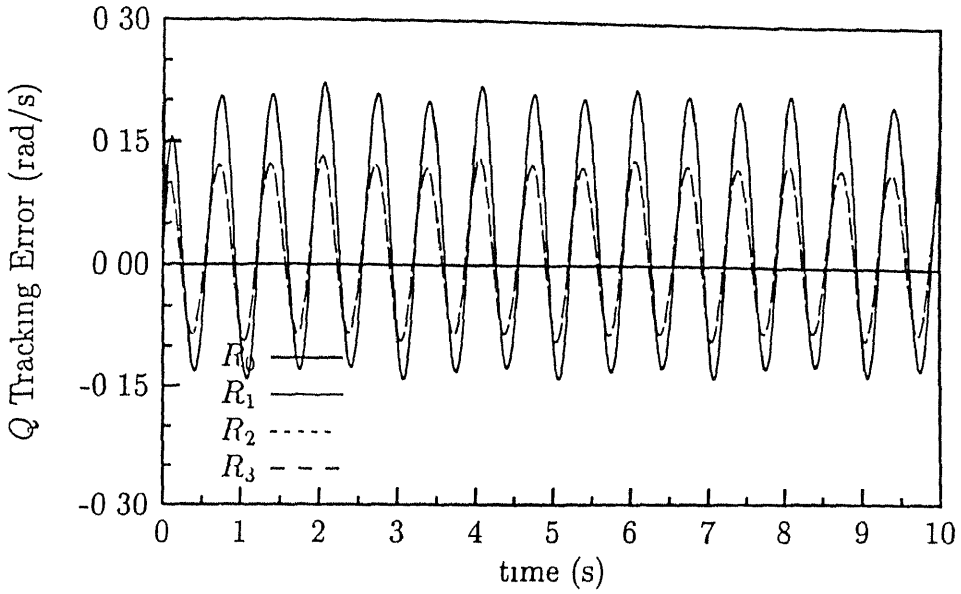

Fig. 5.6 The $S_Q = Q - Q_a$ response The R_2 and R_3 are seen to be overlapping

and S_v errors are inter-dependent (as shown in Appendix G) and the effect of varying the gains K_x and K_v simultaneously needs further study

The tracking error of the input dynamics $(u - u_a)$ is as shown in Figs 5 10, 5 11, and 5 12 It is seen from these figures that the S_u error (5 28) remains inside the selected boundary layer thicknesses ($\phi_{u_i} = 50\ 0$)

It may be concluded that as the K_v gain terms are increased the S_v error, introduced due to the input dynamics, decreases Thus it is seen that the input dynamics can be easily incorporated in a SMC approach with an attendant increase in velocity and position tracking errors, which can however be minimized by choosing appropriate gains as shown above The simulation results validate the control design method for the MIMO case The various loop errors are seen to be bounded though by unknown quantities A detailed parametric study of the involved feedback gains needs to be done for their proper selection

This chapter so far considers the development of a SMC design method for the case of specified first order input dynamics However, the method is not limited to this class of systems only and may be easily extended to the case of higher order input dynamics

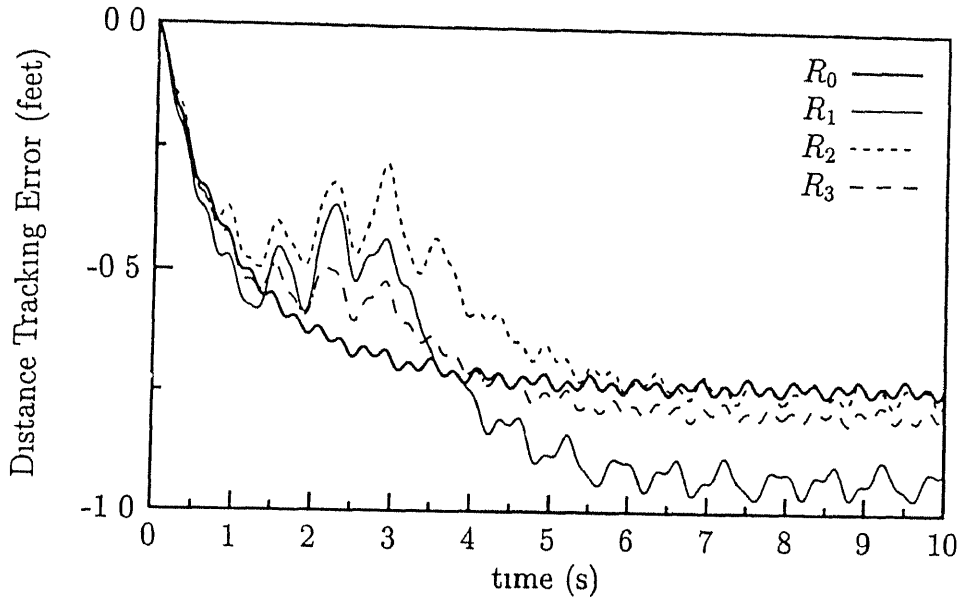

Fig. 5.7 The $p_x - p_{x_d}$ responses

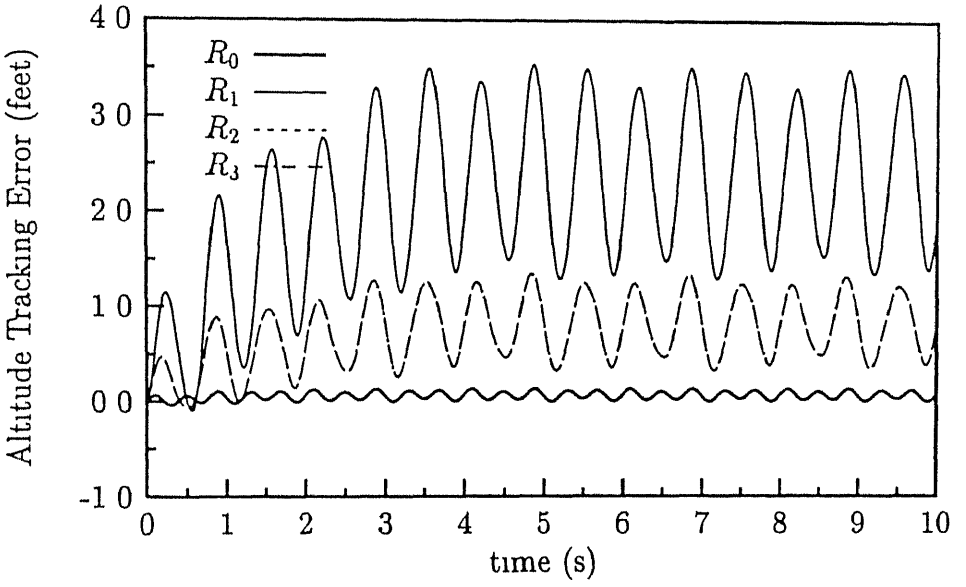

Fig. 5.8· The $p_z - p_{z_d}$ responses Note that the R_2 and R_3 responses overlap

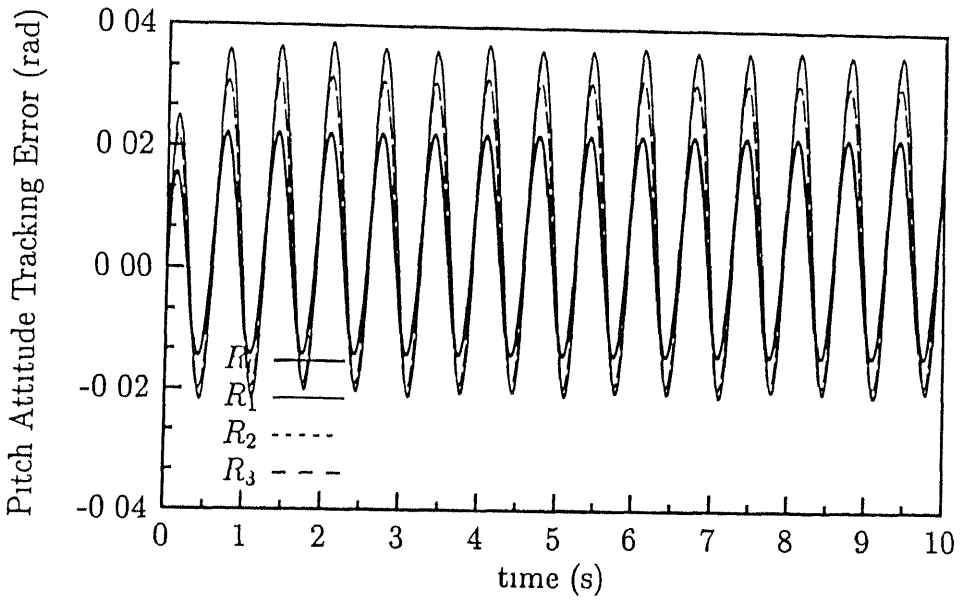

Fig. 5.9 The $\theta - \theta_d$ responses The R_2 and R_3 responses almost overlap

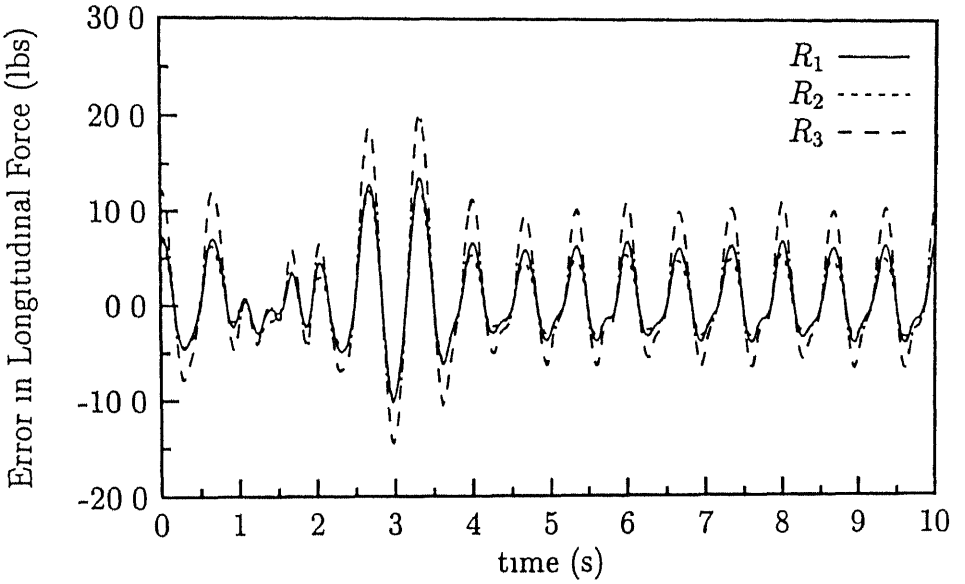

Fig. 5 10 The $F_x - F_{x_a}$ responses

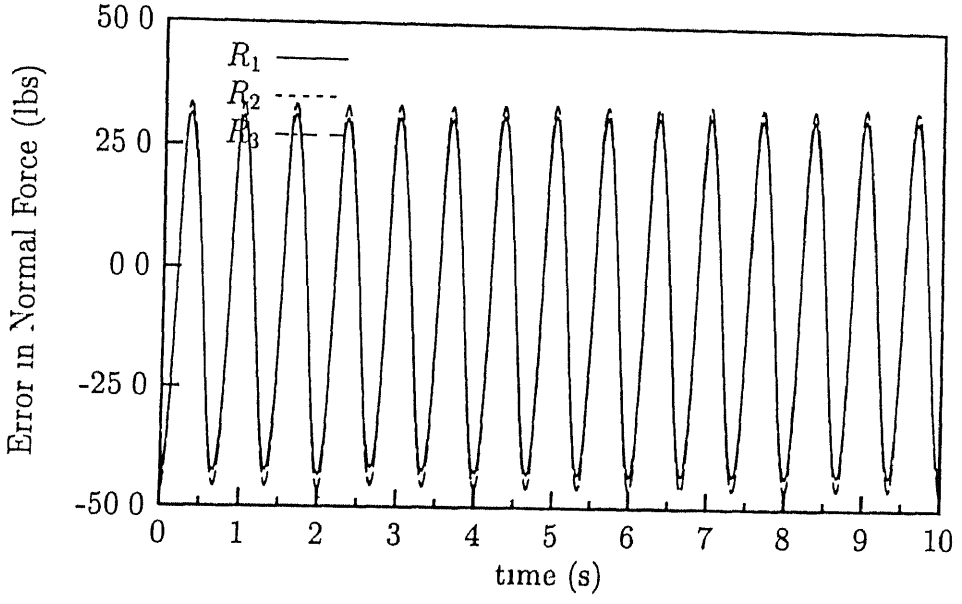

Fig. 5.11 The $F_z - F_{z_a}$ responses

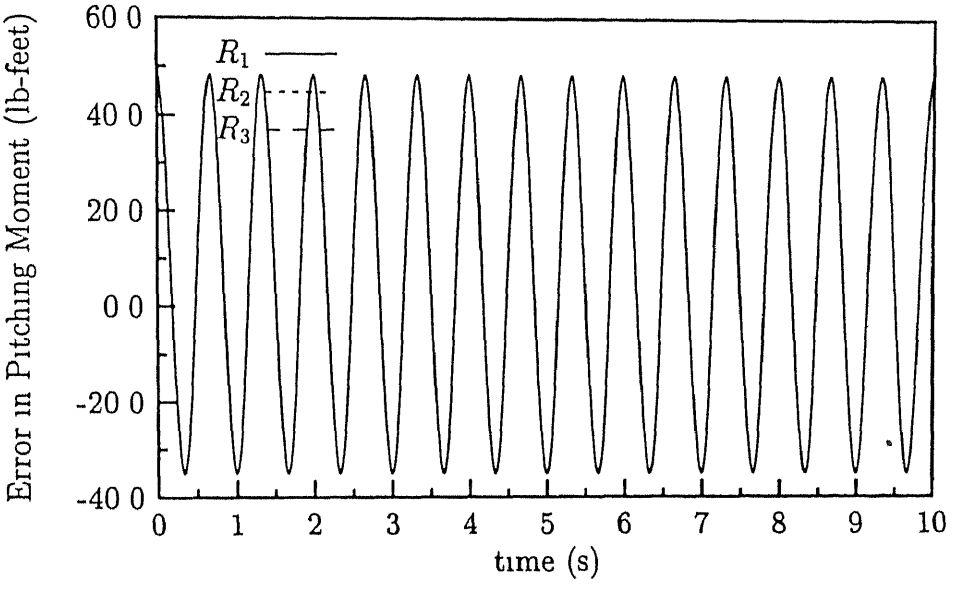

Fig. 5 12 The $M - M_a$ responses

using the ML analysis as was done in Section 4 4 1 The derivations for $\mathbf{u}_a$ in (5 32) and $\mathbf{u}_a = \mathbf{T}_u + \mathbf{d}'_u$ as in (5 46) and (5 47) would still remain the same as in Section 5 3 In case of specified second order input dynamics, for e g , another derivative of $\mathbf{T}_u$ would be required and the $\mathbf{d}'_u$ term would be passed on to the inner loops as was done in Sections 4 2 and 4 4 1 From its definition in (5 46), $\mathbf{T}_u$ would require another derivative of the desired model responses Thus the simple disturbance propagation method offered by the ML approach may be utilized to handle higher order input dynamics also

5.4 Conclusions

In this chapter, a robust control law design method, using a ML strategy, for a nonlinear system with specified input dynamics under unmatched uncertainties is developed The method does away with the requirement of higher order derivatives of the disturbances and uncertainties, leading to a simplified robustness analysis A discontinuous SMC law or its continuous approximation is designed in the inner-most loop so that the control inputs track a desired input signal generated in the outer loops Thus, the method results in continuous control inputs with discontinuities in its first or second derivatives only Since, it has been developed using a model following (MF) framework, higher order derivatives of the model (desired) responses are needed The method uses a full state feedback, including a measurement of the applied inputs The method is first developed for a SI nonlinear spring-mass-damper system It is shown that accelerometer signals are not necessary, although if present, they can be made use of Simulation results for the problem establish the applicability of the method The method is then applied to the MI aircraft problem with unmatched uncertainties as considered in Section 4 3 The bounds for the position and velocity errors are developed Results obtained from numerical simulation for different gain sets are presented and compared The ML strategy based SMC law synthesis method for a system with a specified input dynamics thus offers a alternate approach to the problem Also, the involved robustness issues are much easily tackled in this framework as compared to the other methods

Chapter 6

Conclusions & Scope for Further Work

The thesis is a study on some practical application aspects of the SMC design method The nonlinear longitudinal dynamics of a generic aircraft with the force-moment vector as the input has been treated as a benchmark problem The capability of generating a desired force-moment vector, given the airframe and engine characteristics, needs further study The control laws are developed under the assumption that an inverse map from the force space to the actual control surface deflections exists Although control laws have been developed for the longitudinal dynamics only, the method may easily be extended to the complete aircraft dynamics The main results of the study are as follows

1 A new method of selection of parameters for the constant plus proportional rate reaching law based SMC based on the criterion of the time to a pre-specified level of output tracking error (OTE) is proposed It is established the method guarantees a robust performance in the reaching phase also and gives faster tracking performances as compared to controllers based on the reaching time criterion.

2 The SMC has been used to design controllers for the aircraft dynamics which is nonlinear in the input This is achieved by using a force control approach (FCA), treating the force-moment vector as pseudo-inputs It is assumed that there are methods to generate any forces and moments as commanded by the

control law The error between the commanded and the generated forces is modelled as a bounded multiplicative uncertainty The conventional MIMO SMC design method is extended to include this uncertainty Analytical control laws are developed for the tracking and trimming modes for the longitudinal aircraft dynamics in the presence of matched uncertainties

3 The multi-loop (ML) strategy has been utilized to propose a method of designing SMC laws in the presence of unmatched disturbances and uncertainties The position and velocity tracking errors are derived and shown to be uniformly ultimately bounded Analytical control laws are synthesized for the tracking mode and verified through numerical simulation using the parameters of the F-16 aircraft

4 Using the better disturbance propagation property of the ML approach, a procedure for the selection of the gain of the switching term is proposed which permits extension of the conventional SMC design methods to the unmatched uncertainty case The switching surface parameters can be selected using the developed bounds on the output tracking error

5 The ML structure has been extended to generate SMC laws for systems with specified input dynamics in the presence of matched and unmatched uncertainties and disturbances Robustness analysis has been carried out and the ultimate boundedness of the position, velocity and input tracking errors are established Simulation results are obtained for a nonlinear spring mass system and the aircraft longitudinal dynamics and establish the efficacy of the proposed approach

Thus, the present work establishes that the ML (multi-loop) strategy can be used to advantage in designing SMC laws for mechanical and in particular aircraft systems, considering some of the practical issues involved With the FCA as proposed in this study, and an estimate of the aircraft mass and inertia parameters, the developed control laws can be used to generate force-moment specifications to be met by the aerodynamics and propulsion groups at preliminary design stages of a development

project for the aircraft to have desired the HQs The explicit model following structure allows for easy alterations in the desired model responses at any design stage or even in flight

The capabilities of the SMC method need to be extended for it to become a powerful alternative to the conventional FCS design methods For this, further studies along the following directions will be beneficial

1 The work relies on the existence of a map from the force space to the effector space The capability of varying all the components of the force-moment vector independently needs further study It will be interesting to find out the minimum number of control effectors required for this purpose and their design This issue needs further detailed study, before the FCA (force control approach) can actually be applied to the full envelope FCS design problem

2 The control laws developed in this work use a full state feedback The case of output feedback and the design of nonlinear observers based on the SMC approach to generate estimates of the remaining states should be studied

3 It is desirable to extend the present study to include bounded control input and rate saturations

4 The specification of model responses based on the handling quality (HQ) requirements and its selection in the case of an existing airframe with a given limited force generation capability should be studied The advantage of a model following approach may be utilized by specifying different linear model responses for different operating conditions, which could depend not only on the input and rate saturations but also on the need to limit some particular states of the aircraft These model responses may then be scheduled instead of the controllers as in the gain-scheduled FCS design approach This could also be achieved by specifying the desired response through a single nonlinear system

5 The control laws synthesized in this work are analog Most of the controller implementations, however, are now done on digital computers Thus it is desirable

to consider SMC design for sampled data feedback systems

6 The results for second order systems (c f Chapter 2) would be of use for many mechanical systems, for e g , robot applications Thus, further study needs to be carried out to develop better estimates of the time to reach a specified level of output tracking error

References

[1] McRuer D and Graham D , " Eighty Years of Flight Control Triumphs and Pitfalls of the Systems Approach ," *Journal of Guidance Control and Dynamics*, vol 4 no 4, pp 353–362, 1981

[2] Burns B R A , " Fly-by-Wire and Control Configured Vehicles - Rewards and Risks ," *Aeronautical Journal*, vol 79, pp 231–246, Feb, 1975

[3] Simpson A and Hitch H P Y , " Active Control Technology ," *Aeronautical Journal*, vol 81, pp 231–246, June 1977

[4] Bera R K , "Control configured vehicles- goals and challenges," Project Document PD CF 8932, National Aeronautical Laboratory, Bangalore, India, September 1989

[5] Bera R K , "A conceptual framework for fighter flight control systems," Project Document PD CF 9009, National Aeronautical Laboratory, Bangalore, India, April 1990

[6] Gal-Or B , " Editorial Western vs Eastern Fighter Technologies Beyond 2000 ," *International Journal of Turbo and Jet Engines*, vol 11, pp 113–118, 1994

[7] Gal-Or B , " Thrust Vectoring for Flight Control and Safety A Review ," *International Journal of Turbo and Jet Engines*, vol 11, pp 119–136, 1994

[8] " Fighters for 2000 AD ," *Vayu*, vol no 2, pp 39–44, 1997

[9] Belov A , " The Su-30 Family ," *Vayu*, vol no 3, pp 38–45, 1997

[10] Lewis F L and Stevens B , *Aircraft Control and Simulation* John Wiley Inter-Science, 1992

[11] Yedavalli R K , " Robust Control Design for Aerospace Applications ," *IEEE Transactions on Aerospace and Electronic Systems*, vol 25 no 3, pp 314–324, 1989

[12] Houpis C H , Sating R R , Rasmussen S , and Sheldon S , " Quantitative Feedback Theory Technique and Application ," *International Journal of Control*, vol 59 no 1, pp 39–70, 1994

[13] Gangsaas D , Bruce K R , Blight J D , and Ly U , " Application of Modern Synthesis to Aircraft Control Three Case Studies ," *IEEE Transactions on Automatic Control*, vol 31 no 11, pp 995–1014, 1986

[14] Adams R J , Sparks A , and Banda S S , " Full Envelope Multivariable Control Law Synthesis for a High Performance Test Aircraft ," *Journal of Guidance Control and Dynamics*, vol 16 no 5, pp 948–955, 1993

[15] Blight J D , Dailey R L , and Gangsaas D , " Practical Control Law Design for Aircraft using Multivariable Techniques ," *International Journal of Control*, vol 59 no 1, pp 93–137, 1994

[16] Shue S P , Sawan M E , and Rokhsaz K , " Mixed H_2/H_∞ Method Suitable for Gain Scheduled Aircraft Control ," *Journal of Guidance Control and Dynamics*, vol 20 no 4, pp 699–706, 1997

[17] Enns D , Bugajski D , Hendrick R , and Stein G , " Dynamic Inversion an evolving methodology for flight control design ," *International Journal of Control*, vol 59 no 1, pp 71–91, 1994

[18] Moorhouse D J and Citrus K D , " The Control System Design Methodology of the STOL and Maneuver Technology Demonstrator ," *International Journal of Control*, vol 59 no 1, pp 221–238, 1994

[19] Shamma J S and Athans M , " Analysis of Gain-scheduled control for non-linear plants ," *IEEE Transactions on Automatic Control*, vol 35 no 8, pp 898–907, 1990

[20] Shamma J S and Athans M , " Gain Scheduling Potential hazards and Remedies ," *IEEE Control System Magazine*, vol 12 no 3, pp 101–107, 1992

[21] Slotine J J E and Li W , *Applied Nonlinear Control* Prentice Hall, 1991

[22] Isidori A , *Nonlinear Control Systems* Newyork Springer-Verlag, 1989

[23] Smith G A and Meyer G , " Aircraft Automatic Flight Control System with Model Inversion ," *Journal of Guidance Control and Dynamics*, vol 10 no 3, pp 269–275, 1987

[24] Lane S H and Stengel R F , " Flight control design using nonlinear inverse dynamics ," *Automatica*, vol 24 no 4, pp 471–483, 1988

[25] Vukobratović M and Stojić R , *Modern Aircraft Flight Control* , vol 109 of *Lecture Notes in Control and Information Sciences* Berlin Springer-Verlag, 1988

[26] Singh S N , " Decoupled Ultimate Boundedness Control of Systems and Large Aircraft maneuver ," *IEEE Transactions on Aerospace and Electronic Systems*, vol 25 no 5, pp 677–688, 1989

[27] Romano J J and Singh S N , " I-O map inversion, zero dynamics and Flight Control ," *IEEE Transactions on Aerospace and Electronic Systems*, vol 26 no 6, pp 1022–1028, 1990

[28] Durham W C , Lutze F H , Barlas M R , and Munro B C , " Nonlinear model-following control application to airplane control ," *Journal of Guidance Control and Dynamics*, vol 17, no 3, pp 570–577, 1994

[29] Sun X D and Clarke T , " Advanced aircraft flight control using nonlinear inverse dynamics ," *IEE Proceedings on Control Theory and Applications*, vol 141 no 6, pp 418–426, 1994

[30] Adams R J and Banda S S , " Robust flight control design using dynamic inversion and structured singular value synthesis ," *IEEE Transactions on Control System Technology*, vol 1 no 2, pp 80–91, 1993

[31] Sparks A and Banda S S , " Application of Structured Singular Value Synthesis to a Fighter Aircraft ," *Journal of Guidance Control and Dynamics*, vol 16 no 5, pp 940–947, 1993

[32] Sparks A , Buffington J , and Banda S S , " Fighter aircraft lateral directional axes full envelope Control law design ," *International Journal of Control*, vol 59 no 4, pp 893–924, 1994

[33] Utkin V I , *Sliding Modes and their Applications in Variable Structure Systems* Moscow Mir Publishers, 1978

[34] Utkin V I , " Variable Structure systems with Sliding Mode ," *IEEE Transactions on Automatic Control*, vol 22 no 2, pp 212–222, 1977

[35] DeCarlo R A , Zak S H , and Matthews G P , " Variable Structure Control of nonlinear multivariable systems A Tutorial ," *Proceedings of the IEEE*, vol 76 no 3, pp 212–232, 1988

[36] Hung J Y , Gao W , and Hung J C , " Variable Structure Control A Survey ," *IEEE Transactions on Industrial Electronics*, vol 40 no 1, pp 2–21, 1993

[37] Gao W and Hung J C , " Variable Structure Control of Nonlinear Systems A New Approach ," *IEEE Transactions on Industrial Electronics*, vol 40 no 1, pp 45–55, 1993

[38] Drazenovic B , " The Invariance conditions in Variable Structure Systems ," *Automatica*, vol 5, pp 287–295, 1969

[39] Franklin J A , " Application of nonlinear inverse methods to the control of powered lift aircraft over the low speed flight envelope ," *International Journal of Control*, vol 59 no 1, pp 321–335, 1994

[40] Calise A J and Kramer F S , " A Variable Structure approach to Robust control of VTOL Aircraft ," *Journal of Guidance Control and Dynamics*, vol 7 no 5, pp 620–626, 1984

[41] Singh S N , " Asymptotically decoupled discontinuous control of systems and Nonlinear Aircraft maneuver ," *IEEE Transactions on Aerospace and Electronic Systems*, vol 25 no 3, pp 380–391, 1989

[42] Hedrick K J and Gopalswamy S , " Nonlinear Flight Control Design via Sliding Methods ," *Journal of Guidance Control and Dynamics*, vol 13 no 5, pp 850–858, 1990

[43] Thukral A and Innocenti M , " Controls Design Challenge A Variable Structure Approach ," *Journal of Guidance Control and Dynamics*, vol 17 no 5, pp 942–949, 1994

[44] Fossard A J , " Helicopter Control law based on Sliding Mode with Model following ," *International Journal of Control*, vol 57 no 5, pp 1221–1235, 1993

[45] Col Francis M S , " X-31 An international success story ," *Aerospace America*, pp 22–27,32, February 1995

[46] Gal-Or B , Sherbaum V , Lichtsinder M , and Turgemann M , " Complete Thrust Vectoring Flight Control for Future Civil Jets, F-22 Superiority Fighter and Cruise Missiles, Part I Vectored F-22, F-16 and F-15 ," *International Journal of Turbo and Jet Engines*, vol 10, pp 1–17, 1993

[47] Durham W C, " Constrained control allocation ," *Journal of Guidance Control and Dynamics*, vol 16 no 4, pp 717–725, 1993

[48] Durham W C , " Constrained control allocation 3 moment problem ," *Journal of Guidance Control and Dynamics*, vol 17 no 2, pp 330–336, 1994

[49] Snell S A , Enns D F , and Garrard Jr W L , " Nonlinear inversion flight control for a supermaneuverable aircraft ," *Journal of Guidance, Control, and Dynamics*, vol 15 no 4, pp 976–984, 1992

[50] Azam M and Singh S N , " Invertibility and trajectory control for nonlinear maneuvers of aircraft ," *Journal of Guidance Control and Dynamics*, vol 17 no 1, pp 192–200, 1994

[51] Spurgeon S K , " Choice of discontinuous control component for robust sliding mode performance ," *International Journal of Control*, vol 53 no 1, pp 163–179, 1991

[52] Spurgeon S K and Davies R , " A Nonlinear Control Strategy for Robust Sliding Performance in the Presence of Unmatched Uncertainty ," *International Journal of Control*, vol 57 no 5, pp 1107–1123, 1993

[53] Liao T L , Fu L C , and Hsu C F , " Output Tracking Control of Nonlinear Systems with Mismatched Uncertainties ," *Systems and Control Letters*, vol 18, pp 39–47, 1992

[54] Emel'yanov S V , Korovin S K , and Levant A , " Higher Order Sliding Modes in Control Systems ," *Differential Equations*, vol 29 no 11, pp 1627–1647, 1993

[55] Levant A , " Sliding Order and Sliding Accuracy in Sliding Mode Control ," *International Journal of Control*, vol 58 no 6, pp 1247–1263, 1993

[56] Zhou F and Fisher D G , " Continuous sliding mode control ," *International Journal of Control*, vol 55 no 2, pp 313–327, 1992

[57] Ramirez H S , " Dynamical Sliding Mode Control Strategies in the Regulation of Nonlinear Chemical Processes ," *International Journal of Control*, vol 56 no 1, pp 1–21 1992

[58] Ramirez H S , " On the Dynamical Sliding Mode Control of Nonlinear Systems ," *International Journal of Control*, vol 57 no 5, pp 1039–1061, 1993

[59] Ramirez H S , Zribi M , and Ahmad S , " Dynamical Sliding Mode Control Approach for Vertical Flight Regulation in Helicopters ," *IEE Proceedings on Control Theory and Applications*, vol 141 no 1, pp 19–24, 1994

[60] Chiacchiarini H G , Desages A C , Romagnoli J A , and Palazoglu A , " Variable Structure Control with a Second-order Sliding Condition Application to a Steam Generator ," *Automatica*, vol 31 no 8, pp 1157–1168, 1995

[61] Choi S , Park D , and Jayasuriya S , " A Time varying Sliding surface for fast and robust tracking control of Second-order Uncertain Systems ," *Automatica*, vol 30 no 5, pp 899–904, 1994

[62] Bartoszewicz A , " A Comment on 'A Time varying Sliding surface for fast and robust tracking control of Second-order Uncertain Systems' ," *Automatica*, vol 31 no 12, pp 1893–1895, 1995

[63] Bartoszewicz A , " Time-varying Sliding Modes for Second-order Systems," *IEE Proceedings on Control Theory and Applications*, vol 143 no 5, pp 455–462, 1996

[64] Mudge S K and Patton R J , " Enhanced Assessment of Robustness for an Aircraft's Sliding Mode Controller ," *Journal of Guidance Control and Dynamics*, vol 11 no 6, pp 500–507, 1988

[65] Bartolini G and Zolezzi T , " Control of Nonlinear Variable Structure Systems ," *Journal of Mathematical Analysis and Applications*, vol 118 no 1, pp 42–62, 1986

[66] Hauser J , Sastry S , and Meyer G , " Nonlinear control design for slightly NMP systems application to V/STOL aircraft ," *Automatica*, vol 28 no 4, pp 665–679, 1992

[67] Li Z , Chai T Y , and Wen C , " Systematic Design of Robust Controllers for Nonlinear Uncertain Systems ," *International Journal of Control*, vol 62 no 4, pp 871–892, 1995

[68] Li Z , Chai T Y , Wen C , and Soh C B , " Robust Output Tracking for Nonlinear Uncertain Systems ," *Systems and Control Letters*, vol 25, pp 53–61, 1995

[69] Ogata K , *Modern Control Engineering* Prentice Hall of India, 1992

[70] Hui S and Zak S D , " Robust Control Synthesis for Uncertain/Nonlinear Dynamical Systems ," *Automatica*, vol 28 no 2, pp 289–298, 1992

[71] Qu Z , " Global Stabilization of Nonlinear Systems with a Class of Unmatched Uncertainties ," *Systems and Control Letters*, vol 18, pp 301–307, 1992

[72] Qu Z , " Robust Control of Nonlinear Uncertain Systems under Generalized matching Conditions ," *Automatica*, vol 29 no 4, pp 985–998, 1993

[73] Cong L and Landers P H , " Robust Control of MIMO Nonlinear Systems with Mismatched Uncertainties ," *International Journal of Control*, vol 62 no 4, pp 961–981, 1995

[74] Wu W and Chou Y S , " A New Systematic Design of High-Gain Feedback for Nonlinear Systems with Unmatched Uncertainties ," *International Journal of Control*, vol 62 no 6, pp 1471–1489, 1995

[75] Zhao F and Utkin V I , " Adaptive Simulation and Control of Variable-structure Control Systems in Sliding Regimes ," *Automatica*, vol 30 no 5, pp 899–904, 1994

[76] Chang F J , Twu S H , and Chang S , " Adaptive Chattering Alleviation of Variable Structure Systems Control ," *IEE Proceedings on Control Theory and Applications*, vol 137 no 1, pp 31–39, 1990

[77] Elmali H and Olgac N , " Robust Output Tracking Control of Nonlinear MIMO Systems via Sliding Mode Technique ," *Automatica*, vol 28 no 1, pp 145–151, 1992

Appendix A

The S response

The s dynamics is shown to be given in (2 18) as

$$s = -\epsilon s - \eta' \mathrm{sgn}[s], \tag{A 1}$$

where, η' depends on disturbances and uncertainties and is thus an unknown function of the time variable t However, it is known to be bounded and $\eta' \geq \eta$, where η is a constant, for all t Let the response of the above system be indexed by the gain of the switching term, i e as $s_{\eta'}$ Here, the decay performance of $s_{\eta'}$ is studied In particular, consider the case of s decaying from an initial positive value of s_0 at $t = 0$ The above reaching law shows that $s = 0$ is an equilibrium point of the system and further that once s reaches zero, it will stay there for all future time instants Starting from a positive s_0, the s will always be non-negative The sgn[s] term is thus replaced by $+1$ in the above equation Thus, the s dynamics becomes

$$\begin{aligned} s &= -\epsilon s - \eta', \text{ or} \\ &= -\epsilon s - \eta + (\eta - \eta'(t)) \end{aligned} \tag{A 2}$$

The $\eta - \eta'(t) = n(t)$ term is seen to be non-positive The solution of the above equation may be written [69] as

$$s_{\eta'}(t) = s_0 e^{-\epsilon t} + \int_0^t e^{-\epsilon(t-\tau)}[-\eta + n(\tau)]d\tau, \text{ or}$$

$$\leq \quad s_0 e^{-\epsilon t} + \int_0^t e^{-\epsilon(t-\tau)}[-\eta]d\tau, \tag{A 3}$$

since $n(\,) \leq 0$ for all t For negative initial values of s_0, it can be similarly shown that

$$s_{\eta'}(t) \geq s_0 e^{-\epsilon t} + \int_0^t e^{-\epsilon(t-\tau)}[\eta]d\tau, \tag{A 4}$$

The right hand side of the above inequalities (A 3) and (A 4) represents s_η, i e the initial condition response of

$$s = -\epsilon s - \eta \mathrm{sgn}[s] \tag{A 5}$$

These inequalities may be rewritten as a single inequality as

$$|s_{\eta'}(t)| \leq |s_\eta(t)|, \tag{A 6}$$

which implies that if $\eta'(t) > \eta$ for all t, the decay of s exhibited by (A 1) is guaranteed to be better than the response of (A 5) as given in (A 6) Therefore, the reaching time, i e the time taken to arrive at $s = 0$ starting from s_0 will be bounded as

$$t_{reach} \leq \frac{1}{\epsilon} \ln \left(\frac{\epsilon |s_0| + \eta}{\eta} \right), \tag{A 7}$$

which is the reaching time for (A 5) [37] The (A 6) also implies that increasing the magnitude of η leads to a faster decay of s and lower reaching times

If, the sgn[s] term is replaced by a continuous approximation as sat[s/ϕ] in (A 5), where ϕ represents an appropriately selected boundary layer thickness, then the s dynamics is given by $s = -\epsilon s - \eta \mathrm{sat}(s/\phi)$ The time taken from an initial condition of s_0 at $t = 0$ to reach the boundary layer may be evaluated as

$$t_{reach} = \frac{1}{\epsilon} \ln \left(\frac{\epsilon |s_0| + \eta}{\epsilon \phi + \eta} \right) \tag{A 8}$$

Appendix B

Proof of Claim 1

The following proof shows how a $\delta > 0$ may be selected, under the assumptions in the Claim 1 and starting from the premise that the (2 32) is true, i e ,

$$Q = \delta P + H \tag{B 1}$$

The P and Q matrices in the above equation are as given in (2 25) and (2 29) respectively

Proof:

From the P and Q matrices as given, the elements of the symmetric matrix $H = Q - \delta P$ from (B 1) are obtained as

$$\begin{aligned} h_{11} &= 2\alpha^2\epsilon - \delta(\alpha^2 + \beta) \\ h_{12} &= 2\alpha\epsilon - \beta - \delta\alpha \\ h_{22} &= 2\epsilon - \delta, \end{aligned} \tag{B 2}$$

where, h_{ij} represents the element $H(i,j)$ It is required that H be at least a positive semi-definite matrix The positive definiteness of this matrix would require that $h_{11}, h_{22} > 0$ and $\det[H] > 0$, where $\det[\,]$ represents the determinant of its argument The two former inequalities gives

$$\begin{aligned} \delta &< 2\epsilon\frac{\alpha^2}{\alpha^2 + \beta}, \text{ and} \\ \delta &< 2\epsilon \end{aligned} \tag{B 3}$$

It is seen that these inequalities are in agreement with one another For the last condition, the det$[H]$ may be easily obtained from its elements as defined in (B 2) as $h_{11}h_{22} - h_{12}^2$ and after some algebraic simplification it may be written as

$$\det[H] = \beta[\delta^2 - 2(\alpha + \epsilon)\delta + 4\alpha\epsilon - \beta] \tag{B 4}$$

The positive definiteness of P and Q imposes the condition that $0 < \beta < 4\alpha\epsilon$ as has been discussed in Section 2 3 Since $\beta > 0$, the term factored out in the above equation is dropped in the further developments The above equation thus shows that $\det[H]/\beta$ is thus a quadratic function (Q_f) in δ as

$$Q_f(\delta) = \delta^2 - 2(\alpha + \epsilon)\delta + 4\alpha\epsilon - \beta, \tag{B 5}$$

and the constant term in the above equation is seen to be positive from the bounds to be satisfied by β as given in (2 30) The roots r_1, r_2 of this quadratic equation may be easily calculated as

$$r_1, r_2 = (\alpha + \epsilon) \pm \sqrt{(\alpha - \epsilon)^2 + \beta} \tag{B 6}$$

Note that $\sqrt{(\alpha - \epsilon)^2 + \beta}$ can always be represented as $(\alpha - \epsilon) + \delta_1$ where $\delta_1 > 0$ may be uniquely found Thus, the roots in (B 6) may be simplified to get

$$r_1, r_2 = 2\alpha + \delta_1, 2\epsilon - \delta_1 \tag{B 7}$$

Note that a small positive value for β would imply a small δ_1 It can be shown that even for values of β as large as permissible by its bounds, the $r_2 = 2\epsilon - \delta_1 > 0$ Since the coefficient of the second order term in Q_f in (B 5) is seen to be positive, it implies that the Q_f has a minimum, and the corresponding value of δ $(= \delta_m)$ which gives the function minimum can be evaluated as

$$\delta_m = \alpha + \epsilon, \tag{B 8}$$

which being the arithmetic mean of r_1 and r_2 will always lie between the two roots. Combined with the fact that $Q_f = 0$ at the roots $\delta = r_1$ and r_2 (B 7), it is seen that the $Q_f \leq 0$ is possible only for values of δ between the two roots and it would be

positive everywhere outside of this set Moreover, at $\delta = 0$ the value of Q_f is seen to be $4\alpha\epsilon - \beta$, which is positive as discussed earlier

Thus it is evident that a positive δ can always be selected from the sets given by $(0, 2\alpha]$ or $(0, 2\epsilon)$, whichever is smaller The two may be combinedly expressed by letting $\gamma = \min[2\alpha, 2\epsilon]$, where $\min[\ ,\ ]$ is taken to give the minimum of its arguments Thus, the permissible values of δ may be specified by an open set as

$$\delta \in (0, \gamma) \tag{B 9}$$

Moreover, in the limit of $\beta \to 0$, a choice of $\delta \to \gamma$ would be achieved It is thus established that a positive δ always exists which would result in H being a positive definite matrix, thus satisfying the Claim 1 ■

Appendix C

Proof of Claim 2

The arguments of the candidate Lyapunov function $V(\ ,\ )$ in (2 40) are omitted when no confusion is likely to arise Note that this candidate function is not differentiable on the planes $S_p = 0$ and $S_q = 0$ However, it is possible to use the generalized Lyapunov theorem, which allows non-differentiability of the Lyapunov function in a set of measure zero [41, 60] It is obvious that V is positive definite function with $V(0,0) = 0$, and positive everywhere else in the e-e plane The at least negative semi-definiteness (n s d) of V is established next for the two cases

Proof· Using (2 31), The time derivative of (2 40) may be derived following the steps as outlined in Section 2 3 and gives the V here as

$$V = -y^T Q y + 2y^T P \bar{q} + M \left[S_p \mathrm{sgn}[S_p] + S_q \mathrm{sgn}[S_q] \right], \qquad \text{(C 1)}$$

except for the two planes where the function is not differentiable Note that $\bar{q}$ is different for the Cases CP and CQ as they have different switching surfaces S_p and S_q However the P is common for both the cases It has been selected as P in (2 25) for the Case CP Thus, the $y^T P \bar{q}$ may be rewritten as $S_p h_i$, where $h_i = -\eta' \mathrm{sgn}[S_i]$ and the subscripts $i = p, q$ represents the cases CP and CQ respectively Moreover it follows from $\eta' \leq \eta_M$ that the maximum value of $|h_i| = \eta_M$ The S_p and S_q as required in the above equation and are evaluated as follows With h_i as defined above, the $e = -ae - be + h_i$ from (2 20), for the case represented by the subscript i, and

$a = pq, b = p + q$ from (2 8), the $S_p = e + pe$ may be simplified as

$$\begin{aligned} S_p &= -ae - (b-p)e + h_i \\ &= -pqe - qe + h_i, \text{ or} \\ S_p &= -qS_p + h_i \end{aligned} \tag{C 2}$$

Similarly, S_q can be obtained as

$$S_q = -pS_q + h_i \tag{C 3}$$

Thus the time derivative of the candidate Lyapunov function as in (C 1) may be rewritten for the case 'i', using the $y^T P\bar{q} = S_p h_i$ as defined above and S_p and S_q as in (C 2) and (C 3), as

$$\begin{aligned} \dot{V}_i &= -y^T Qy + 2S_p h_i + M\left[(-qS_p + h_i)\text{sgn}[S_p] + (-pS_q + h_i)\text{sgn}[S_q]\right], \text{ or} \\ &= -y^T Qy + 2S_p h_i - M[q|S_p| + p|S_q|] + M[\text{sgn}[S_p] + \text{sgn}[S_q]]h_i \end{aligned} \tag{C 4}$$

It is seen from Fig C 1, that the two planes, $S_p = 0$ and $S_q = 0$, divide the $e - \dot{e}$ plane into four regions $\dot{V}_i$ as evaluated above is checked for sign definiteness in each of these regions for the two cases First the Case CP is considered

Case CP

In this case ($i = p$) and $h_p = -\eta' \text{sgn}[S_p]$ Thus, it is obvious that

$$\begin{aligned} h_p &> 0, \textit{ when } S_p < 0, \text{ and} \\ h_p &< 0, \textit{ when } S_p > 0 \end{aligned} \tag{C 5}$$

Let $\dot{V}_p$ represent $\dot{V}$ for this case Note that, the $-y^T Qy - M[q|S_p| + p|S_q|]$ term in $\dot{V}_i$ in (C 4) is always negative definite The sign definiteness of the remaining terms are established in the four regions

1 Region 1 In this region $S_p > 0$ and $S_q > 0$ Thus, $[\text{sgn}[S_p] + \text{sgn}[S_q]] = 2$ and $\dot{V}$ in (C 4) reduces to

$$\dot{V}_p = -y^T Qy - M[q|S_p| + p|S_q|] + 2S_p h_p + 2Mh_p \tag{C 6}$$

With $h_p < 0$ (C 5), it can be seen that $\dot{V}_p < 0$ in this region

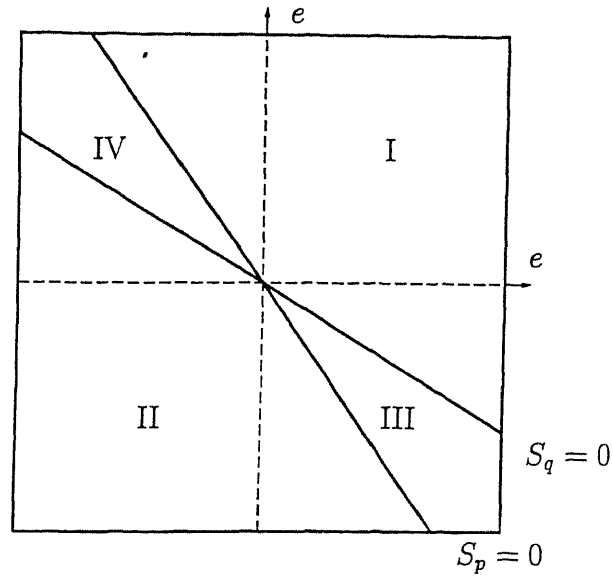

Fig C.1 The e–e plane

2 Region 2 In this region $S_p < 0$ and $S_q < 0$ and V becomes

$$V_p = -y^T Q y - M[q|S_p| + p|S_q|] + 2S_p h_p - 2Mh_p \qquad \text{(C 7)}$$

In this region, $h_p > 0$ which makes $V_p < 0$

3 Region 3 In this region $S_p > 0$ and $S_q < 0$ and with $[\text{sgn}[S_p] + \text{sgn}[S_q]] = 0$, V may be obtained as

$$V_p = -y^T Q y - M[q|S_p| + p|S_q|] + 2S_p h_p \qquad \text{(C 8)}$$

From (C 5), $h_p < 0$ ensures that V_p is negative

4 Region 4 In this region $S_p < 0$ and $S_q > 0$ and V becomes

$$V_p = -y^T Q y - M[q|S_p| + p|S_q|] + 2S_p h_p \qquad \text{(C 9)}$$

$h_p > 0$ in this region, and thus the time derivative of V can be seen to be negative.

The above checks establish that V in (2 40) is a Lyapunov function for Case CP Note that the $S_p h_p$ term in the above equations may be rewritten as $-\eta'|S_p|$ which is always

negative The V_p in the four regions as in (C 6) - (C 9) may be jointly expressed by the following inequality

$$V_p \leq -y^T Q y - M[q|S_p| + p|S_q|] - 2\eta'|S_p| \tag{C 10}$$

It is evident that V in (2 40) remains positive definite with the V_p above being negative definite for all $M \geq 0$, and thus the V is seen to be a valid Lyapunov function for the CP case

The candidate function is next checked for the Case CQ

Case CQ·

In this case with $i = q$, h_q is given as $-\eta'\mathrm{sgn}[S_q]$, and thus,

$$\begin{aligned} h_q &> 0, \ when\ S_q < 0, \text{ and} \\ h_q &< 0, \ when\ S_q > 0 \end{aligned} \tag{C 11}$$

Let V_q represent V for this case

1 Region 1 In this region $S_p > 0$ and $S_q > 0$ V in (C 4) reduces to

$$V_q = -y^T Q y - M[q|S_p| + p|S_q|] + 2S_p h_q + 2M h_q \tag{C 12}$$

With $h_q < 0$ from (C 11), it can be seen that $V_q < 0$ in this region

2 Region 2 In this region $S_p < 0$ and $S_q < 0$ and V becomes

$$V_q = -y^T Q y - M[q|S_p| + p|S_q|] + 2S_p h_q - 2M h_q \tag{C 13}$$

In this region, $h_q > 0$ which makes $V_q < 0$

3 Region 3 In this region $S_p > 0$ and $S_q < 0$ and V becomes

$$V_q = -y^T Q y - qM|S_p| - pM|S_q| + 2S_p h_q \tag{C 14}$$

Note that the first three terms are negative, however the last term is positive as $h_q > 0$ (C 11) The above equation may be rewritten as

$$V_q = -y^T Q y - pM|S_q| - (qM - 2h_q)|S_p| \tag{C 15}$$

It is known that η' and therefore $|h_q|$ is bounded Thus if $(qM - 2h_q) > 0$, then V_q becomes negative in this region

4 Region 4 In this region $S_p < 0$ and $S_q > 0$ and V becomes

$$V_q = -y^T Q y - qM|S_p| - pM|S_q| + 2S_p h_q \tag{C 16}$$

As in the Region 3, here also the first three terms are negative, but with $h_q < 0$ (C 11), the last term is positive Rewriting the above equation as

$$V_q = -y^T Q y - pM|S_q| - (qM + 2h_q)|S_p| \tag{C 17}$$

If $(qM+2h_q) > 0$, then the time derivative of V can be seen to be negative Here, h_q is negative and hence the inequality is the same as in the previous region

Thus it is seen that, if

$$M > \frac{2|h_q|}{q} = \frac{2\eta_M}{q}, \tag{C 18}$$

then V (2 40) becomes a Lyapunov function for Case CQ, since $|h_q| \leq \eta_M$ In particulai, if M is selected as

$$M = \frac{2\eta_M}{q - \delta_q}, \tag{C 19}$$

where $0 < \delta_q < q$, then $qM - 2h_q$ term in (C 15) and (C 17) may be replaced by $\delta_q M$ The V_q in (C 12) - (C 17) for the four regions may then be rewritten jointly as

$$V_q \leq -y^T Q y - pM|S_q| - \delta_q M|S_p| \tag{C 20}$$

This proves the claim ■

Appendix D

The Aircraft Parameters, Disturbances, and Uncertainties

In this work, the model responses are generated by

$$\triangle X = A_m \triangle X + B_m \triangle U_p, \tag{D 1}$$

where $\triangle X = X - X_{eq}$, where $X = [V_t,\ \alpha,\ Q,\ \theta]^T$ represents the vector of desired state trajectories and $\triangle U_p = U_p - U_{eq}$, where U_p represents the pilot inputs, namely the elevator stick and throttle gear deflections The X_{eq} and U_{eq} denotes the quantities at the equilibrium condition Note that the aircraft states in the chapters are taken as $[U,\ W,\ Q,\ \theta]^T$ Thus, appropriate transformations for the first two states needs to be performed The remaining states (namely, p_x and p_z) not specified in the above equation evolve according to (3 1) The matrices A_m and B_m were taken as

$$A_m = \begin{bmatrix} 23580E+0 & 48254E+3 & -35039E+2 & -60960E+3 \\ -30237E-3 & -11753E+1 & 85488E+0 & -81518E-2 \\ -24369E-2 & -12663E+2 & -58805E+1 & -45627E+1 \\ 00000E+0 & 00000E+0 & 10000E+1 & 00000E+0 \end{bmatrix}$$

$$B_m = \begin{bmatrix} 40239E+0 & 17039E+0 \\ -31570E-4 & -21507E-2 \\ 00000E+0 & -18243E+0 \\ 00000E+0 & 00000E+0 \end{bmatrix} \quad \text{(D 2)}$$

The above model gives desired trajectories in the $V_t - \alpha$ terms where as these are required to be given in the $U - W$ frame in the chapters The quantities may be transferred from $V_t - \alpha$ reference frame to the $U - W$ using the following formulae [10]

$$\begin{aligned} U &= V_t \cos(\alpha), \text{ and} \\ W &= V_t \sin(\alpha), \end{aligned} \quad \text{(D 3)}$$

or inversely as

$$\begin{aligned} V_t &= U^2 + W^2, \text{ and} \\ \tan(\alpha) &= W/U \end{aligned} \quad \text{(D 4)}$$

The U_d and W_d required in the work are evaluated by taking the derivative of D 4 which on simplification using (D 3) gives

$$\begin{aligned} U_d U_d + W_d W_d &= V_{t_d} V_{t_d}, \text{ and} \\ -W_d U_d + U_d W_d &= V_{t_d}^2 \alpha_d \end{aligned} \quad \text{(D 5)}$$

The above equation may be solved for U_d and W_d, in terms of the known V_{t_d}, α_d, and therefore U_d, W_d and the time derivatives V_{t_d} and α_d to get

$$\begin{aligned} U_d &= \frac{U_d V_{t_d}}{V_t} - W_d \alpha_d, \text{ and} \\ W_d &= \frac{W_d V_{t_d}}{V_t} + U_d \alpha_d \end{aligned} \quad \text{(D 6)}$$

The second derivatives of the model response are developed by taking a time derivative of (D 1) and simplifying it to get

$$\begin{aligned} \Delta X &= A_m \Delta X + B_m \Delta U_p, \text{ or} \\ \Delta X &= A_m^2 \Delta X + A_m B_m \Delta U + B_m \Delta U_p \end{aligned} \quad \text{(D 7)}$$

Thus, the second derivatives V_{t_d} and α_d are easily calculated Note that they contain the derivative of the applied pilot inputs It now remains to transform these into U_d and W_d as are required in (5 43) For this, taking another time derivative of (D 5) and rearranging terms, it is seen that

$$\begin{aligned} U_d U_d + W_d W_d &= V_{t_d}^2 + V_{t_d} V_{t_d} - U_d^2 - W_d^2, \text{ and} \\ -W_d U_d + U_d W_d &= 2V_{t_d} V_{t_d} \alpha_d + V_{t_d}^2 \alpha_d \end{aligned} \tag{D 8}$$

The above linear equations may be solved for the unknowns U_d and W_d to get

$$\begin{aligned} U_d &= \frac{1}{V_{t_d}^2}[U_d(V_{t_d}^2 + V_{t_d} V_{t_d} - U_d^2 - W_d^2) - W_d(2V_{t_d} V_{t_d} \alpha_d + V_{t_d}^2 \alpha_d)], \text{ and} \\ W_d &= \frac{1}{V_{t_d}^2}[W_d(V_{t_d}^2 + V_{t_d} V_{t_d} - U_d^2 - W_d^2) + U_d(2V_{t_d} V_{t_d} \alpha_d + V_{t_d}^2 \alpha_d)] \end{aligned} \tag{D 9}$$

The remaining second order derivative in (5 43, i e the Q_d is directly available from (D 7)

The uncertainties and disturbances considered considered in this work are

- **Uncertainty in the Mass and Inertia:** The nominal values of reciprocal of aircraft mass, $\hat{R_m} = 1\ 5 \times 10^{-3}$, and inverse of the pitching moment of inertia, $\hat{c}_7 = 1\ 75 \times 10^{-5}$ have been used The range of their possible variations have been taken as $1\ 0 \times 10^{-3} \leq R_m \leq 2\ 0 \times 10^{-3}$ and $1\ 0 \times 10^{-5} \leq c_7 \leq 2\ 5 \times 10^{-5}$ The actual values of these parameters as used in the simulation are reported in Fig D 1 The bounds D_{b1} and D_{b2} can be evaluated as 1/3 and 3/7 respectively

- **Uncertainty in Aerodynamic Inversion and/or Modeling:** It is assumed that a maximum 20 percentage of error can occur, which means that $|\delta_{ae}| \leq 0\ 20$ For simulation purposes two different sets of variation in δ_{ae} has been used as

$$\begin{array}{ll} UC1 \quad \textit{Uncertainty set } 1 & UC2 \quad \textit{Uncertainty set } 2 \\ \delta_{ae}(1) = 0\ 05 + 0\ 145\cos(3\pi t) & \delta_{ae}(1) = -0\ 19, \\ \delta_{ae}(2) = -0\ 02 + 0\ 15\cos(5\pi t), \text{ and} & \delta_{ae}(2) = 0\ 175, \text{ and} \\ \delta_{ae}(3) = 0\ 1 + 0\ 08\cos(3\pi t) & \delta_{ae}(3) = 0\ 185 \end{array} \tag{D 10}$$

for the 3-component force vector

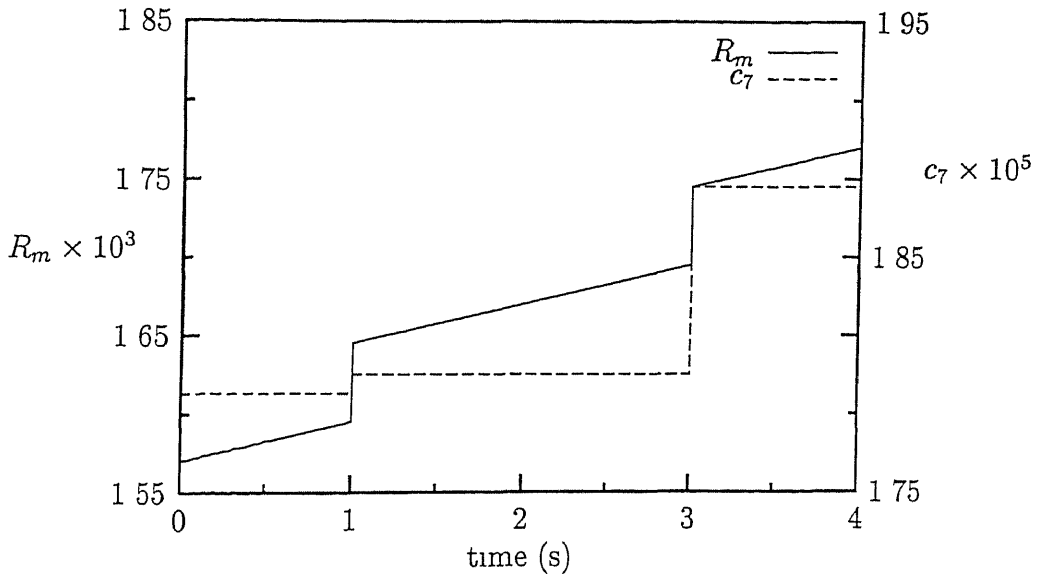

Fig D 1 Variation in the R_m and the c_7 parameters of the aircraft

- **External Disturbances in the governing differential equation** For simulation purposes the external disturbances were assumed to be

$$\begin{aligned} d_U &= 0\ 05 + 0\ 25\cos(3\pi t), \\ d_W &= -0\ 05 + 0\ 25\cos(7\pi t), \text{ and} \\ d_Q &= 0\ 05 + 0\ 15\cos(5\pi t) \\ d_\theta &= 0\ 04 + 0\ 25\cos(3\pi t), \\ d_x &= -0\ 74d0 + 0\ 25\cos(7\pi t), \text{ and} \\ d_z &= 0\ 05d0 + 0\ 85\cos(5\pi t) \end{aligned} \tag{D 11}$$

with $D_U = 0\ 3$, $D_W = 0\ 3$, and $D_Q = 0\ 3$ Note that the other disturbance terms are unmatched Their bounds are taken as $D_\theta = 0\ 3$, $D_X = 1\ 0$, and $D_Z = 1\ 0$

The boundary layer thicknesses have been selected as $\phi = [0\ 5,\ 0\ 5,\ 0\ 005]$ for the tracking mode and $\phi = [0\ 5,\ 0\ 01,\ 0\ 01]$ for the trimming mode

Appendix E

Time Derivatives of Functions

The definitions and notations of time derivatives of smooth scalar, vector and matrix functions of a vector of variables used in this work is given here The vector of variables is taken as $\mathbf{x} = [x_1,\ x_2,\quad ,x_n]^T \in \mathcal{R}^n$ and $\mathbf{x}$ is assumed to be available Also arguments of the functions are omitted where they are not likely to create confusion

Derivative of a Scalar Function

Let $f(\mathbf{x})$ be a scalar function Then its time derivative is given using Lie derivatives [21, 22] as

$$\frac{df}{dt} = \frac{\partial f}{\partial x_1}x_1 + \quad + \frac{\partial f}{\partial x_n}x_n = L_{\mathbf{x}}f \tag{E.1}$$

In this work, the above Lie derivative will be expressed as

$$\frac{df}{dt} = L_{\mathbf{x}}f = R_f\mathbf{x} \tag{E 2}$$

R_f represents a $1 \times n$ element row vector formed from f as defined above

Derivative of a Vector Function

Let $\mathbf{f}(\mathbf{x}) = [f_1,\ f_2,\quad ,f_m]^T$ be a $m \times 1$ vector function Then using the above notation, its derivative is given as

$$\frac{d\mathbf{f}}{dt} = \begin{pmatrix} L_{\mathbf{x}} f_1 \\ L_{\mathbf{x}} f_2 \\ \\ L_{\mathbf{x}} f_m \end{pmatrix} = \begin{pmatrix} R_{f_1}\mathbf{x} \\ R_{f_1}\mathbf{x} \\ \\ R_{f_1}\mathbf{x} \end{pmatrix} = M_f \mathbf{x}, \tag{E 3}$$

where $M_{\mathbf{f}}$ may be rewritten using (E 2) and the above equation as

$$M_f = \begin{bmatrix} \frac{\partial f_1}{\partial x_1} & \frac{\partial f_1}{\partial x_2} & \frac{\partial f_1}{\partial x_n} \\ \frac{\partial f_2}{\partial x_1} & \frac{\partial f_2}{\partial x_2} & \frac{\partial f_2}{\partial x_n} \\ \\ \frac{\partial f_m}{\partial x_1} & \frac{\partial f_m}{\partial x_2} & \frac{\partial f_m}{\partial x_n} \end{bmatrix} \tag{E 4}$$

M_f represents a $m \times n$ matrix formed from the components of the vector function $\mathbf{f}$ as defined above

Derivative of a Matrix Function

Let $A(\mathbf{x})$ represent a $m \times p$ matrix function By definition,

$$\frac{d[A(\mathbf{x})]}{dt} = \left[\frac{da_{ij}(\mathbf{x})}{dt}\right], \tag{E 5}$$

where, $a_{ij}(\mathbf{x})$ represents the element in the i^{th} row and j^{th} column of A Since a_{ij} is a scalar function, its time derivative may be written using (E 2) as

$$\frac{da_{ij}}{dt} = R_{a_{ij}}\mathbf{x} \tag{E 6}$$

The derivative of A (E 5), using the above equation can be expressed in a matrix product form as

$$\frac{d[A]}{dt} = \begin{bmatrix} R_{a_{11}} & & R_{a_{1p}} \\ R_{a_{21}} & & R_{a_{2p}} \\ & & \\ R_{a_{m1}} & & R_{a_{mp}} \end{bmatrix} \begin{bmatrix} \mathrm{x} & 0 & & 0 \\ 0 & \mathrm{x} & 0 & \\ & 0 & & 0 \\ 0 & & 0 & \mathrm{x} \end{bmatrix}, \tag{E 7}$$

where 0 in the above equation represent a n column zero vector Using the definition of a Kronecker product, and defining the first matrix in the above product as J_A, the above equation may be rewritten as

$$\frac{d[A]}{dt} = J_A[I_p \otimes \mathrm{x}] \tag{E 8}$$

where, I_p denotes a $p \times p$ identity matrix, $\otimes$ represents the Kronecker product In the J_A as defined in (E 7) it is clear that, since $R_{a_{ij}}$ represents a $1 \times n$ row vector, the matrix will be a $m \times np$ matrix Also, the $[I_p \otimes \mathrm{x}]$ matrix will be a $np \times p$ matrix by definition Thus the time derivative of A results in a $m \times p$ matrix The J_A matrix as defined above is seen from (E 7) to contain the partial derivatives of a_{ij} with respect to x as

$$J_A = \begin{bmatrix} \frac{\partial a_{11}}{\partial x_1} & \frac{\partial a_{11}}{\partial x_2} & & \frac{\partial a_{11}}{\partial x_n} & \frac{\partial a_{12}}{\partial x_1} & \frac{\partial a_{12}}{\partial x_2} & & \frac{\partial a_{1p}}{\partial x_n} \\ \frac{\partial a_{21}}{\partial x_1} & \frac{\partial a_{21}}{\partial x_2} & & \frac{\partial a_{21}}{\partial x_n} & \frac{\partial a_{22}}{\partial x_1} & & & \\ & & & & & & & \\ \frac{\partial a_{m1}}{\partial x_1} & \frac{\partial a_{m1}}{\partial x_2} & & \frac{\partial a_{m1}}{\partial x_n} & \frac{\partial a_{m2}}{\partial x_1} & \frac{\partial a_{m2}}{\partial x_2} & . & \frac{\partial a_{mp}}{\partial x_n} \end{bmatrix} \tag{E 9}$$

Appendix F

The Uniform Ultimate Boundedness of Systems

Definition 1 (Global uniform ultimate boundedness) *[52]*

An uncertain feedback system with state $\mathbf{x}(t)$ *is said to be globally uniformly ultimately bounded with respect to a set* $S \subset \mathcal{R}^n$, *if*

1 *for each uncertainty realization and for each* $(t_0, \mathbf{x}(t_0)) \in \mathcal{R} \times \mathcal{R}^n$ *there exists at least one solution* $\mathbf{x}(\,)\quad [t_0, t_1) \rightarrow \mathcal{R}^n,\ t_1 > t_0,$

2 *given any real number* $\delta > 0$, *there exists a real number* $d(\delta) > 0$ *such that, for any solution* $\mathbf{x}(\,)$ *with* $||\mathbf{x}(t_0)|| \leq \delta$, $||\mathbf{x}(t)|| < d(\delta)$ *for all* $t \in [t_0, t_1)$ *all solutions can thus be continued over* $[t_0, \infty]$,

3 *for every* $\mathbf{x}(t_0) \in \mathcal{R}^n$, *there exists a non-negative constant* $T(\mathbf{x}(t_0), S) \in \mathcal{R}^+$ *such that, for every solution* $\mathbf{x}(\,)$ *with* t_0 *arbitrary,* $\mathbf{x}(t) \in S$ *for all* $t \geq t_0 + T(\mathbf{x}(t_0), S)$

Using the above definition, the global uniform ultimate boundedness of the following system is established The S_{x_1} dynamics in (4 12) may be written in general form as

$$x = -kx + d, \tag{F 1}$$

where $x \in \mathcal{R}$, $k > 0$, and d represents the unknown uncertainty term which is given to be bounded with $|d| < D$ The subsequent developments follow the steps as outlined in [52, 70] Select the candidate Lyapunov function as

$$V(x) = \frac{1}{2}x^2 \tag{F 2}$$

Its time derivative may be calculated as $V = -kx^2 + xd$ With the bound on d as specified above, it is seen that

$$V \leq -kx^2 + D|x| \tag{F.3}$$

Note that $|x| = \sqrt{2V}$ from (F 2) Thus, $V \leq -2kV + D\sqrt{2V}$ It is evident from this equation that $V < 0$ if $V > r_1 - \epsilon$, where $\epsilon > 0$ is a small constant, and $r_1 = \epsilon + D^2/(2k^2)$ Define the set $S = x \quad \frac{1}{2}x^2 \leq r_1$ From the fact that $V < 0$ if $V > r_1 - \epsilon$, it is seen that if $x(t_0) \in S$ then $x(t) \in S$ for all $t \geq t_0$ The (F 3) may be rewritten as

$$V \leq -2kV + D\sqrt{2V} \tag{F.4}$$

The time taken for V to change from V_0 at $t = t_0$ to V_1 at $t = t_1$ may be evaluated as

$$t_1 - t_0 \leq \frac{1}{k} \ln \left[\frac{k\sqrt{2V_0} - D}{k\sqrt{2V_1} - D} \right] \tag{F 5}$$

Thus, if $x(t_0) \notin S$, then the trajectory will reach S in a finite time given by

$$t_1 - t_0 \leq \frac{1}{k} \ln \left[\frac{k\sqrt{2V_0} - D}{k\sqrt{2r_1} - D} \right] \tag{F.6}$$

All conditions for uniform ultimate boundedness are thus satisfied

Appendix G

The Error Bounds

The $\mathbf{S}_v$ is shown to satisfy the bounds as in (5 51) Putting $\alpha_i = [|\mathbf{B}_1|\phi_u + \mathbf{D}_1 + D_t(|\mathbf{f}_1 - \mathbf{T}_a|)]_i$, it may be rewritten in a simpler form component-wise as

$$
\begin{aligned}
|S_U| &\leq \frac{\alpha_U + D'_{2U}}{K_U[1 - D_t(1,1)]} \\
|S_W| &\leq \frac{\alpha_W + D'_{2W}}{K_W[1 - D_t(2,2)]} \\
|S_Q| &\leq \frac{\alpha_Q + D'_{2Q}}{K_Q[1 - D_t(3,3)]}
\end{aligned}
\tag{G 1}
$$

Similarly, the $|S_{x_i}|$ are given to be bounded as in (5 52) and using the bounds on the B_2 matrix in (4 29), these may be expressed as

$$
\begin{aligned}
K_x|S_x| &\leq S_U + S_W + D_{2x}, \\
K_z|S_z| &\leq S_U + S_W + D_{2z}, \text{ and} \\
K_\theta|S_\theta| &\leq S_Q + D_{2\theta}
\end{aligned}
\tag{G.2}
$$

The bounds $\mathbf{D}'_2$ as required in (G 1) are given in (4 43) and are seen to involve the bounds on the position errors, i e $|\mathbf{S}_x|$ Using the bounds on the position errors as

above in (4 43) gives

$$\begin{pmatrix} D'_{2U} \\ D'_{2W} \\ D'_{2Q} \end{pmatrix} = \begin{pmatrix} K_x D_{2x}|cos(\theta)| + K_z D_{2z}|sin(\theta)| \\ +D_{2\theta}\left[|U_d sin(S_\theta)| + |W_d cos(S_\theta)| + D_{2x} + D_{2z}\right] \\ +2D_{2\theta}[|S_U| + |S_W|] \\ K_x D_{2x}|sin(\theta)| + K_z D_{2z}|sin(\theta)| \\ +D_{2\theta}\left[|U_d cos(S_\theta)| + |W_d sin(S_\theta)| + D_{2x} + D_{2x}\right] \\ +2D_{2\theta}[|S_U| + |S_W|] \\ K_\theta D_{2\theta} \end{pmatrix}, \text{ or,}$$

$$= \begin{pmatrix} \beta_U + 2D_{2\theta}[|S_U| + |S_W|] \\ \beta_W + 2D_{2\theta}[|S_U| + |S_W|] \\ K_\theta D_{2\theta} \end{pmatrix}, \qquad \text{(G 3)}$$

where, β_U, β_W are positive quantities and are obviously defined It is seen from the above equation that D'_{2Q} does not depend on any of the velocity error bounds Thus the bounds $|S_Q|$ and the $|S_\theta|$ may be directly evaluated as defined in (G 1) and (G 2) respectively However, the $|S_U|$ and the $|S_W|$ bounds are implicitly defined and may be evaluated as follows

Using the above developed bounds for $\mathbf{D}'_2$ (G 3), and putting $\alpha'_i = \alpha_i + \beta_i$, $i = U, W$, $q_1 = K_U[1 - D_t(1,1)]$, and $q_2 = K_W[1 - D_t(2,2)]$, the $|S_U|$ and $|S_W|$ in (G 1) may be rewritten as

$$|S_U| \leq \frac{\alpha'_U + 2D_{2\theta}[|S_U| + |S_W|]}{q_1}, \text{ and}$$

$$|S_W| \leq \frac{\alpha'_W + 2D_{2\theta}[|S_U| + |S_W|]}{q_2} \qquad \text{(G 4)}$$

The above inequalities may be expressed as set of simultaneous linear inequalities in matrix form as

$$\begin{bmatrix} 1 - 2D_{2\theta}/q_1 & -2D_{2\theta}/q_1 \\ -2D_{2\theta}/q_2 & 1 - 2D_{2\theta}/q_2 \end{bmatrix} \begin{pmatrix} |S_U| \\ |S_W| \end{pmatrix} \leq \begin{pmatrix} \alpha'_U/q_1 \\ \alpha'_W/q_2 \end{pmatrix} \qquad \text{(G 5)}$$

Note that α'_i, $i = U, W$ and q_1, q_2 are always positive The solution $|S_U|$ and $|S_W|$ of the above equation should be positive to be practically meaningful This may be easily established using the following theorem

Theorem 1 (Forbenius-Perron) *[21] Consider a square matrix A with nonnegative elements Then the largest eigenvalue ρ_1 of A is nonnegative Furthermore, consider the equation*

$$(I - \rho^{-1}A)\mathbf{y} = \mathbf{z}, \tag{G 6}$$

where, $\mathbf{y}, \mathbf{z}$ are vectors, I is the identity matrix of appropriate dimensions and all components of the vector $\mathbf{z}$ are nonnegative

If $\rho > \rho_1$, then the above equation admits a unique solution $\mathbf{y}$, whose components y_i are all nonnegative

From (G 5), it is seen that the $\mathbf{z} = [\alpha'_U/q_1 \ \alpha'_W/q_2]^T$ has all its components positive, and the A matrix, as in the above theorem, is seen from (G 5 to be

$$A = \begin{bmatrix} 2D_{2\theta}/q_1 & 2D_{2\theta}/q_1 \\ 2D_{2\theta}/q_2 & 2D_{2\theta}/q_2 \end{bmatrix} \tag{G 7}$$

The eigenvalues of the A matrix are easily obtained as 0 and $2D_{2\theta}/(q_1+q_2)$ According to the above theorem, if the largest eigenvalue is less than 1 0, then the (G 5) is guaranteed to have a positive solution for the norm of the error bounds Now, by definition $q_1 + q_2 = K_U[1 - D_t(1,1)] + K_W[1 - D_t(2,2)]$, and since $D_{2\theta}$ is a known bounded quantity, sufficiently large positive values for K_U and K_W can be selected to make the non-zero eigenvalue less than 1 0 Thus, the error bounds may be obtained by solving the simultaneous linear equation set in (G 5) Further, once the $|\mathbf{S}_v|$ are guaranteed to be positive, the positiveness of $|\mathbf{S}_x|$ is obvious from its definition in (4 45) Similar results are presented in [70] using a different approach

APPENDIX 1
ERRATA

The following corrections are to be included in the thesis

1) **Ref: Pg-6: 5th Line-**

"*Using this result, is proposed*" should be corrected to

This result has been used to propose a new method of selection of controller parameters, which gives a lower time to OTE

2) **Ref: Pg-9: 15th Line-**

"*Application of the unmatched uncertainty*" should be corrected to

The ML approach is then applied to a third order nonlinear system with unmatched uncertainties and disturbances A new method of selecting the gain of the switching term is proposed Further it is shown that the conventional SMC may be extended to tackle the unmatched uncertainty case with the proposed gain selection

3) **Ref: Pg-72: 18th Line-**

"*The Δae in the simulation*" The 'Δae ' in this line should be corrected to 'Δ_{ae}'

4) **Ref: Pg-94: 14th Line-**

"*As seen earlier in this chapter*" should be corrected to

As discussed in Section 4 2, the effect of disturbances in the outer loops is easily passed on to the inner loop This simple propagation of disturbances results in a simplified robustness analysis, as will be shown in this chapter

5) **Ref: Pg-94: 21st Line-**

"*Following the developments in the innermost loop*" should be corrected to

Following the developments in Chapter 4, the tracking of position variables is done in the outer loop by generating augmented velocity command signals These augmented velocity signals are tracked in the inner loop by synthesizing augmented input command signals A SMC law is then designed to track the commanded input signals in the innermost loop

6) **Ref: Pg-116: 10th Line-**

"*In this chapter, is developed*" should be corrected to

In this chapter, the ML strategy has been used to develop a robust control law design method for a nonlinear system with specified input dynamics under unmatched uncertainties and disturbances

Date 7 /12/1998

G K Singh,
Roll No 9210464